Universidad de Santiago de Compostela
Facultad de Medicina y Odontología
Departamento de Medicina

Teranóstica en el ictus isquémico: nanopartículas vectorizadas hacia la zona peri-infarto

Ischemic stroke theranostic: peri-infarct guided nanoparticles

Tesis doctoral
Jesús Agulla Freire
2012

UNIVERSIDADE DE SANTIAGO

DE COMPOSTELA

TERANÓSTICA EN EL ICTUS ISQUÉMICO: NANOPARTÍCULAS VECTORIZADAS HACIA LA ZONA PERI-INFARTO

ISCHEMIC STROKE THERANOSTICS: PERI-INFARCT REGION GUIDED NANOPARTICLES

TESIS DOCTORAL

PhD Thesis

Jesús Agulla Freire

2012

El **Prof. Dr. José Castillo Sánchez**, Catedrático del Departamento de Medicina de la Universidad de Santiago de Compostela, Coordinador del Laboratorio de Investigación en Neurociencias Clínicas (LINC) y Director del Área de Neurociencias del Hospital Clínico Universitario de Santiago de Compostela, y los doctores **Pedro Ramos Cabrer** y **Tomás Sobrino Moreiras** (colaboradores docentes del Departamento de Medicina de la Universidad de Santiago de Compostela),

CERTIFICAN:

Que el presente trabajo titulado "**Teranóstica en el ictus isquémico: nanopartículas vectorizadas hacia la zona peri-infarto**" ha sido realizado bajo su dirección, por el licenciado en biología molecular **D. Jesús Agulla Freire**, y se encuentra en condiciones de ser presentado y defendido como Tesis Doctoral ante el tribunal correspondiente en la Universidad de Santiago de Compostela.

Santiago de Compostela, Enero de 2012

Prof. Dr. José Castillo Sánchez

Dr. Pedro Ramos Cabrer

Dr. Tomás Sobrino Moreiras

Prof. Dr. José Castillo Sánchez (MD, PhD), Professor of Neurology in the Department of Medicine of the University of Santiago de Compostela, head of the Clinical Neurosciences Research Laboratory and Director of the Neurosciences Section at the University Clinical Hospital, **Pedro Ramos Cabrer (PhD)** and **Tomás Sobrino Moreiras (PhD)**,

CERTIFY:

That the present research study entitled "**Ischemic stroke theranostic: peri-infarct guided nanoparticles"** has been carried out under their supervision by **Jesús Agulla Freire**, graduate in Biology, and that the document meets all requisites for its defense under the corresponding PhD committee proposed by the University of Santiago de Compostela.

Santiago de Compostela, January 2012

Prof. José Castillo Sánchez (MD, PhD)

Pedro Ramos Cabrer (PhD) Tomás Sobrino Moreiras (PhD)

Este trabajo ha sido financiado con subvenciones concedidas por la Xunta de Galicia: Consellería de Sanidade (Código PS09/32) y Consellería de Industria (Código 09CSA057918PR) y el proyecto INCITE 08PXIB927229PR); por el ministerio de ciencia e innovación (MCIN, proyecto SAF 2008-02190 y proyecto SAF 2001-30517); por el Instituto de Salud Carlos III (Proyecto PI11/02161, proyecto CP09/00074 y RETICS-RD06/0026); y por el grupo Ferrer Internacional, S.A. Se agradece especialmente a la Unión Europea por la financiación otorgada a través de fondos FEDER.

This work has been supported with grants from Xunta de Galicia: Consellería de Sanidade (Code PS09/32) y Consellería de Industria (Code 09CSA057918PR and project INCITE08PXIB927229PR) and proyect INCITE 08PXIB927229PR); also by the Spanish Ministry of Science and Innovation (MCIN, project SAF 2008-02190 and SAF 2011-30517); the Instituto de Salud Carlos III (Project PI11/02161, CP09/00074 and RETICS-RD06/0026); and from Ferrer internacional, S.A. The EU is deeply acknowledged for the founding of this work through FEDER funds.

APPRECIATIONS

My sincere gratitude towards José Castillo (MD, PhD), for giving me the opportunity to start my research career at the Clinical Neurosciences Research Laboratory. I also want to thank my PhD co-directors Pedro Ramos (PhD) and Tomás Sobrino (PhD) for their support during this somewhat tortuous period. To all the members of ANEVAS and the laboratory, without their help it would have been impossible to finish this thesis. I deeply appreciate the support of the Photophysics and Molecular Photochemistry group directed by Dr. Wajih Al-Soufi at the University of Santiago de Compostela, as well as the Molecular Imaging and Image Guided Interventions group directed by Prof. Holger Grüll and the Biomedical NMR group directed by Prof. Klaas Nicolay at the Eindhoven University of Technology.

I want to thank David for all his support both technically and academically, we shared a great part of the work that helped engendered this document. Also I want to thank Isabel with whom I raced to finished the thesis, you have been a great player, but sorry, I win. To my college sweetheart for her unreserved support, I'm sorry for all the trouble I have caused you, but for what I've heard, this is only the beginning. Just remember that as a great poet once said: "…life can be a challenge, life can seem impossible, it's never easy when so much is on the line". And thanks to Pedro, the brain behind it all, without his might we would still be stalled at the beginning, you have been the "Clay" that held it all together.

Thank you everyone

ABBREVIATIONS

- ***2D-PAGE*** , Bi-dimensional Poly-Acrylamide Gel Electrophoresis
- ***ADC***, Apparent Diffusion Coefficient
- ***AMPA***, 2-Amino-3-hydroxy-5-Methyl-4-isoxazol Propionic Acid
- ***ATP***, Adenosin Tri-Phosphate
- ***BBB***, Blood Brain Barrier
- ***BCNU***, Bis-ChloroethylNitrosoUrea
- ***BDNF***, Brain Derived Neurotrophic Factor
- ***BSA***,Bis(StearylAmide)
- ***C-GSF***, Granulocyte Colony-Stimulating Factor
- ***CBF***, Cerebral Blood Flow
- ***CDDS***, Chemical Drug Delivery Systems
- ***CEST***, ChEmical Shift saturation Transfer
- ***CHAPS***, CHolAmidopropyl-dimethylammonio-PropaneSulfonate
- ***CMT***, Carrier-Mediated Transport
- ***CNS***, Central Nervous System
- ***COFRADIC***, COmbined FRActional DIagonal Chromatography
- ***COX-2***, CyclOXigenase-2
- ***CSF***, CerebroSpinal FLuid
- ***CT***, Computed Tomography
- ***DC***, Drug Content
- ***DLS***, Dynamic Light Scattering
- ***DSPC***, DiStearoylPhosphatidylCholine
- ***DSPE***, 1,2-Distearoyl-Sn-glycero-3-PhosphoEthanolamine
- ***DTPA***, DieThylenetriaminePentaacetic Acid
- ***DTT***, DiThioThreitol
- ***DWI***, Diffusioin Weighted Imaging
- ***EAAT***, Excitatory Amino-Acid Transporter
- ***EGF***, Epidermal Growth Factor
- ***EPO***, ErythroPOeitin
- ***FDA***, Food and Drug Administration
- ***FGF***, Fibroblast Growth Factor
- ***FOV***, Field Of View
- ***GABA***, Gamma-AminoButyric Acid
- ***Gd***, Gadolinium

- ***GDNF***, Glial-Derived Neurotrophic Factor
- ***GFAP***, Glial Fibrillary Acidic Protein
- ***GOT***, Glutamate-Oxaloacetate Transaminase
- ***Hb***, Hemoglobin
- ***HPLC***, High-Performance Liquid Chromatography
- ***hs-tk***, herpes simplex thymidine kinase
- ***HSP***, Heat Shock Protein
- ***icv***, itracerebroventricular
- ***IL-2***, InterLeukin-2
- ***iNOS***, inducible Nitric Oxide Synthase
- ***IPG***, Immobilized PH Gradient
- ***ISF***, InterStitial Fluid
- ***iv***, intravenous
- ***LC***, Liquid Chromatography
- ***Mab***, Monoclonal antibody
- ***MALDI***, Matrix-Assisted Laser Desorption/Ionization
- ***MCA***, Middle Cerebral Artery
- ***MCT***, MonoCarboxylic acid Transporter
- ***MI***, Molecular
- ***MMP***, Matrix MetalloProteinase
- ***MRI***, Magnetic Resonance Imaging
- ***MS***, Mass Spectrometry
- ***MSC***, Mesenchymal Stem Cell
- ***NGF***, Nerve Growth Factor
- ***NIHSS***, National Institutes of Health Stroke Scale
- ***nNOS***, nuclear Nitric Oxide Synthase
- ***NM***, Nuclear Medicine
- ***NMDA***, N-Methyl- D-aspartate
- ***NO***, Nitric Oxide
- ***NVU***, NeuroVascular Unit
- ***OB***, Olfatory Bulb
- ***PAGE***, PolyAcrylamide Gel Electrophoresis
- ***PBS***, Phosphate-Buffered Saline
- ***pCPP:SA***, 1,3 bis-para-CarboxyPhenoxyPropane: Sebacic Acid
- ***PCR***, Polymerase Chain Reaction
- ***PE***, PhycoErythrin

- ***PEG***, PolyEthylene Glycol
- ***PET***, Positron Emission Tomography
- ***PGA***, Poly(Glycolic Acid)
- ***PHDCA***, Poly-HexaDecylCyanoAcrylate
- ***PLA***, Poly(Lactic Acid)
- ***PLGA***, Poly(Lactide-co-Glycolide Acid)
- ***PNA***, Peptide Nucleic Acids
- ***PVDF***, PolyVinylidene DiFluoride
- ***PWI***, Perfusion Weighted Imaging
- ***rES***, reticuloEndothelial System
- ***RMS***, Rostral Migratory Stream
- ***RMT***, Receptor-Mediated Transport
- ***ROS***, Reactive Oxygen Species
- ***rt-PA***, recombinant tissue Plasminogen Activator
- ***SATA***, N-Succinimidyl S-AcetylThioAcetate
- ***SDF-1***, Stromal Cell-Derived Factor-1
- ***SDS***, Sodium Dodecyl Sulfate
- ***SVZ***, SubVentricular Zone
- ***TBST***, Tris-Buffered Saline + TWEEN-20
- ***TCEP***, Tris(2-CarboxyEthyl)Phosphine
- ***TE***, Echo Time
- ***TEAB***, TetraEthylAmmonium Borohydride
- ***TEM***, Transmission Electron Microscopy
- ***TIA***, Transient Ischemic Attack
- ***TIE***, Tyrosine kinase with Immunoglobulin-like and EGF-like domains
- ***TOF***, Time Of Flight
- ***TR***, Repetition Time
- ***TTC***, 2, 3, 5-Triphenyl-2H-Tetrazolium Chloride
- ***VASO***, VAscular-Space-Occupancy
- ***VEGF***, Vascular Endothelial Growth Factor
- ***WHO***, World Health Organization

INDEX

1. INTRODUCTION

1.1. Stroke

Stroke is a cerebrovascular disease, consequence of the alteration of normal cerebral blood flow, which results in a transitory or permanent deficit of the function of one or more parts of the brain. Alternatively one could define stroke as all those alterations, via ischemic or hemorrhagic mechanisms, that affect some part of the brain in a transitory or permanent manner, to such extent that induced metabolic or biochemical alterations would lead to cell death, and alteration of the nervous system. The World Health Organization (WHO) has defined stroke as the fast clinical development of focal signs of alteration of cerebral function without any other apparent origin that the vascular one.[1]

Stroke can be classified, attending to the nature of the lesion, in ischemic stroke and intracerebral hemorrhage. However, alternative classifications of this cerebrovascular disease can be used attending to other parameters such as stroke subtype, the progression profile, neuroimaging characteristics, nature, size and topography of the lesion, and the mechanisms of induction and etiology.[2]

1.1.1. Ischemic Stroke

Ischemic stroke is the most common type of stroke. All those secondary encephalic alterations that lead to a failure of blood supply, both qualitatively and quantitatively are included under this term. The term focal brain ischemia is used when only one part of the brain is affected, while global brain ischemia involves the affectation of the whole brain.

Focal ischemic stroke is classified in: 1) transitory ischemic attack (TIA) and 2) cerebral infarction. TIA is defined as the focal or

monocular cerebral dysfunction with symptoms that last for less than 24 hours, whose origin is a vascular insufficiency caused by an arterial thrombus or embolism, associated to arterial, cardiac or hematologic disease.[3]

TIA patients present higher risk of subsequent major stroke (cerebral infarct) and other vascular episodes, mainly coronary, and the outcome of each individual is extraordinarily variable.

Within the term ischemic stroke several etiologic subtypes are included (figure 1):[4]

- *Atherothrombotic infarction:* generally middle or large sized infarcts with cortical, subcortical, carotid or vertebro-basilar topography, in patients with presence of one or several cerebrovascular risk factors. It is imperative the presence of clinically generalized atherosclerosis, or the demonstration of occlusion or stenosis (> 50% occlusion or <50% plus two or more vascular risk factors) in cerebral arteries, with an established correlation to the patient's clinic.
- *Lacunar infarction or small vessel disease:* small sized infarct (<15 mm of diameter), localized in the distribution territory of the penetrating arterioles. Although micro-atheromatosis and lipohialinosis of penetrating arterioles are the most frequent pathologic substrate in lacunar infarcts, other less frequent potential causes are cardiac embolism, arterial embolism, infectious arthritis or prothrombotic state.
- *Cardioembolic infarction:* generally medium (1.5-3 cm of diameter) or large (>3 cm of diameter) sized infarcts, with symptoms frequently started during awakening. It is mandatory the presence of a demonstrated embolic cardiopathy, and the absence of significant concomitant arterial occlusion or stenosis.
- *Infarction of non-habitual origin:* infarcts of any size, in patients without known vascular risk factors, where cardioembolic, lacunar or atherotrombotic infarcts have been discarded.

- *Infarction of undetermined etiology:* brain infarcts of medium or large size with more than two potential etiologies or unknown origin.

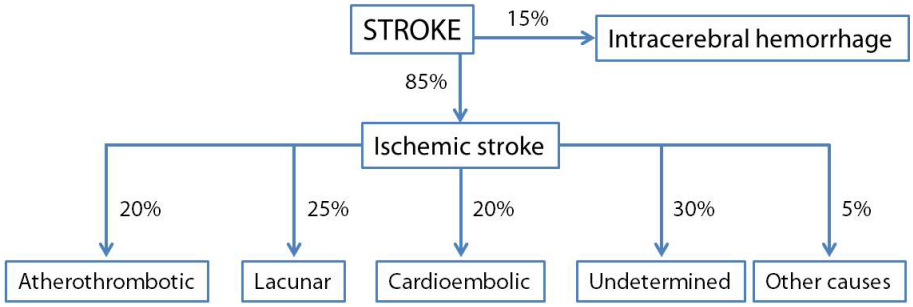

Figure 1. Classification of stroke attending to its etiopathogenic origin.

1.1.2. Biochemistry of cerebral ischemia

The acute obstruction of one of the large brain arteries, such as the Middle Cerebral Artery (MCA), induces an instantaneous reduction of blood flow in the corresponding irrigation area (focal ischemia). Such reduction of blood supply is not homogeneous in the affected area and can change within minutes or hours, especially if blood supply is reinstated.[5]

Ischemia becomes severe in the so-called ischemic core, the portion of tissue closest to the affected blood vessel, while a gradient of perfusion is established in its periphery, the so-called penumbra, where the reduction of blood flow is less severe, due to the blood supply carried out by collateral arteries of the non-ischemic neighbor tissue.[6] The impact of brain ischemia will depend on the severity and duration of the reduction of blood flow.

After the onset of brain ischemia, a sequence of molecular events are triggered in the short and the long term, initiated with an energetic failure in cells, related to the interruption of oxidative phosphorylation processes and the deficient production of adenosine tri-phosphate (ATP) (Figure 2).

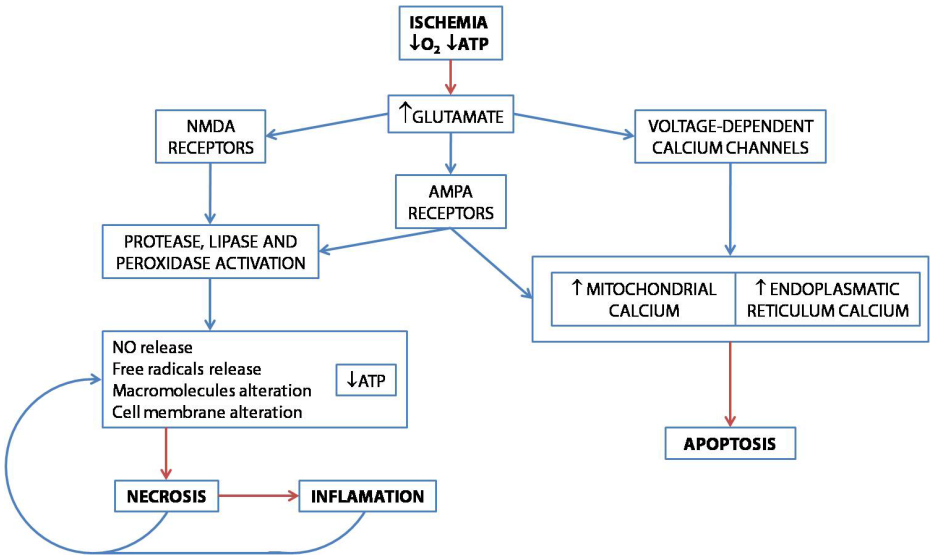

Figure 2. Sequence of main physiopathological events in cerebral ischemia.

The cessation of transmembrane ionic gradients due to the failure of sodium-potassium-ATPase pumps, and other ATP-dependent ionic pumps, is the key step of the physiopathological mechanisms in stroke, especially of cell death in the ischemic core, when the vascular occlusion last for a few minutes.[7] Neurons and glial cells suffer an extreme depolarization because of the entrance of sodium, chloride, calcium and water into the cytoplasm.[8] In addition, potassium leaves the cell, inducing a sudden increment of its extracellular levels.[9] The energetic failure, and the associated ionic changes, originate an increment in glutamate, a hyperexcitability of N-methyl- D-aspartate glutamatergic receptors (NMDA), and of a-amino- 3-hydroxy-5-methyl-4-isoxazol propionic acid receptors (AMPA), which induces an even higher increase of intracellular calcium (Figure 3).[10-12]

The increase of intracellular calcium does not exclusively depend on the activation of glutamate receptors, but also in the stimulation of calcium voltage-dependent channels.

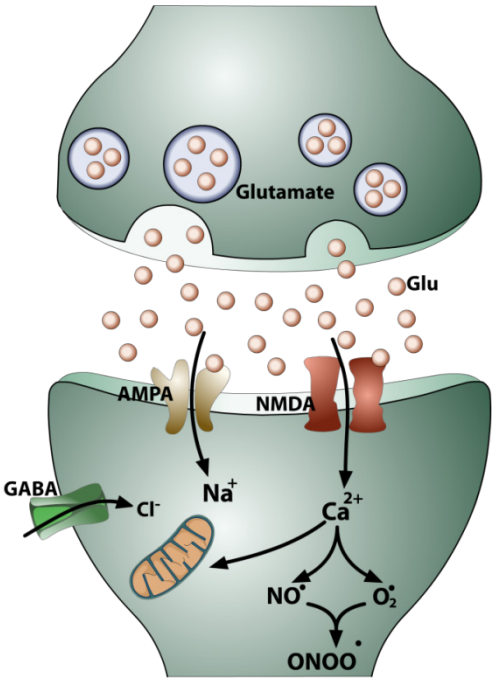

Figure 3. Role of glutamate on the stimulation of AMPA and NMDA receptors.

Hyperexcitability causes a depolarization phenomenon in the periphery of the infarct, which increases the energetic cost while the membrane tries to re-polarize itself.[6, 13-14] Calcium increment, together with acidosis and peri-infarct depolarization, contribute to initiate the damage. Later, inflammation and activation of apoptotic phenomena contribute to increase the lesion.[12, 15] During ischemia, and particularly during reperfusion, free radicals are generated. These are highly reactive species produced at both the initial and late stages of brain ischemia, via different physiopathological mechanisms. In first place, oxygen reactive species are produced by the metabolism of arachidonic acid and the activity of neuronal NO (Nitric Oxide) synthase (nNOS).

During intermediate stages, free oxygen radicals are provided by the infiltration of neutrophils in the ischemic area. At later stages, they are produced via the synthesis and activation of inducible NO synthase enzymes (iNOS) and cycloxigenase-2

(COX-2).[16-17] Ischemic stroke triggers a series of complex molecular events, among which activation and expression of genes are included. Some of those events arise from the immediate reaction of neurons to damage,[18] and others are associated to cellular processes that determine the near fate of the affected neurons,[19] or coordinate the repair mechanisms of tissues.[20-21]

Ischemic cellular death can take place in two different ways. The most common one is necrosis,[22] which is the result of the acute energetic failure, and it is characterized by a loss of morphology and, in the end, cellular lysis, which also triggers inflammatory processes.[23] On the other hand, apoptotic or programmed cell death can be observed when energy-dependent intracellular mechanisms are activated, leading to a regulated cell degradation. Cell debris are later removed by phagocytic cells without inflammatory reaction.[15, 24]

1.1.3. Therapeutic approaches for the treatment of stroke

1.1.3.1. Thrombolysis and neuro-interventionism

Pharmacological or mechanical (thrombectomy) thrombolysis is the strategy that reports higher benefits for the patient, in terms of neurological outcome. The most common thrombolytic agent is the recombinant tissue plasminogen activator or rt-PA. Both therapies have pushed for the creation of stroke units inside hospitals, which in turn have improved the management of stroke patients. Nevertheless only 3-7% of stroke patients are currently treated by these procedures. Such reduced numbers may be due to different factors, including the narrow therapeutic window and the high risks associated with the treatment. Current neuroprotective strategies are aimed at both widening the therapeutic window, and the risk factors associated to therapy.[25-28]

The therapeutic window associated with intravenous thrombolytic treatment is 4.5 hours. The extension of this window may be possible by selecting candidate patients with a large "penumbral area" (the area of the brain susceptible to damage unless otherwise protected within the first 24-48 hours). There have been several approaches to identify the ischemic penumbra, based on neuroimaging criteria such as the DWI/PWI mismatch[29] or the so-called Clinical/DWI uncoupling.[30]

An early treatment with anti-excitatory drugs or induction of hypothermia could also help to maintain the penumbra for extended periods of time, hence prolonging the therapeutic window for reperfusion. However, these approaches have only been successfully applied on experimental studies, so far.

Reperfusion is associated with a higher rate of hemorrhagic events. Therefore the maintenance of the blood-brain barrier integrity (i.e. with metalloproteinase inhibitors), fluid homeostasis (by regulating aquaporin and inhibiting endothellin) and disabling free radicals after a reperfusion treatment, will also turn out to be viable neuroprotective strategies during the acute phase of a stroke.[31]

1.1.3.2. Neuroprotection

Neuroprotection is a term that conglomerates a variety of strategies aimed at reducing cell death after an ischemic event, without disturbing tissue reperfusion. So far, a plethora of compounds have been proposed to block the pathway leading to ischemia-induced cell death at different steps. Most of these compounds have shown positive effects in experimental studies, tough none of them have shown a clear beneficial effect in clinical studies.[32-33] Neuroprotective drugs can be classified into seven different groups, regarding their action mechanism.

Calcium blockers

Calcium plays an important role in stroke pathophysiology. The blockage of calcium channels stops neuronal Ca^{2+} intake,

hence reducing cell death. Nimodipine is an example of this family of compounds. With more than 200 published experimental studies, only half of them proved the efficacy of the drug. None of the members of this family of compounds have proved a clear neuroprotective activity on clinical studies.[34-36] Among the reasons for this fact, it could be mentioned that on the studies that generated positive results, animals were mostly treated within the first 15 minutes post-ischemia, which is not translatable to the clinical settings.

Glutamate antagonists

Glutamate is the main excitatory amino acid in the central nervous system. After an ischemic event, an excitotoxic response is generated leading to cell death. Glutamate activates NMDA and AMPA receptors. NMDA receptors mediate cellular calcium and sodium intake. Several non-competitive blocking drugs against NMDA receptors have been synthesized, such as MK-801 (dizocilpine). Used as a neuroprotective compound, MK-801 rendered positive results in animal models of stroke. Nevertheless, the subsequent clinical trial had to be stopped due to adverse effects.[37]

NMDA competitive antagonist drugs have been also synthesized and used in animal models of stroke, like CGS 19755 (selfotel) and GV15526 (gavestinel). Though both compounds produced encouraging results in experimental studies, but they showed no effect in clinical trials.

Natural NMDA antagonists, such as magnesium, have also been used as neuroprotective compounds. Magnesium sulphate has showed a brain infarct reduction up to 60% in animal models, treated even 6 hours after ischemia onset. Once again, this results could not been translated to the clinics, since it showed no effect in clinical trials.[38]

As for NMDA, AMPA receptors have also been targeted for neuroprotective strategies. AMPA antagonists like ZK200755 have

shown moderate neuroprotective effects in animal models. Results of its clinical trials have never been published.[31, 34, 39]

Plasmatic glutamate scavengers

Under normal physiologic conditions, glutamate present at the synaptic junction is captured by neurons and astrocytes through specific excitatory amino-acid transporters (EAATs). Nonetheless, under ischemic conditions these transporters do not function properly, leading to the accumulation of glutamate in the extracellular space.

EAATs are also present at the luminal side of endothelial cells in brain capillaries, and facilitate the passing of glutamate from the brain to blood. In this sense, it has been recently published that the increase of glutamate gradients between brain and blood facilitates the dumping of glutamate from the extracellular space to circulating blood, offering in this way an alternative strategy to protect brain cells during ischemia. Those strategies are based on metabolizing plasmatic glutamate by the action of the resident enzyme glutamate-oxaloacetate transaminase (GOT), with or without the complementary addition of oxaloacetate, the glutamate co-substrate on the reaction catalyzed by GOT. This neuroprotective strategy has been successfully tested on animal models by our research group, leading to a significant reduction on brain infarct volume on animal models of stroke. In parallel, an association between elevated levels of GOT on blood and good outcome following stroke has been found in two clinical retrospective studies, pointing to the potential translationality of this neuroprotective strategy to the clinical setting.[40-42]

Antioxidants

Oxidative stress is another mechanism implicated on cell death after an ischemic event. Antioxidants could therefore play a role as neuroprotective drugs. The most successful antioxidant tested has been NXY-059. This drug reduced brain infarct by 66% in animal models, when injected 5 hours after occlusion. The first

clinical trial generated positive results, improving patient's functional outcome. However a second clinical trial was negative. A possible explanation of this discrepancy could be the low efficacy this drug has to get across the BBB, which may affect the bioavailability of the drug to the brain, depending on the administration characteristics.[43-45]

Phospholipid precursors: citicoline

Citicoline or CDP-choline is a precursor on the synthesis of phosphate-choline, which is integrated in the membrane of neurons. It has been shown that citicoline inhibits norepinephrine and dopamine levels on the CNS, and restores mitochondrial ATPase activity.

On animal models citicoline lowered phospholipase 2 activation after brain ischemia, reducing arachidonic acid formation and hence the production of free radicals; therefore inhibiting oxidative stress. Another effects claimed for this drug are its capacity to reduce excitotoxicity and the stimulation of brain plasticity.[46]

In preclinical studies, the treatment with citicoline immediately after reperfusion led to an improvement on functional deficits after a period of 28 days. A pool-data analysis published in 2002 showed a 33% increment in complete recovery after mild or severe stroke (NIHSS≥ 8) when the treatment was started within the first 24 hours and maintained for 6 weeks thereafter.[32, 47-49]

Nitric oxide pathway transduction regulators

One example of this kind of drugs would be lubezol, a compound capable of deregulate the glutamate-induced nitric oxide synthase pathway. This compound has shown hippocampal neuroprotection from nitric oxide toxicity. In experimental studies it has shown a 50 % infarct volume reduction upon injecting the drug 3 hours after ischemia induction. Nevertheless no clinical trial rendered positive results, having one of them to be stopped due to an increase in the treatment group mortality.[37]

Other compounds

Several studies have been performed using other neuroprotective agents such as leukocyte inhibitors (enlimomab), neuronal potassium channel activators (BMS-204352), membrane fluidity modifiers (piracetam), opioid antagonists (namefene), growth factors employed as intracellular calcium regulators (FGF), and much more. None of them have shown the definitive efficacy of pharmacological neuroprotection.[37]

1.1.3.3. Neurorepair

Neurorepair strategies involve the restoration of brain function, either by regeneration of damaged cerebral tissue (neurogereneration) or by the establishment of alternative neuronal pathways to carry out the altered function (brain plasticity). These processes work at a long term, hence the therapeutic window for these approaches are more relaxed than those needed for thrombolytic or neuroprotective therapies. Preclinical data show that functional recovery improved upon using neuroreparative approaches that start more than 24 hours after the onset of symptoms. The group of therapies aimed at recovering the neurological function after stroke is diverse, and not restricted to neurons, since the repair of the neurovascular unit includes also procedures aimed at the enhancing of angiogenesis and synaptogenesis. Thus, neurorepair treatments may include intracerebral or systemic use of stem cells, pro-neurogenic, pro-angioigenic and/or pro-synaptogenic drug injection.

Neurogenesis after brain ischemia

In the adult brain there are niches for the production of neural stem cells, localized in the subventricular region of the lateral ventricles (SVZ) and the dentate gyrus of the hippocampus. Under normal physiological conditions, the neuroblasts produced in the SVZ migrate to the olfactory bulb to

differentiate in new neurons. It has been shown that following focal brain ischemia in the rat, an increase in neuroblast formation occurs in the ipsilateral hemisphere, and that these neuroblasts migrate to regions surrounding the lesion.[50] This effect has been also shown in humans (figure 4).[51] The enhancement of natural occurring endogenous neurorepair mechanisms is a promising trend on stroke treatment.

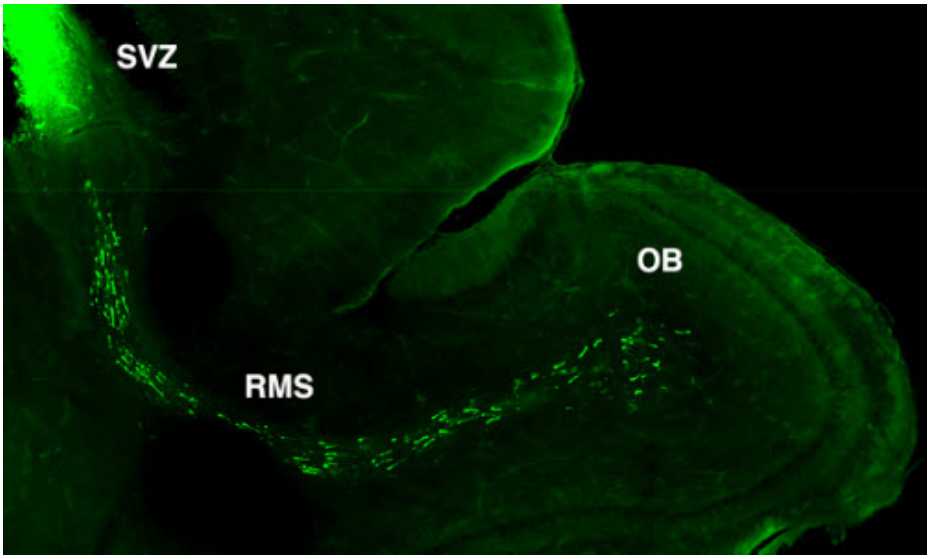

Figure 4. Progenitor stem cells recruited to an ischemic lesion from the subventricular zone. SVZ, subventricular zone; RMS, rostral migratory stream; OB, olfactory bulb (from Oudin et al.[52])

After an ischemic event, adult progenitor stem cells seem to recover embryonic signals, which lead them to proliferate and eventually differentiate into neurons, which get integrated into pre-existing neural circuits. It has been shown that when the subventricular zone is damaged by ionizing radiation, animals suffering from an ischemic lesion suffer from more severe neurological deficits, as compared to non-radiated.

Even though newborn cells are recruited after an ischemic insult, most of them do not get integrated into neuronal circuits, for several reasons, like the highly inflammatory environment at the

lesion site. Recently, several strategies have been employed to enhance endogenous neurogenesis. Thus, a greater number of newly differentiated neurons may be available, which should increase the chance of these neurons to survive and integrate in neuronal networks, therefore improving functional recovery. Both cellular and pharmacological therapies have been used to achieve this goal. All of them have in common the activation of the phosphatidylinositol-3-kinase (PI3-Akt) pathway. This pathway is involved in cell survival, proliferation, differentiation and migration.[53] Treatment with mesenchymal stem cells stimulate parenchymal cells to produce neurotrophic factors, such as brain derived neurotrophic factor (BDNF), which in turn activate the Akt pathway. Meanwhile, systemic erythropoietin also activates Akt, increasing neurogenesis.[54-55]

Angiogenesis after brain ischemia

Development of the cerebral vascular system occurs mainly due to angiogenic processes. During adult life however, endothelial cell proliferation ceases under normal physiological conditions. Nonetheless, upon an ischemic event brain capillaries surrounding the lesion proliferate, and new vessels are formed between 2 and 28 days after the onset of stroke. During their early stages, newly created vessels are highly permeable wearing off this phenomenon as maturation takes place.[56-59]

The angiogenic process involves a multi-step procedure that comprises endothelial cell proliferation and migration, tubule formation, branching and anastomosis. Vascular endothelial growth factor (VEGF) and its receptor (VEGFR2) initiate the angiogenic process, being angiopoietin 1 and 2 and their receptor (TIE-2) responsible for the maturation, stabilization and vascular remodeling.[60] As mentioned above, overexpression of all the angiogenic elements remains for at least 28 days, inside the rodent ischemic brain tissue. VEGF and VEGF2 overexpression promotes vascular ramification, being the newly formed vessels highly permeable. Meanwhile angiopoietins and TIE2 overexpression stimulate vessel maturation leading to the formation of fully functional brain blood vessels. VEGF treatment

as well as any therapy aimed at producing VEGF, VEGF2, angiopoietin or TIE2 overexpression increases angiogenesis in the peri-infarct region. Mesenchymal stem cell treatment, for example, induces VEGF, angiopoietin 1 and Tie2 overexpression, leading to an increase in agiogenesis.[60]

The angiogenic process is essential for brain recovery after cerebral ischemia. Without restoring the blood flow very it is highly unlikely that recovery can occur at the peri-infarct region. A correlation between the number of blood vessels in the periphery of the lesion and patient survival has been shown, in clinical studies.[37] In experimental studies both cellular and pharmacological therapies have been used to increase angiogenesis, producing an increment in the functional recovery of ischemic animals.[61]

Neurogenesis & angiogenesis

Neurogenic and angiogenic processes after cerebral ischemia are not isolated but rather closely intermingled. Neurogenesis in the peri-infarct region cannot occur without angiogenesis, since the latter is responsible for restoring the oxygen and nutrient supply to newly formed neurons. Furthermore, endothelial cells produce growth factors that allow the neurons to survive, and that regulate metabolic activity of neural precursors. Endothelial cells secrete stromal cell-derived factor-1 (SDF-1), VEGF and matrix metalloproteinases (MMPs) that induce and facilitate neural progenitor cell migration to the infarct surrounding tissue. On the other hand, neural progenitor cells overexpress angiopoietin 2 and VEGFR2 leading to an increase in angiogenesis.[62]

Several *in vitro* and *in vivo* studies corroborate the relationship between angiogenesis and neurogenesis.[63-64] *In vitro* neural progenitor cells stimulate tubule formation resembling capillaries. In animal models of ischemia Tie2 inhibitors not only reduce angiogenesis, but also neuroblast migration to the peri-infarct area. On the other hand, neural progenitor cell grafting in the infarct region induced angiogenesis. Therefore neurogenesis

and angiogenesis seem to be highly related, and both working together promote neural remodeling and improve neurologic function after brain ischemia.[65-66]

The role of oligodendrocytes, astrocytes and axons in neurorepair

In the brain parenchyma there are not only neurons, but other cellular components as well. Oligodendrocytes, astrocytes and the development of fully functional axons by neurons are also involved on neurorepair. Following stroke, axon growth by neurons is highly impaired. Also astrocytes proliferate forming a glial scar that surrounds the lesion. Astrocytes release proteoglycans that inhibit axonal growth. Hence there should be mechanisms aimed at reducing glial scar formation, to stimulate axonal growth for an efficient neurorepair.[67]

Treatment with mesenchymal stem cell (MSC) induces an increase in axonal density surrounding the ischemic lesion. Such increment can be appreciated at least for a year after the treatment. MSCs reduce the release of axonal growth inhibitory proteins, allowing for axonal growth and neurite formation.[67]

Mature oligodendrocytes are responsible for the myelin sheath that covers the neuron's axon, allowing it to perform properly. These oligodendrocytes come from non-myelinating oligodendrocytes located at the corpus callosum, the striatum and the subventricular zone, in the adult brain. Mesenchymal stem cell transplants increases oligodendrocyte progenitors in the ischemic hemisphere, as well as the overall number of mature oligodendrocytes in the peri-infarct region. EPO or sildenafil treatment after ischemia increases the number of myelinated axons in the tissue surrounding the lesion. Hence cellular or pharmacological therapies can be used to promote oligodendrocyte proliferation and axonal regeneration.[67]

Stem cells and neurorepair

The main goal of neurorepair is the restoration of brain tissue lost after an ischemic event. Using stem cells to substitute the

damaged tissue could look like an obvious approach, but this would imply stem cells to remain immature for a determined period of time, to later differentiate into neurons, glial cells and endothelial cells. Furthermore, newly formed tissue should be functional, and replace the loss of function caused by the lesion. However, it may be also possible that grafted cells do not repair damaged tissues by themselves, but release trophic factors instead, allowing neural survival in the ischemic penumbra, or enhance endogenous neurogenesis and angiogenesis.[68-69]

Stem cells are capable of differentiate into multiple tissues as well as proliferate indefinitely. These cells can be; 1) totipotent, meaning capable to differentiate into every kind of tissue both embryonic as well as extra-embryonic, 2) pluripotent, which differentiate into every type of embryonic tissue, or 3) multipotent cells, capable to differentiate into every type of cell that forms a specific tissue.

The most potent stem cells are embryonic stem cells, which are capable to differentiate into every kind of cell that composes the body, including neurons. In mice studies, embryonic stem cells transplanted to the brain were able to graft, differentiate into neurons and glial cells, and integrate themselves in the surrounding neural circuits. Unfortunately, these cells have the capacity to form teratomas.[70-71] This capacity gets reduced as cells differentiate into neural cells, hence there are techniques being developed that would allow for this to happen.[72-73] The heterogeneous cell population obtained by these methods is a drawback for its application, since some cells are left undifferentiated, becoming a potential source for teratomas.

Teratocarcinogeneous cells have also been used, since they are immortalized cells that can be differentiated to neurons upon treatment with retinoic acid. In preclinical studies these cells have shown the capacity to integrate in the brain.[37]

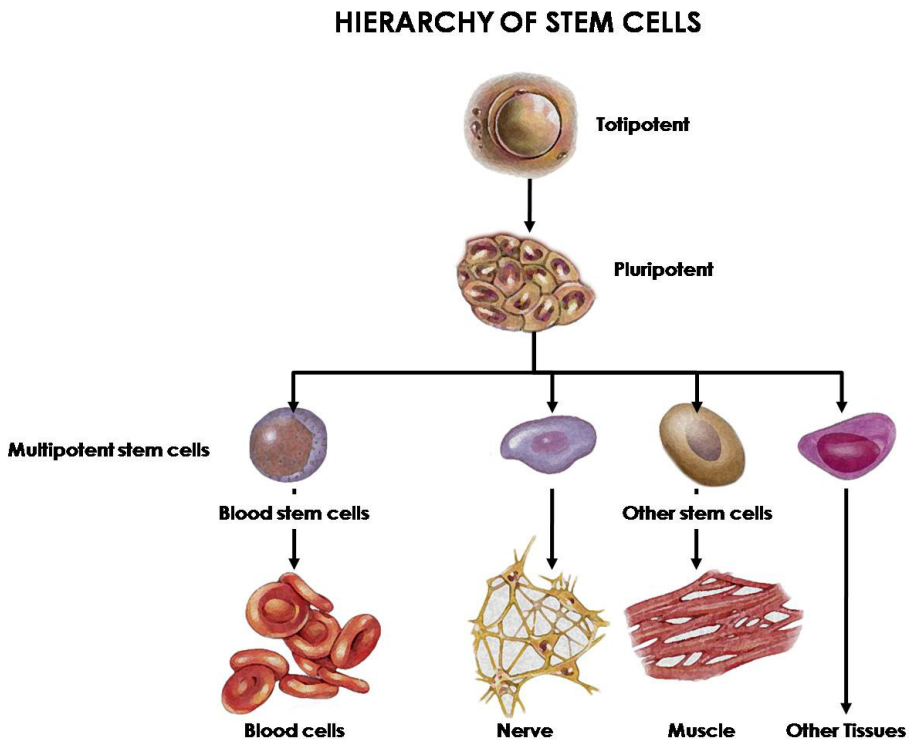

Figure 5. Different types of stem cells and their relationship.

Bone marrow stem cells and umbilical cord blood derived stem cells are the most widely used stem cells. Both are comprised multipotent stem cells. Intravenous injection of these cells reduced infarct volume as well as improved neurological outcome in animal models of stroke.[67] Furthermore, both *in vitro* and *in vivo* studies have shown that these cells have the capacity to differentiate into neurons.[67] Besides systemic injection, multipotent stem cell production can be stimulated by pharmacological means such as the treatment with the granulocyte colony stimulating factor (G-CSF).[74]

1.2. THE PERI-INFARCT REGION

The introduction of the concept of ischemic penumbra by Astrup,[7] and its subsequent development, has been the key for a

change in the consideration of ischemic stroke from a "preventable catastrophe" to a "treatable disease." The "time is brain" aphorism, and the consideration that stroke is a neurological emergency, as a result of the ischemic penumbra concept, has allowed patients to profit from quick treatment by trained medical staff and transfer to specialized stroke units. The penumbra is classically defined as the hypoperfused tissue surrounding the ischemic core, in which blood flow is too low to maintain electric activity but sufficient to preserve ion channels. However, this area is subjected to a wave of deleterious metabolic processes propagated from the core to the neighboring tissue, including excitotoxicity, spreading depression, oxidative stress, and inflammatory response, which lead to the expansion of the ischemic core and the subsequent worsening clinical outcome.

The most relevant definition of ischemic penumbra for clinical practice is based on neuroimaging techniques. It is widely accepted that brain tissue with reduced blood perfusion, as seen in MR perfusion-weighted imaging (PWI) but not included into the lesion core, as seen in MR diffusion weighted imaging (DWI), indicates potentially salvageable tissue. Thus, the combination of PWI and DWI images has led to the PWI/DWI mismatch concept.[75] Although it is generally accepted that hyperintense signal on DWI represents the lesion core, quantitative measurements of apparent diffusion coefficients (ADC) reveal that during ischemia, ADC values decline before energy metabolism fails, indicating that the increase in DWI signal intensity is not restricted to the infarct core.[75] Therefore, the discrimination between penumbra and infarct core by DWI is not always clear, because DWI signal increases in both sites.[76] In addition, PWI-detectable flow decreases are pathophysiologically relevant only when they interfere with adequate oxygen supply to the tissue. Thus, the PWI/DWI mismatch includes not only the penumbra periphery, but also surrounding intact tissue.[75] Nowadays, neuroscientists are able to delineate the ischemic penumbra using alternatives to this hemodynamic concept. Among others, tissue hypoxia can be

determined by MR spectroscopy, anoxic depolarization depicted by manganese enhanced MRI, tissue acidosis shown by pH-weighted MRI, and others. However, none of these methodologies is able to provide clear-cut threshold values to differentiate among ischemic core, penumbra, and surrounding intact brain tissue by themselves, and a multimodality approach is generally recommended.[75-76] Most of these MRI-based methods are unfortunately restricted to experimental models and state-of-the-art brain imaging systems, and must be fully validated for the human brain before they can be translated into clinical practice.[77]

Although the definition of the penumbra by imaging techniques is currently of great value, in clinical terms, an alternative definition of "tissue-at-risk", that is generally called peri-infarct region, may be more suitable, from a strategic point of view for the development of new therapeutic approaches on stroke. The peri-infarct region is therefore defined as a "no men's land" between the infarct core, with a front of toxic mediators of damage spreading out from it, and the healthy tissue, from where tissue's healing and repair mediators are trying to access to the affected but still viable tissue (figure 6). It is clear that the peri-infarct definition and spatiotemporal dynamics do not necessarily match the specifications of the ischemic penumbra.

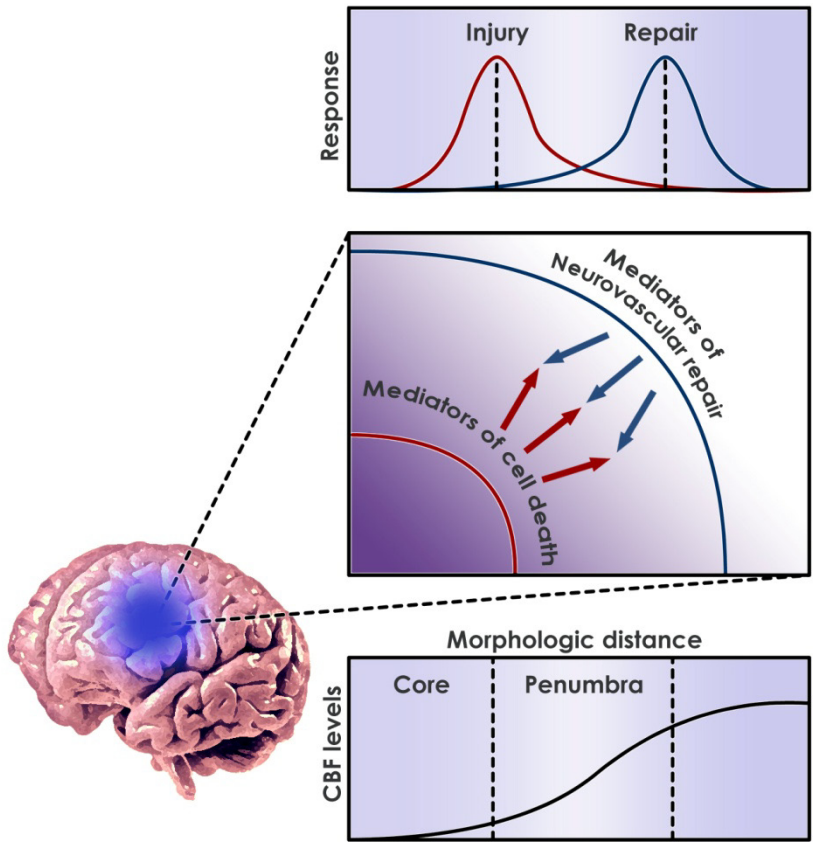

Figure 6. Peri-infarct region, defined as the battlefield between mediators of damage, from the infarct core, and mediators of healing and repair, form normal tissue. (Taken from Lo et al.[78])

1.2.1. New targets in ischemic stroke

A definition of "tissue-at-risk" alternative to the ischemic penumbra must take two main aspects in consideration. The first one is the fact that the real limits of affected tissue are not well delineated by the DWI-PWI mismatch, as mentioned above. A second, and more important aspect, is the fast caducity of the penumbra with time. The ischemic penumbra disappears a few hours after the onset of stroke, either because it is incorporated into the ischemic core, or because perfusion is restored in, at least, part of this territory. However, the normalization of

perfusion does not warranty delayed damage to the affected tissue, by mechanisms like cellular apoptosis. Therefore, progressing damage on the affected tissue, that last for days after normal perfusion restoration remains unveiled for conventional neuroimaging techniques.

Alternatively to the use of neuroimaging, one could consider the identification of the peri-infarct tissue based on molecular markers of the cascade of molecular events that take place at the peri-infarct tissue.[77]

The main factor responsible for the extension of the ischemic damage is, as discussed before, the fact that a decrease in cerebral blood flow yields reduced adenosine 5-triphosphate and failure of Na/K pumps, increasing extracellular glutamate and activating glutamate-mediated channels (N-methyl-D-aspartate and 2-amino-3-hydroxy-5-methyl-4-isoxazolepropionic acid), ending in an increase of intracellular calcium.[79] Intracellular calcium participates in the formation of free radicals through the activation of nitric oxide synthase, which promotes nitric oxide formation and the subsequent synthesis of the highly toxic peroxynitrite radicals.[80] Thus, the spread of glutamate from the ischemic core to its periphery is a mechanism that induces irreversible damage to tissue. Glutamate acts as a mediator of peri-infarct depolarizations, or spreading depression, which originates a marked disruption of ionic homeostasis and causes acidosis and increases energy demand and neurotransmitter effluxes, all starting from the core and propagating through its periphery to increase infarct volume.[81-82]

Deleterious processes propagating from the core to the peri-infarct tissue can induce additional mechanisms of damage, which include oxidative stress, nitric oxide overproduction, release of inflammatory cytokines (e.g. tumor necrosis factor- and interleukin-6), expression of adhesion molecules (e.g. intercellular molecule adhesion-1 and vascular cellular adhesion molecule), and production of matrix metalloproteinases.[83] Protein synthesis and apoptosis are also considered active processes on the peri-infarct core.

A reduction on protein synthesis is one of the earliest and most sensitive metabolic consequences of ischemia,[84] and stress proteins such as heat shock protein 70 are upregulated.[83] Correlations have been found between regions of expression of heat shock proteins and the peri-infarct tissue, although this is considered as the region of suppressed synthesis of proteins with preservation of adenosine 5-triphosphate levels.[85] Apoptosis also contributes to the recruitment of peri-infarct tissue to the core of the lesion. In fact, apoptosis is considered the prototypical form of cell death in the peri-infarct tissue.

Any of the aforementioned mechanisms involve multiple molecular markers that could be used for the definition of a peri-infarct region, and should be explored to see which one could better delineate the spatiotemporal dynamics of the so-called "tissue-at-risk", "salvable tissue" or "peri-infarct tissue", which should become the real target for stroke treatment.

1.3 THERANOSTICS

1.3.1. Introduction

The term "theranostics" refers the combination of the dual role of diagnostics and therapeutics on a single action. The term was first coined about a decade ago and was used to describe diagnostic tests developed to guide personalized therapies.[86]

Definitions and strategies used in theranostics do match most of the objectives of the definition of the peri-infarct region. In theranostics, an specific organ, tissue or group of cells (a tumor, for example) are selected as target, then a search for molecular markers that specifically characterize such target is performed and, finally, molecular constructs with diagnostic and therapeutic capacities are build, to locate, delimitate and treat the target, leaving the rest of tissues unaffected. This is the principle of personalized medicine.

Numerous types of entities have been described in the literature, with the potential to be used as theranostic agents in targeted therapies in the body (small molecules, peptides, linear polymers, proteins, dendrimers, liposomes, nanoparticles, cells, etc.).[87-94]

In the following sections we review the concepts involved in theranostics, with the aim to set the basis of a novel concept on the definition of new targets (peri-infarct tissue) and therapeutic approaches (targeted interventions), for the treatment of stroke.

1.3.2. Molecular imaging for diagnosis

Molecular imaging (MI) is a term that describes the field that encompasses new and old imaging modalities that seeks to present patient-specific and disease-specific molecular and genetic information in conventional 2-dimensional and 3-dimensional anatomic imaging readouts. The foundations of MI are based on the fusion of a "promoter" agent that will be altered in a particular environment or disease state with an observable "reporter" agent that would register any change in the signal or contrast from the promoter. The most commonly used modalities in MI research have been optical-based near-infrared or visible light sensors, bioluminescence, cameras sensitive to the firefly luciferase-luciferin generation of green light, nuclear medicine (NM)-based single-photon and positron tomography, and most recently, magnetic resonance (MR).

Optical Imaging

Optical imaging techniques developed early for molecular and cellular biology use a wide variety of wavelengths. The noninvasive imaging *in vivo* with light photons has largely come from the advances in targeted bioluminescence probes, near-infrared fluorochromes, activated near-infrared fluorescence agents, and primarily from light emitted from the luciferase entity (reporter) in the presence of a substrate (luciferin).[95-96] Most fundamental to the widespread use of *in vivo* optical imaging of

stroke or ischemia in living subjects is the difficulty of detecting light from the brain, primarily because of the presence of the skull. Nonetheless, advances in the use of near-infrared for diagnosis have been made. Identifying hypoxic tissue has therapeutic implications for multiple disease states including stroke, where it allows us to determine the area of healthy tissue susceptible to develop into infarct. Tissue oxygenation can be measured directly using near-infrared oximetry to measure fractional oxygenation of Hb. This approach has been used intrasurgically in pigs to study regional myocardial oxygenation.[97-98] In a related method, sensors using quenching of the near-infrared fluorescent or phosphorescent lifetime of inorganic crystals by O_2 have been used for imaging PO_2 in cutaneous melanoma compared with adjacent skin that was clinically normal.[99] Also noninvasive early detection of brain edema has been accomplished in mice, using near-infrared light scattering.[100]

Nuclear Medicine Molecular Imaging

Nuclear medicine molecular imaging methods such as single photon emission CT and PET are much more relevant and indeed have been used for decades in stroke and neuronal applications such as brain mapping, blood flow mapping, metabolism, and so on. The advent of small single photon emission CT (micro single photon emission CT), PET (micro PET), and CT scanners has advanced NM methods for stroke research in the recent years. NM relies solely on the design and use of injected MI probes to provide the imaging signal contrast. The term "probe" is commonly used to refer to the tracer, beacon, smart probe, reporter agent, contrast agent, and/or nanoparticle used. The biggest advantages of NM PET aside from the near-picomolar probe sensitivity is that existing probes can be modified with a radiolabel while minimally perturbing the parent molecule, again indirectly related to the exquisite sensitivity of NM to the radiolabel.[101] Because NM relies on injected tracers, soft tissue contrast and resolution was poor. With the advent of PET/CT hybrids, however, 2-dimensional and

3-dimensional fusions provide both agent sensitivity and tissue contrast. The PET/CT hybrid is a potent methodology in stroke. Aside from the excellent usefulness of CT in stroke with hemorrhage detection, CT angiography, CT perfusion as well as xenon-enhanced CT, the PET/CT hybrid will allow for the addition of PET detection of receptor ligands, cerebral metabolism and blood flow, neuronal integrity as well as hypoxia and apoptosis markers.[97, 102-103]

Magnetic Resonance Imaging

MR contrast for molecular imaging in stroke research is derived from 4 major sources: endogenous contrast from the water proton dynamics in the microenvironment, endogenous chemical shifts of proton-bearing metabolites such as lactate, injection of exogenous contrast agents that report water proton changes, and from detection of heteronuclei.

MR has a high specificity and sensitivity to the water hydrogen proton. MR using other nuclei such as carbon-13 or fluorine-19 is much less efficient. This occurs because of the Boltzmann Distribution; that is, that at 1.5 Tesla, only approximately 5 to 10 protons per million ever contribute to the MR signal. New methods of dynamically increasing this inherently low signal magnetization by as much as 5 orders of magnitude are now available, termed "hyperpolarization".[97, 104-106] Using metabolically active carbon-13 labeled sugars, hyperpolarized MR could be routinely used in patients with stroke for mapping dynamic glucose consumption, pH, oxygen extraction, and blood flow all in one examination.

Mapping water proton dynamics in clinical stroke is the backbone of diffusion-weighted and perfusion-weighted imaging. Arterial spin-labeling of vascular flow protons can be clinically used to generate quantitative blood flow maps in a noninvasive manner.[107] Vascular-space-occupancy (VASO) MRI has been used recently to map the vascular space occupancy in the brain and can do so in 3-dimension and in near real-time.[108-109] This may prove ideal for mapping intracranial

pressures, sickle cell dynamics, vasospasm effects, and cerebral blood volume changes in neurovascular diseases.[110] Another noninvasive MRI method (CEST or chemical shift saturation transfer) exists for pH imaging, in this case amide–water proton exchange interactions are mapped, since each nucleic acid contains amide protons, it allows *in vivo* pH imaging.[111] This technique has been shown sensitive to ischemic tissue acidosis and may serve as a new surrogate metabolic imaging marker for stroke.[112-113] CEST has been shown to be more reliable identifying the penumbra region compared to PWI/DWI studies.[114]

MR spectroscopy is another modality of NMR that allows us to evaluate individual molecules; unfortunately this technique needs millimolar concentrations to produce reliable data. An approach to solve this issue comes from the exogenous contrast agent field. MR contrast agents generally differentiate into the T1-shortening and T2*-shortening applications.

T1 shortening has been largely the domain of gadolinium-chelated agents. The gadolinium chelates can be designed so they bind to various *in vivo* compounds (such as blood pool albumin or clot-rich fibrin), receptors, antibodies, and so on. Other designs provide specifically active gadolinium chelates that alter tertiary structure (and thus their proton relaxivity) in the presence of lactate, sugars, differing pH, calcium, and a host of other interesting agents.[115] However, the lowest concentrations of the gadolinium chelates needed is still in the micromolar range. Other T1-shortening agents are manganese ions, which are small enough to enter the neuronal white matter tracts through the eye (for example) and provide a trace of not only white matter integrity and structure, but also differences in tract activations.[116]

The use of T2*-shortening agents containing superparamagnetic iron particles can provide a larger contrast effect than corresponding concentrations of the T1-shortening gadoliniums. This has been widely used for *in vivo* cell tracking.[117-119] Iron nanoparticles can bind specifically over time (in lymph nodes for

example), hence iron receptor binding or collection in cells or clots could be used for clinical applications.[110] Because of the ultrasmall particle size, iron can be conveniently labeled to various *in vivo* receptors, agents, micelles, liposomes, nanotubes, and so on. In addition, iron nanoparticles can be easily dual- or triple-labeled for eventual PET/MR or optical/MR hybrid imaging. Nanoparticle structure can also be modified providing a multispectral effect of the particle, a chemical shift of sorts, caused by the microenvironment surrounding the particular nanocarrier used.[120] In this direction, the structure of the chelate around the gadolinium can have a profound effect on the local proton T1-shortening effect and has allowed the synthesis, for example, of lactate-sensitive contrast agents.[121-122] Nevertheless, these agents can operate down only to the micromolar range. Other lanthanide nuclei used as chemical shift agents such as europium have been found to have also effects over CEST. These so called paraCEST agents can lower the sensitivity to the nanomolar range.[123-124]

Hyperpolarization is another approach to molecular imaging that can rival paraCEST sensitivity. This technique increases nuclei magnetization 100000-fold providing a strong MR signal even with a single pulse. Metabolites such as piruvate or bicarbonate can be hyperpolarized, and serve as a tool to monitor the metabolism of such compounds *in vivo*.[110, 125]

The ability of imaging dynamic processes of apoptosis, hypoxia, ischemia, and in general, activation of genetic expressions such as the cascading changes in proteomics *in vivo* will reveal themselves as an essential tool for enhanced stroke diagnosis.

1.3.3. Drug delivery for treatment

Drug delivery to the brain has always been challenging due to the special condition of the cerebral tissue. The restricted access to the brain due to its innate physical and chemical properties has engendered a wide variety of strategies aimed at enhancing drug concentration in the brain.

In specific pathologies a specific area in the brain is affected. Targeting this specific area would improve outcome and reduce adverse side effects caused by the potential treatments.

Theranostics is a natural extension of Molecular imaging, considering that the very same molecules that are used as imaging probes for the imaging of targeted tissues can allocate different drugs within their structure, that perform after stabilization and transportation to the target site by the molecular probe, can be released there in a controlled fashion, performing an effective therapeutic effect, by concentrating the drug at the target site, and reducing (undesirable) secondary effects on healthy tissue.

The transport and controlled release of therapeutic drugs by molecular imaging probes, carrying out a theranostic effect in this way, is of special relevance when the target is within the brain parenchyma. The central nervous system (CNS) is highly protected in mammals, and it is very difficult to reach it by many substances that may be present on circulating blood, such is the case for systemically administered therapeutic drugs. Therefore it is important to learn about the barriers of the CNS and how to circumvent them, if one intends to deliver a theranostic agent that aims to target the peri-infarct region.

1.3.4. Barriers of the CNS

There are three barriers regulating the molecular exchange between the blood and neural, tissue or its fluid spaces:

- The blood brain barrier (BBB) which is formed by the interaction between glial cells and endothelial cells that separates blood and brain interstitial fluid (ISF).
- The choroid plexus epithelium between blood and ventricular cerebrospinal fluid (CSF).
- The arachnoid epithelium between blood and sub-arachnoid CSF.

Due to the limits imposed by these barriers, neurons are rarely located at more than 8–20 μm away from a brain capillary.[126] This structural configuration makes the BBB as the main barrier controlling the immediate microenvironment of brain cells.

The BBB is formed by a monolayer of endothelial cells, connected to each other by tight junctions, together with astrocyte end-feet processes, perivascular neurons and pericytes (figure 7). Both pericytes and endothelial cells are enclosed by the basal lamina. All the elements described above constitute the "neurovascular unit" (NVU).[127] The most important site of the BBB lies at the cerebral microvessels. Endothelial cells are very polarized, exhibiting very low pinocytic activity, they also possess a high number of mitochondria, needed for the multiple active transport mechanisms found in these cells.[128] The blood-brain barrier (BBB) provides protection to brain cells and preserves brain homeostasis.

Astrocytes that form the NVU are also responsible for the homeostasis and regulate the ion distribution in the brain,[129] but their end feet cover only partially the blood vessels. In contrast to endothelial cells and pericytes, astrocytes are not connected to other cells by tight junctions, and they do not have a common basal membrane. Therefore, polar molecules (such as proteins) can enter the interstitial liquid and be directly transported to the pericytes and the endothelial cells.[130]

1.3.5. Transport mechanisms across the BBB

The BBB is permeable to small and lipophilic molecules, but larger molecules are not transported across unless there is an active transport system available for them.[131] This is one of the main problems for the delivery of drugs to the brain. An additional problem is the very effective drug efflux systems (P-glycoprotein) existing on the cells, which pump the drug back out of them. We will review next the particularities of the transport of different sort of substances through the BBB.

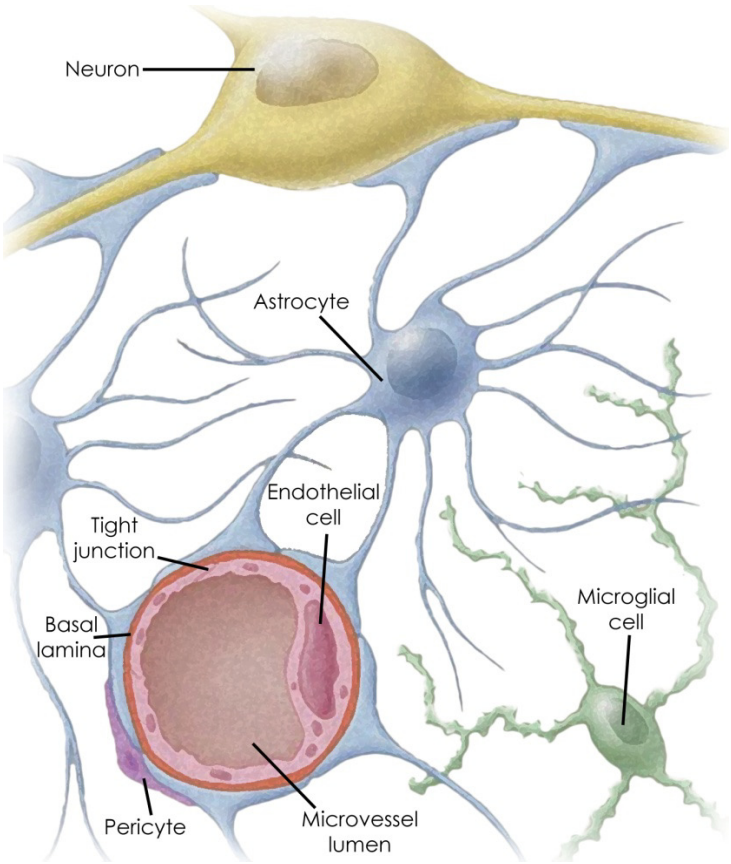

Figure 7. Barriers to the Central Nervous System.

Transport of ionic compounds

The monocarboxylic acid transporter (MCT) can move various anionic compounds across the BBB.[132-133] For example, MCT1 present in the BBB acts as a transport mechanism for lactic acid and other monocarboxylic compounds.[134] Cationic compounds can enter the brain either by passive diffusion or by carrier-mediated transport. This is the mechanism used by several drugs to cross the BBB.[135-140] Choline, an endogenous hydrophilic amine, has been demonstrated to be taken up by a carrier-mediated transport mechanism.[135-136, 139]

Transport of proteins

Peptides are usually large, hydrophilic, and unstable, hence efficient permeation into the brain generally does not occur for them.[141] However, certain small peptides are transported by carrier-mediated transport mechanisms, and others can cross the BBB by receptor-mediated or absorptive-mediated transcytosis.[142]

Absorptive-Mediated transcytosis

Absorptive-mediated transcytosis is triggered by electrostatic interactions between the positively charged moiety of the peptide and the negatively charged plasma membrane surface region.[143-146] This transport mechanism also functions in other tissues such as kidney and liver.[144]

Receptor-Mediated transcytosis

To get peptides to cross the BBB they need to be manipulated. Sometimes this is achieved by synthesis of chimeric peptides, formed by the covalent binding of the non-permeable but pharmacologically effective portion of the peptide to an appropriate vector that can be transported across the BBB.[144] In this case, the chimeric peptide is first transported into the brain endothelial cytoplasm by receptor-mediated or absorptive-mediated endocytosis. The intact chimeric peptide is then transferred into the brain's interstitial space by receptor-mediated exocytosis. Subsequently, the binding between the vector and the pharmacologically active peptide is cleaved and, finally, the released peptide exerts its pharmacological effect in the brain.[143-144, 147-148]

Efflux by P-Glycoprotein

Sometimes, drugs exhibit lower accumulation in the brain than would be expected from their lipophilic properties.[149-150] This phenomenon seems to be accompanied by overexpression of the transmembrane P-glycoprotein at the blood-brain barrier.[151-152] P-glycoprotein molecules are located at the luminal side of

the endothelial cells and their function is to serve as an energy dependent efflux pump, transporting drugs out of cells, and thus decreasing their accumulation in the cytoplasm. The consequence of this mechanism is the reduction of the efficiency of the drug.[151-153] P-glycoprotein has a very broad substrate specificity.[154-156]

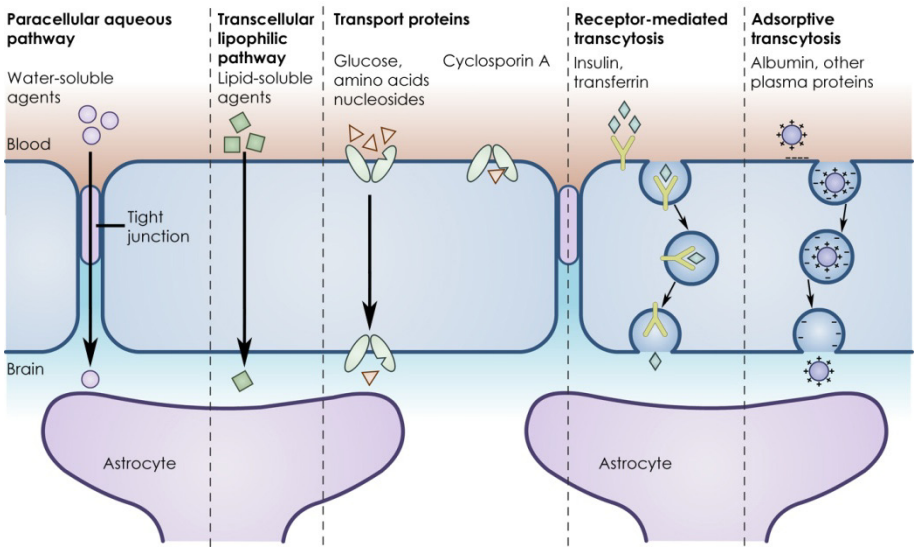

Figure 8. Transport mechanisms across the BBB.

Given the highly selective nature of the BBB, the question arises as how drugs that usually do not cross the BBB can still be delivered to the brain. An estimated 99% of all potential drugs are clinically useless because the BBB prevents them from getting into the brain.[142] Thus, finding ways to overcome the BBB are of great clinical significance.

1.3.6. Administration routes

Various strategies have been used for the delivery of drugs to the brain, including osmotic and chemical opening of the BBB, and the use of transport/carrier systems like liposomes and other nanoparticles, to bypass the BBB. Some routes of direct

administration to the brain are non-invasive, such as the intranasal route, whereas others involve the entry into the CNS by devices and needles such as in case of intra-thecal and intracerebro-ventricular delivery.[144] In the next section we discuss the main approaches to deliver drugs to the CNS.

Interstitial delivery

The most direct way of circumventing the BBB is to deliver drugs directly to the brain interstitium. By directing agents uniquely to an intracranial target, interstitial drug delivery can theoretically yield high CNS drug concentrations with minimal systemic exposure and toxicity. Furthermore, with this strategy, intracranial drug concentrations can be sustained, which is crucial in treatment with many chemotherapeutic agents.[157]

Several techniques have been developed for delivering drugs directly to the brain interstitium. One such methodology is the Ommaya reservoir or implantable pump as discussed earlier under intraventricular/intra-thecal route. This technique, however, does achieve truly continuous drug delivery. More recently, several implantable pumps have been developed that possess several advantages over the Ommaya reservoir. This can be implanted subcutaneously and refilled by subcutaneous injection and are capable of delivering drugs as a constant infusion over an extended period of time.[158] Furthermore, the rate of drug delivery can be varied using external handheld computer control units. Currently each of the three different pumps available for interstitial CNS drug delivery operates by a distinct mechanism. The Infusaid pump uses the vapor pressure of compressed Freon to deliver a drug solution at a constant rate; the MiniMed PIMS system uses a solenoid pumping mechanism, and the Medtronic SynchroMed system delivers drugs via a peristaltic mechanism. The distribution of small and large drug molecules in the brain can be enhanced by maintaining a pressure gradient during interstitial drug infusion to generate bulk fluid convection through the brain interstitium or by increasing the diffusion gradient by maximizing the concentration of the infused agent as a supplement to simple

diffusion. Another recent study shows that the epidural delivery of morphine encapsulated in multivesicular liposomes (Depo-Foam drug delivery system) produced a sustained clearance of morphine and a prolonged analgesia, and the results suggest that this delivery system is without significant pathological effects at the dose of 10mg/ml morphine after repeated epidural delivery in dogs.[159-162]

Intra-ventricular / Intra-thecal route

One strategy for bypassing the BBB that has been studied extensively both in laboratory and in clinical trials is the intralumbar injection or intreventricular infusion of drugs directly into the CSF. Drugs can be infused intraventricularly using an Ommaya reservoir, a plastic reservoir implanted subcutaneously in the scalp and connected to the ventricles within the brain via an outlet catheter. Drug solutions can be subcutaneously injected into the implanted reservoir and delivered to the ventricles by manual compression of the reservoir through the scalp.[163-164]

When compared to vascular drug delivery, intra-CSF drug administration theoretically has several advantages. Intra-CSF drug administration results in an immediate elevation in CSF drug concentrations. Since, the drug is somewhat contained within the CNS, a smaller dose can be used, potentially minimizing systemic toxicity. Furthermore, drugs in the CSF encounter minimized protein binding and decreased enzymatic activity relative to drugs in plasma, leading to longer drug half-life in the CSF. Finally, because the CSF freely exchanges molecules with the extracellular fluid of the brain parenchyma, delivering drugs into the CSF could theoretically result in therapeutic CNS drug concentrations.[165]

However, this delivery method has not lived up to its theoretical potential for several reasons. These include a slow rate of drug distribution within the CSF and increase in intracranial pressure associated with fluid injection or infusion into small ventricular volumes. It results in to high clinical incidence of hemorrhage,

CSF leaks, and neurotoxicity and CNS infections. The success of this approach is limited by the CSF-brain barrier, composed of barriers that limit drug diffusion into the brain parenchyma. Because the extracellular fluid space of the brain is extremely tortuous, drug diffusion through the brain parenchyma is very slow and inversely proportional to the molecular weight of the drug. For macromolecules, such as proteins, brain parenchymal concentrations following intra-CSF administration are essentially undetectable. For these reasons, intra-CSF chemotherapy in the treatment of intraparenchymal CNS tumors has not proven to be effective. The greatest utility of this delivery methodology has been in cases where high drug concentrations in the CSF and/or the immediately adjacent parenchyma are desired, such as in the treatment of carcinomatous meningitis or for spinal anesthesia/analgesia.[166]

Intra-thecal and intracerebral drug administration differs fundamentally from systemic drug administration in terms of pharmacokinetic characteristics determining brain tissue concentration, where the available dose reaching the target organ is 100%. However, there are large gradients inside the tissue with very high local concentrations at the site of administration (the ventricular surface or tissue site of injection) and zero concentration at some distance for macromolecules. Since, they have low diffusion coefficients, the gradients will be even steeper than what has been measured for small molecular weight drugs. After intracerebro-ventricular (icv) injection, the rate of elimination from the CNS compartment is dominated by cerebrospinal fluid dynamics. Clinical examples of intra-thecal small drug delivery are the icv administration of glycopeptide and aminoglycoside antibiotics in meningitis, the intraventricular treatment of meningeal metastasis, intra-thecal injection of baclofen for treatment of spasticity and the infusion of opioids for severe chronic pain.[167-168] These examples have in common the fact that the drug targets in all instances are close to the ventricular surface. Superficial targets may also be accessible for some macromolecular drugs.[169-170]

Olfactory Pathway

An alternative CNS drug delivery strategy that has received relatively little attention is the intranasal route. Drugs delivered intranasally are transported along olfactory sensory neurons to yield significant concentrations in the CSF and olfactory bulb. In recent studies, intranasal administration of wheat germ agglutinin horseradish peroxidase resulted in a mean olfactory bulb concentration in the nanomolar range. In theory, this strategy could be effective in the delivery of therapeutic proteins such as brain-delivered neurotrophic factor (BDNF) to the olfactory bulb as a treatment for Alzheimer's disease. The nasal drug delivery to the CNS is thought to involve either an intraneuronal or extraneuronal pathway. Recent evidence of direct nose-to-brain transport and direct access to CSF of three neuropeptides bypassing the bloodstream has been shown in human trials, despite the inherent difficulties in delivery.[171-172] The difficulties that have to be overcome include an enzymatically active, low pH nasal epithelium, the possibility of mucosal irritation or the possibility of large variability caused by nasal pathology, such as common cold. An obvious advantage of this method is that it is noninvasive relative to other strategies. In practice, however, further study is required to determine if therapeutic drug concentrations can be achieved following intranasal delivery.

Systemic route

Given the highly selective nature of the BBB, the question arises as to how drugs that usually do not cross the BBB can still be delivered to the brain. Because the BBB prevent the drugs getting into the brain, finding ways to overcome the BBB are of great clinical significance. The most favorable method to overcome this issue is to manipulate or "trick" the BBB, so that neurologically active compounds can be given systemically by oral, intramuscular, or intravenous application. Here, several different approaches are possible: osmotic opening of the BBB or pharmacologically by raising the lipophilicity of the drug using chimeric molecules or by attaching drugs to nanoparticles.[173]

1.3.7. Strategies for enhanced brain drug delivery

1.3.7.1. Drug manipulation

Lipophilic analogues

CNS penetration is favored by low molecular weight, lack of ionization at physiological pH, and lipophilicity. Delivery of poorly lipid-soluble compounds to the brain requires some way of getting past the BBB. There are several possible strategies, such as transient osmotic opening of the BBB, exploiting natural chemical transporters, high dose chemotherapy, or even biodegradable implants. But all of these methods have major limitations: they are invasive procedures, have toxic side effects and low efficiency, and are not sufficiently safe. A possible strategy is to smuggle compounds across as their lipophilic precursors. Because drug's lipophilicity correlates so strongly with cerebrovascular permeability, hydrophobic analogues of small hydrophilic drugs ought to more readily penetrate the BBB.[174] This strategy has been frequently employed, but the results have often been disappointing. Immunoliposomes (antibody-directed liposomes) have been recognized as a promising tool for the site-specific delivery of drugs and diagnostic agents. However, the *in vivo* use of classical immunoliposomes is hampered by the very rapid clearance of immunoliposomes from the circulation by the reticuloendothelial system.[175-176] Avoidance of this obstacle is possible if gangliosides[177] PEG-derivatized lipids[178] are inserted within the bilayer of conventional liposomes, as these modifications prolong considerably the liposome half-life in the circulation. Liposomes coated with the inert and biocompatible polymer PEG are widely used and are often referred to as "sterically stabilized" or "stealth liposomes".[179] PEG coating is believed to prevent recognition of liposomes by macrophages due to reduced binding of plasma proteins.[178, 180] Unfortunately, it has been difficult to combine steric stabilization of liposomes with efficient immunotargeting. PEG coating of liposomes can create steric hindrances for antibody-target interaction.[181-182] It

has therefore been proposed to attach a cell-specific ligand to the distal end of a few lipid-conjugated PEG molecules rather than conjugate the ligand to a lipid head-group on the surface of a PEG-conjugated liposome. This has been done with folic acid[183] and monoclonal antibodies[184-187] to target liposomes to cells in tissue culture and organs *in vivo*.

Prodrugs

Brain uptake of drugs can be improved via prodrug formation. Prodrugs are pharmacologically inactive compounds that result from transient chemical modifications of biologically active species. The chemical change is usually designed to improve some deficient physicochemical property, such as membrane permeability or water solubility. After administration, the prodrug, by virtue of its improved characteristics, is brought closer to the receptor site and is maintained there for longer periods of time. Here it gets converted to the active form, usually via a single activating step.[188] Unfortunately, simple prodrugs suffer from several important limitations. Going to extremes on the lipophilic precursor scale, a possible choice for CNS prodrugs is coupling the drug to a lipid moiety, such as fatty acid, glyceride or phospholipids. Such prodrug approaches were explored for a variety of acid-containing drugs, like levodopa, GABA, Niflumic acid, valproate or vigabatrin are coupled to diglycerides or modified diglycerides.[189] While increased lipophilicity may improve movement across the BBB, it also tends to increase uptake into other tissues, causing an increased tissue burden.

Chemical Drug Delivery

Chemical drug delivery systems (CDDS) represent novel and systematic ways of targeting active biological molecules to specific target sites or organs based on predictable enzymatic activation. They are inactive chemical derivatives of a drug obtained by one or more chemical modifications so that the newly attached moieties are monomolecular units (generally comparable in size to the original molecule) and provide a site-specific or site enhanced delivery of the drug through multi-step

enzymatic and/or chemical transformations.[190-192] During the chemical manipulations, two types of bio removable moieties are introduced to convert the drug into an inactive precursor form. A target or moiety is responsible for targeting, site-specificity, and lock-in, while modifier functions serve as lipophilizers, protect certain functions, or fine-tune the necessary molecular properties to prevent premature, unwanted metabolic conversions. The CDDS is designed to undergo sequential metabolic conversions, disengaging the modifier functions and finally the target or moiety, after this, fulfils its site- or organ-targeting role.

Carrier Mediated Drug Delivery

Carrier-mediated transport (CMT) and receptor-mediated transport (RMT) pathways are available for certain circulating nutrients or peptides. The availability of these endogenous CMT or RMT pathways means that portals of entry to the brain for circulating drugs are potentially available. In the brain capillary endothelial cells, which make up the BBB, there are several transport systems for nutrients and endogenous compounds. They are:

a) The hexose transport system for glucose and mannose.
b) The neutral amino acid transport system for phenylalanine, leucine and other neutral amino acids.
c) The acidic amino acid transport system for glutamate and aspartate.
d) The basic amino acid transport system for arginine and lysine.
e) The β-amino acid transport system for β-alanine and taurine.
f) The monocarboxylic acid transport system for lactate and short-chain fatty acids such as acetate and propionate.
g) The choline transport system for choline and thiamine.
h) The amine transport system for mepyramine.
i) The nucleoside transport system for purine bases such as adenine and guanine, but not pyrimidine bases.
j) The peptide transport system for small peptides such as encephalins, the thyrotropin releasing hormone, arginine, vasopressin, etc.[193-194]

Utilization of differences in the affinity and the maximal transport activity among these transport systems expressed at the BBB is an attractive strategy for controlling the delivery and retention of drugs into the brain.

Receptor/Vector Mediated Drug Delivery

Receptor-mediated drug delivery to the brain employs chimeric peptide technology, wherein a non-transportable drug is conjugated to a BBB transport vector. The latter is a modified protein or receptor-specific monoclonal antibody that undergoes receptor-mediated transcytosis through the BBB in-vivo. Conjugation of drug to transport vector is facilitated with chemical linkers, avidin-biotin technology, polyethylene glycol linkers, or liposomes. Multiple classes of therapeutics have been delivered to the brain with the chimeric peptide technology, including peptide-based pharmaceuticals, such as a vasoactive peptide analogs or neurotrophins such as brain-derived neurotrophic factor, anti-sense therapeutics including peptide nucleic acids (PNAs), and small molecules incorporated within liposomes. The attachment of the drug that normally does not undergo transport through the BBB to a BBB transport vector such as the mAb, results in the formation of a chimeric peptide, provided the bifunctionality of the conjugate is retained. That is, the chimeric peptide must have not only a BBB transport function, but also a pharmaceutical function derived from the attached drug. Certain drugs may not be pharmacologically active following attachment to a BBB transport vector. In this case, it may be desirable to attach the drug to the transport vector via a cleavable disulfide linkage that ensures the drug is still pharmacologically active following release from the transport vector owing to cleavage of the disulfide bond. Depending on the chemistry of the disulfide linker, a molecular adduct will remain attached to the drug following disulfide cleavage, and the molecular adduct must not interfere with drug binding to the drug receptor.[149-150, 195-196] A second consideration with respect to the use of a disulfide linker is that virtually all of the cell disulfide reducing activity may be

contained within the cytosol Therefore, the chimeric peptide must undergo endosomal release following receptor-mediated endocytosis into the target brain cell, in order to distribute to the reductase compartment.

1.3.7.2. Disrupting the Blood Brain Barrier

The second invasive strategy for enhanced CNS drug delivery involves the systemic administration of drugs in conjunction with transient BBB disruption (BBBD). Theoretically, with the BBB weakened, systemically administered drugs can undergo enhanced extravasations rates in the cerebral endothelium, leading to increased parenchymal drug concentrations. A variety of techniques that transiently disrupt the BBB have been investigated; however, albeit physiologically interesting, many are unacceptably toxic and therefore not clinically useful. These include the infusion of solvents such as dimethyl sulfoxide or ethanol and metals such as aluminum; X-irradiation; and the induction of pathological conditions including hypertension, hypercapnia, hypoxia or ischemia.[197] The mechanisms that are responsible for BBBD with some of these techniques are not well understood.

Osmotic disruption

Osmotic opening of the BBB was developed. Intracarotid injection of an inert hypertonic solution such as mannitol or arabinose has been employed to initiate endothelial cell shrinkage and opening of BBB tight junctions for a period of a few hours, and this permits delivery of antineoplasic agents to the brain. Though this treatment is still investigational, the fact that some patients who fail systemic chemotherapy have responded to similar or lower doses of intracarotid drugs is an often-cited argument in favor of the method. One reason for the unfavorable toxic/therapeutic ratio often observed with the hyperosmotic BBBD is that this methodology results in only a 25% increase in the permeability of the tumor microvasculature, in contrast to a 10-fold increase in the permeability of normal brain

endothelium.[198] Osmotic disruption of the BBB has also been suggested as a delivery strategy for recombinant adenoviral vectors for gene transfer to intracerebral tumors, and for magnetic resonance imaging agents for diagnosis of brain metastases using iron oxide conjugates, but there are problems which must be overcome before the routine clinical use of this technique can be realized. Osmotic disruption seems to be most successful in treating primary non-AIDS CNS lymphoma. The risk factors include the passage of plasma proteins, the altered glucose uptake, and the expression of heat shock proteins, microembolism or abnormal neuronal function.

Biochemical Disruption

Recently, new and potentially safer biochemical techniques have been developed to disrupt the BBB. Selective opening of brain tumor capillaries (the blood–tumor barrier), by the intracarotid infusion of leukotriene C4 was achieved without concomitant alteration of the adjacent BBB. In contrast to osmotic disruption methods, biochemical opening utilizes the novel observation that normal brain capillaries appear to be unaffected when vasoactive leukotriene treatments are used to increase their permeability. However, brain tumor capillaries or injured brain capillaries appear to be sensitive to treatment with vasoactive leukotrienes, and the permeation is dependent on molecular size.[199]

1.3.7.3. Drug Delivery from Biological Tissues

Another strategy to achieve interstitial drug delivery involves releasing drugs from biological tissues. The simpler approach to this technique is to implant into the brain a tissue that naturally secretes a desired therapeutic agent. This approach has been most extensively applied to the treatment of Parkinson's disease. Transplanted tissue often did not survive owing to a lack of neovascular innervation. Recently the enhanced vascularization and microvascular permeability in cell-suspension embryonic neural grafts relative to solid grafts has been demonstrated.[200-201]

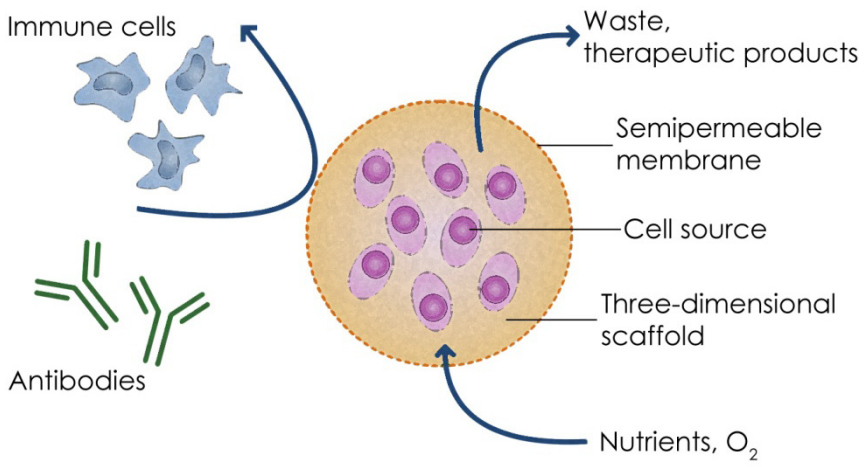

Figure 9. Drug Delivery from Biological Tissues. The model of cell encapsulation depicted above consists of enclosing cells within a three-dimensional polymer scaffold surrounded by a semipermeable membrane that is designed to circumvent immune rejection. The capsule membrane allows the bi-directional diffusion of nutrients, oxygen and waste, and the secretion of the therapeutic product from the encapsulated cells, but prevents immune cells and antibodies, which might destroy the enclosed cells, from entering the capsule. (Adapted from Orive et al.)[202]

An alternative extension of this method is to use gene therapy to develop optimized biological tissue for interstitial drug delivery. Prior to implantation, cells can be genetically modified to synthesize and release specific therapeutic agents. The therapeutic potential of this technique in the treatment of brain tumor was demonstrated. The use of non-neuronal cells for therapeutic protein delivery to the CNS has recently been reviewed. The survival of foreign tissue grafts may be improved by advancements in techniques for culturing distinct cell types. Co-grafted cells engineered to release neurotrophic factors with cells engineered to release therapeutic proteins may enhance the survival and development of foreign tissue. Ideally it would be possible to perform in-vivo genetic engineering to cause specific endogenous brain tissue to express a desired protein, circumventing the ischemic and immunogenic complications encountered with the implantation of foreign tissue grafts. One

such technique that has been successfully used for the treatment of CNS malignancies involves the *in vivo* tumor transduction with the herpes simplex thymidine kinase (HS-tk) gene followed by treatment with anti-herpes drug ganciclovir was achieved by intra-tumoral injection of retroviral vector-producing cells containing the HS-tk gene, rendering the transfected tumor cells susceptible to treatment with ganciclovir. Other vector systems used in CNS gene transfer studies include retroviruses, adenoviruses, adeno-associated viruses, the encapsulation of plasmid DNA into cationic liposomes and neutral and oligodendrial stem cells.[203-204]

Although this approach holds remarkable therapeutic potential in the treatment of CNS diseases, its efficacy has thus far been hindered by a number of obstacles: restricted delivery of vector systems across the BBB, inefficient transfection of host cells, and nonselective expression of the transgene and deleterious regulation of the transgene by the host.

1.3.7.4. Nanoparticles

Approximately 98% of small molecular weight drugs and almost 100% of larger molecular weight peptides and proteins do not cross the blood–brain barrier.[205] Nevertheless, the past few years have seen some notable developments in systemic and local biomaterial-based nanosystems and microsystems for drug delivery.[206] The greatest advantage of systemic drug delivery approaches is their non-invasive nature and use of traditional routes of administration. However, unacceptably large systemic dosages may be needed to achieve therapeutic drug concentrations in the brain. Active targeting (that is, tailoring the surface of a delivery vehicle with site-specific ligands that increase its penetration into the brain tissue) could provide a solution to this limitation.[207-208] The pharmacokinetic properties of these drug delivery systems must increase the bioavailability of the drug and the time it remains in the blood circulation as well as reducing drug clearance by the reticuloendothelial system

(rES).[209] Another option is to use implantable local drug delivery systems to avoid the blood–brain barrier, the side effects of systemic delivery and the necessity to modify the surface of the delivery vehicle.[210] However, local delivery systems require invasive surgery and do not allow dose adjustments once implanted. The main types of nanoparticle systems used for drug deliver are: liposomes, nanospheres, nanocapsules, dendrimers and micelles (figure 10).

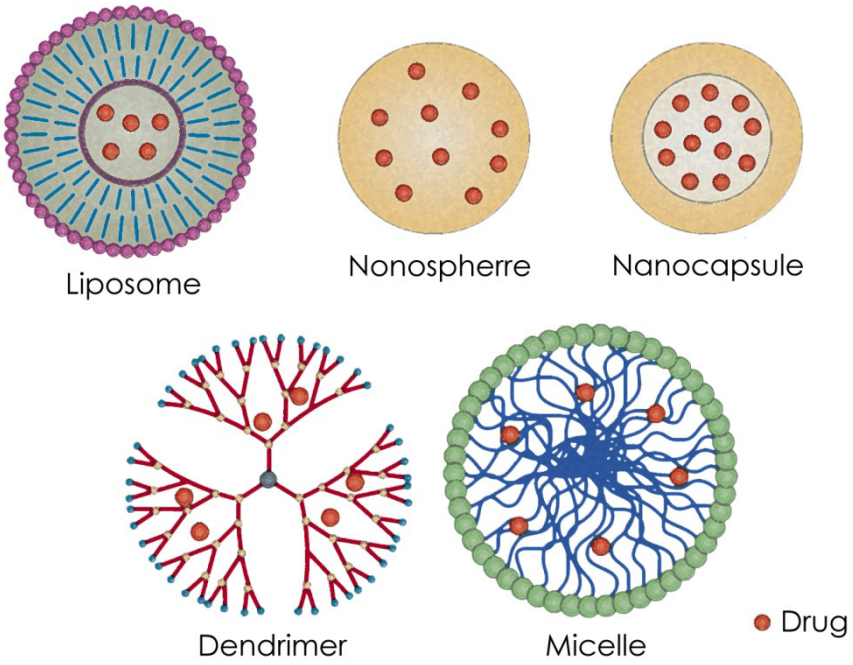

Figure 10. Schematic structure of different nanocarriers (liposomes, nanospheres, nanocapsules, dendrimers and micelles) for drug delivery into the brain. (Adapted from Orive et al.)[202]

Liposomes have a long history as drug carrier systems because of their easy preparation, acceptable toxicity and bio-compatibility profiles, and commercial availability.[211] They are small vehicles with an aqueous inner core enclosed by uni-lamellar or multilamellar phospholipid bilayers.[212-213] Conventional liposomes have relatively short half-lives, modest transport capacity across the blood–brain barrier and rapid rES clearance. These issues can be largely overcome by using

liposomal surface coatings such as polyethylene glycol and maintaining the particle diameter at <100 nm. These modifications reduce liposome aggregation and their recognition by the rES.[179, 214-215] PEGylated liposomes can be also manufactured to increase their access through the blood–brain barrier by receptor or absorptive-mediated transcytosis. The latter can be achieved by coating the liposome surface with monoclonal antibodies to glial fibrillary acidic proteins, transferrin receptors or human insulin receptors.[213, 216] The increasing experience of using liposomes the brain may in the future lead to their use to release neurotrophins and growth factors for brain repair and regeneration.

Liposomes have also been used experimentally to deliver genes to the brain. A plasmid expressing tyrosine hydroxylase, a key enzyme involved in the synthesis of dopamine, was delivered to the dopamine-depleted rat striatum using systemically administered PEG immunoliposome nanoparticles coated with transferrin receptors. The plasmids were expressed throughout the striatum and the nanoparticle delivered gene normalized tyrosine hydroxylase expression levels.[217] Polymeric nanoparticles (which include nanospheres and nanocapsules) are solid carriers ranging from 10 to 1000 nm in diameter made of natural or artificial polymers, which are generally biodegradable and in which therapeutic drugs can be adsorbed, dissolved, entrapped, encapsulated or covalently linked to the particle.[218] The synthetic materials used to prepare nanoparticles include poly(lactic acid) (PLA), poly(glycolic acid) (PGA), poly lactide-co-glycolide (PLGA), poly alkylcyano acrylate and poly anhydride poly bis (p-carboxy phenoxy) propane-sebacic acid (pCPP:SA); natural polymers such as chitosan, alginate and also gelatin have been tested.[219] When systemically administered, nanoparticles are generally more stable than liposomes but are limited by poor pharmacokinetic properties, uptake by the rES and a poor ability to cross the blood–brain barrier. Similar to liposomes, the surface of nanoparticles can be coated with molecules to increase blood–brain barrier permeability and improve pharmacokinetics[220] and even enable targeting for

delivery and imaging purposes. PLGA nanoparticles and microparticles (particle size >1000 nm) have been successfully used to deliver drugs for the treatment of neurodegenerative disorders. For example, using a rat model of Huntington's disease, local sustained administration of PLGA microparticles loaded with nerve growth factor (NGF) protected neurons from intrastriatal injections of the excitotoxin quinolinic acid.[221] These particles can also be loaded with other trophic factors such as glial-derived neurotrophic factor (GDNF), a protein that potently promotes the survival of many types of neurons, or with neurotransmitters such as dopamine and noradrenalin for the treatment of Parkinson's disease.[222] Nanoparticles can also be designed to induce neuroprotection. For example, nanoparticles composed of cerium and yttrium oxides can function as direct antioxidants by inhibiting the reactive oxygen species (ROS) production pathway.[223]

More recently, other configurations of nanocarriers such as solid lipid nanoparticles, micelles and dendrimers have been tested for brain drug delivery. Solid lipid nanoparticles consist of solid lipid matrices stabilized by surfactants. Not only are they easy to prepare but they possess low cytotoxicity and good physical stability and can protect labile drugs from degradation and can provide controlled drug release.[224-225] In a recent study, the efficacy of solid lipid nanoparticles for the delivery of several antineoplasic agents in brain tumor therapy was demonstrated *in vitro* and *in vivo* in rat models of glioma.[226] These nanocarrier systems have been used to enhance brain uptake of a range of other compounds including HIV protease inhibitors such as atazanavir (reyataz; Bristol–Myers Squibb).[227] This suggests that similar approaches could be used for the delivery of drugs to promote neuroprotection, regeneration or repair. One important consideration in the use of nano-sized drug carriers is the largely unknown cytotoxicity that they might possess; especially if used on an intermittent to chronic basis. Micelles form spontaneously in aqueous solutions of amphiphilic block copolymers and have core-shell architectures, whereas dendrimers are repeatedly branched polymer molecules that contain a cascade of

branches grown from one or several cores. Although more extensive studies are needed, polymeric micelles made up of poloxamer block copolymers (Pluronics) and those with TAT-poly(ethylene glycol)-block-cholesterol may open new avenues for the delivery of drugs, including those that aim to promote repair or regeneration of the brain.[228] These systems can trap large amounts of drugs in their core protecting them from degradation and their chemical composition, size and morphology can easily be changed. The surface of polymeric micelles can also be functionalized so that they can cross the blood–brain barrier. Perhaps most importantly, the therapeutic molecules that can be used with these materials are quite varied including proteins, oligonucleotides and imaging agents.[202]

The successful development of efficacious biomaterials capable of brain protection, repair or regeneration will require a uniquely complex interaction among researchers and clinicians.

2. HYPOTHESIS

The peri-infarct tissue is a target area for the treatment of cerebral ischemia. The peri-infarct area presents an specific expression of proteins that can be used to identify and target it.

It is possible to build up theranostic nanosystems that include imaging probes on their structure, and that interact specifically with the peri-infarct tissue, allowing its spatiotemporal characterization *in vivo* (by MRI) and *ex vivo* (by fluorescence microscopy).

The inclusion of a therapeutic agent in the theranostic vehicle will improve the beneficial effect of the drug with respect to the drug administered in its free form.

3. OBJECTIVES

The global objective of this work is the search for a molecular target characteristic of the peri-infarct tissue, and the construction of an effective theranostic agent specific to it, for the enhanced diagnostic and therapeutic treatment of cerebral ischemia.

Particular objectives of the work are:

1. To analyze the protein expression at the peri-infarct region on an animal model of stroke, and select suitable candidates to characterize it.

2. To validate the defined molecular targets by biochemical and histological techniques, and follow the spatiotemporal evolution of the peri-infarct region following cerebral ischemia.

3. To build a liposome-based targeted theranostic agent for the peri-infarct region, with imaging probes for its detection *in vivo* (by MRI) and *ex vivo* (by fluorescence), and able to carry a therapeutic agent on its structure.

4. To demonstrate, *in vitro*, the capacity of the targeted theranostic agent to participate in molecular recognition processes with brain cells.

5. To demonstrate, *in vivo*, the capacity of the targeted theranostic agent to accumulate preferentially at the peri-infarct region on animal models of cerebral ischemia, carrying in this way a diagnostic function.

6. To demonstrate, *in vivo*, the enhanced therapeutic capacity of a neuroprotective drug (citicoline), when transported through the BBB and released preferably at the peri-infarct region by the targeted theranostic agent.

4. MATERIALS AND METHODS

4.1. ANIMAL MODELS OF STROKE

4.1.1. Animal management

In our studies we used Sprague-Dawley rats (Harlan) with a weight of 361±12 g. Animals were kept at controlled conditions of temperature (22±1 °C) and humidity (60±5%), with a 12/12 hours light/dark cycle, and granting free access to food (commercial chow pellets) and tap water. For surgery and MRI rats were anesthetized with sevoflurane (3% in 70% N_2O and 30% O_2). Rectal temperature was monitored and maintained at 37±0.5 °C with a feedback controlled heating system (1025 system, SA Instruments). At the end of the procedures animals were sacrificed under deep anesthesia (8% sevoflurane). All procedures were performed under EU regulations (European Communities Council Directive of 24 November 1986 - 86/609/EEC), with the approval of our institution's ethics committee.

4.1.2. Model of focal permanent ischemia in the rat

Permanent occlusion of the left middle cerebral artery (MCA) was performed by suture of the artery following the method of Shigeno et al.[229] In brief, an incision was practiced along the temporal muscle of the rat. A small (3 mm) hole was drilled in the exposed skull and, the MCA was proximally exposed, where the artery bifurcates in its frontal and parietal branches, and was carefully sutured with a 10-0 Ethilon (polyamide 6) suture (Ethicon Inc.), the absence of blood flow in the artery was visually confirmed under the microscope. Finally, the temporal muscle was gently relocated over the skull and the skin of the animal was sutured. Brain surgery was performed after permanent ligation of the ipsilateral carotid artery.

4.1.3. Model of focal transient ischemia in the rat

Transient focal ischemia was induced in rats by intraluminal occlusion of the middle cerebral artery (MCAO), performed as previously described[230] with some modification. Briefly, under a surgical microscope, the left common, the external, and the internal carotid arteries were dissected from connective tissue through a midline neck incision. The left external carotid artery and the pterygopalatine artery of the internal carotid artery were separated and ligated with 6-0 silk sutures. A 23-mm segment of 3-0 nylon monofilament suture with a silicone rounded tip was inserted into the left common carotid artery stump and advanced into the internal carotid artery around 20 mm from the bifurcation to occlude the origin of the MCA. The intraluminal suture was removed after 90 minutes of occlusion. A laser-Doppler flow probe (tip diameter 1 mm) attached to a flow meter (PeriFlux 5000; Perimed AB) was located over the thinned skull, over the MCAO territory (4 mm lateral to bregma) to obtain a continuous measure of relative cerebral blood flow (CBF) during the experiment. Only animals with a CBF reduction higher than 75% and with reperfusion after occlusion were included in the studies.

4.1.4. Administration of substances

Intraperitoneal injection

Animals treated with citicoline intraperitoneally were briefly anesthetized with sevoflurane 3% in O_2:N_2O/30:70. A 25 gauge needle was inserted in the lower abdomen until it reached the peritoneal cavity, were the drug was injected.

Intravenous injection

Animals treated with citicoline, either free or liposome-bound, were intravenously injected in the jugular vein. First, animals were anesthetized with sevoflurane 3% in O_2:N_2O/30:70. Then a 0.5 cm incision was made in the animal's neck just above the clavicle

1cm to both left and right of the midline. Subcutaneous fat was cut, and the jugular vein was revealed. A 30 gauge needle was used for every injection since after withdrawal, the puncture rapidly closes preventing bleeding. For animals that received serial injections, each jugular was alternatively used to prevent vein damage.

4.1.5. Magnetic Resonance Imaging

MRI studies were conducted on a 9.4T MRI system (Bruker Biospec.). Lesion outcome (lesion volumes and edema formation) were assessed by Diffusion Weighted Images (DWI), during the acute phase or by T2-weighted images at sub-acute and chronic phases of the disease. The whole brain was covered by 14 consecutive, 1 mm thick, rostral-caudal slices. Nanoparticles' uptake and distribution was determined by a T1 map construction after the acquisition of images with different repetition times (8 TRs, following a saturation-recovery scheme) and fitting pixel-by-pixel to mono-exponential equations. Images were processed and analyzed with Bruker's ParaVision software, and with self-developed applications for the software platform Image-J.

4.2. PROTEOMIC ANALYSIS OF PERI-INFARCT TISSUE

4.2.1. Sample processing

For proteomic and Western-Blot analyses, ischemic animals (permanent occlusion of the MCA) were sacrificed by sevoflurane overdose (8% in O_2:N_2O/30:70). Brains were removed and cut into 2 mm thick coronal slices to be stained with a 2% 2, 3, 5-triphenyl-2H-tetrazolium chloride solution (TTC, Panreac). This process stained the intact brain tissue with a pink like color, leaving the ischemic tissue unstained (white). After a 2 minute staining period, the tissue considered as peri-infarct area (a 1mm thick strip in the periphery of the infarcted area), as well as a

matching segment in the contralateral side (used as control tissue), were removed as depicted in Figure 11.

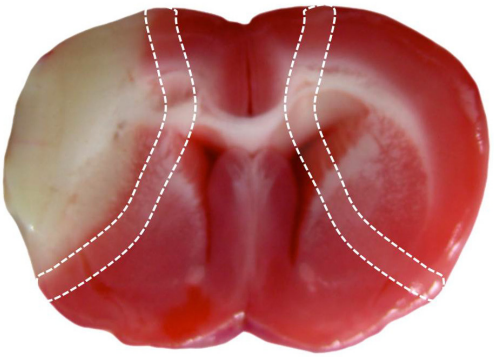

Figure 11. Rat brain coronal slice stained with TTC, the dashed white lines represent the segment of the tissue that was removed for proteomic and Western-Blot analyses.

For inmmunohistochemical validation, a second group of animals were intracardially prefunded with 100 ml phosphate buffer solution to wash out all blood form tissues. After removing the brain, 3 mm thick coronal slices were taken and introduced in a 20% sucrose solution for 1h at 4ºC in a roller bench. This step allowed tissue cryoprotection. Afterwards the slices were carefully dried and place on molds filled with O.C.T. solution (Sakura finetek) and then quickly frozen in 2-methilbutane cooled by liquid Nitrogen. Finally, blocks were stored at -80ºC until further use.

For the evaluation of the HSP72 temporal profile expression, a set of animals was sacrificed at one of the following time points following reperfusion: 6, 12, 24, 48, 72 hours and 5, 7, 10, 14 days. The animals were intracardially perfused with 100ml PBS (pH 7). After removing the brain, 3 mm thick coronal slices were taken and introduced in a 20% sucrose solution for 1h at 4ºC in a roller bench. This step allowed tissue cryoprotection. Afterwards the slices were carefully dried and place on molds filled with O.C.T.

solution (Sakura finetek) and then quickly frozen in 2-methilbutane cooled with liquid Nitrogen. Finally the blocks obtained were stored at -80ºC until further use.

4.2.1.1. Sample sub-fractioning in peri-infarct and contralateral regions

Tissue samples were sub-fractioned into soluble proteins, membrane proteins and insoluble proteins in order to study a broader range of proteins. Special focus was set on membrane proteins, since molecular recognition processes between cells and theranostics agents are expected to take place at this level. Samples were fractioned using a ProteoExtract Native Membrane Protein extraction kit from Calbiochem. According to manufacturer's instructions, samples were homogenized by sonication, this step was performed in 2 ml of cold extraction buffer I (4ºC), adding 10µl of protease inhibitors, for 10 minutes in a roller bench at 4ºC. Afterwards a 16000xg centrifugation step was undergone at 4ºC for 15 minutes. The supernatant (soluble fraction) was removed and frozen. The precipitate was resuspended in 1ml extraction buffer II (4ºC) and 5µl of protease inhibitors were added. The mix was incubated for 30 minutes in a roller bench at 4ºC. Next the mixture was centrifuged at 16000xg for 15 minutes at 4ºC and again the supernatant (in this case the membrane fraction) was removed from the precipitate (insoluble fraction). These three fractions were later used for both bidimensional electrophoresis and COFRADIC (Combined Fractional Diagonal Chromatography) analyses.

4.2.1.2. Sample preparation for bi-dimensional electrophoresis

Protein separation was performed in bidimensional (2D) electrophoresis gels. Protein expression from the peri-infarct region vs. contralateral region was compared for each of the protein fractions (membrane, soluble and insoluble). A total of 6 rats were included for this study. Every gel was performed in duplicate. First, different protein fractions were prepared in

different steps; membrane and soluble proteins were then concentrated by 14000xg centrifugation for 45 minutes in Centricon tubes (Millipore) until the volume was reduced to 500µl. Next, following the addition of 1.5ml cold acetone (4ºC), proteins were incubated for 2h at -20ºC. Finally a 14000xg centrifugation step was performed at 4ºC for 45 minutes to precipitate proteins. 100µl lysis buffer (Urea 7M, thiourea 2M, 4% CHAPS and 3% DTT) was used to resuspend the proteins for 1h in a roller bench at 29ºC.

Insoluble proteins were resuspended in 1ml lysis buffer (Urea 7M, thiourea 2M, 4% CHAPS and 3% DTT) in a roller bench for 3h at 29ºC in order to ensure the precipitate's homogenization. A 14000xg centrifugation was undergone for 45 minutes in order to eliminate the non-homogenized bits. The supernatant was concentrated by a 14000xg centrifugation for 45 minutes in Centricon tubes (Millipore) until the volume was reduced to 500µl. Next, after adding 1.5ml cold acetone (4ºC), proteins were incubated for 2h at -20ºC. Finally a 14000xg centrifugation step was performed at 4ºC for 45 minutes for the proteins to precipitate. 100µl lysis buffer (Urea 7M, thiourea 2M, 4% CHAPS and 3% DTT) was used to resuspend the proteins for 1h in a roller bench at 29ºC.

Finally a modified Bradford method was used to determine protein concentration in all the different fractions.

4.2.2. 2D-PAGE electrophoresis

2D-electrophoresis was performed in two steps. First, proteins were separated according to their isoelectric point. To achieve this, 40µg of protein in 330µl rehydration buffer (7M Urea, 2M thiourea, 4% CHAPS, 0.3% DTT and 0.5% biolites) were loaded onto pH3-10NL IPG (Immobilized pH Gradient) strips. This first dimension was undergone in a Protean IEF Cell system (Bio-Rad, Hercules, CA) applying a 50V current for 12 hours. Afterwards, strip rehydration was performed applying 500V for 15 minutes and 10000V until 30000Vh was reached.

In-between the first and second dimension electrophoresis, an equilibration process was performed by adding SDS buffer which applies a negative charge to all proteins. To accomplish this, IPG strips were submerged for 15 minutes in equilibration buffer with iodineacetomide (50mM Tris, 6M Urea, 30% glycerol, 2% SDS and 25mg/ml iodineacetomide).

Once the equilibration was achieved, the second dimension was performed. In this step, proteins were separated regarding their molecular weight by vertical electrophoresis in polyacrylamide gels. The equilibrated IPG were situated over a 20x26 cm, 12.5% acryl amide gel. A sealing solution (0.5% agarose in 1X electrolyte with bromophenol traces) was applied covering the strip. Separation was achieved using 1X electrolyte (50mM Tris, 384mM Glycine, 0.2% SDS) in the lower chamber and 2X electrolyte in the upper chamber. A 5W/gel current was applied for 15 minutes; afterwards a 15W/gel current was applied until the bromophenol front reached the end of the gel.

4.2.2.1. Protein separation and visualization

Once the 2D-electrophoresis was completed, gel staining was performed to develop the proteins. The staining techniques used were: Flamingo fluorescence (Bio-Rad) for analytic gels (the ones used for the differential protein pattern analysis), and Coomasie staining for preparative gels (the ones used for protein selection and analysis by mass spectrometry).

Flamingo fluorescence staining process started with fixation of the proteins to the gel matrix by submerging the gels in a 40% ethanol, 10% acetic acid solution for two hours. This step immersed protein diffusion. Then 1X Flamingo solution was applied for 3h. Afterwards gels were scanned using a FX-Proplus scanner at a 532 wavelength. Gel pictures were stored for further analysis.

In the Coomassie staining procedure, a first staining step was performed simultaneously with protein fixation. Gels were

immersed in a Coomassie Blue Brilliant R-250 solution with 40% ethanol and 10% acetic acid for 3h. Subsequently gels were unstained with a multiple step process in a 30% ethanol, 10% acetic acid solution. Finally gels were immersed in distilled water overnight. Afterwards gels were scanned in a G5700 densitometer, and images were stored for further use.

4.2.2.2. Differential analysis of protein spots

PDQuest software (Bio-Rad) was used the analysis of the gels' images. Every picture was cut under the same template, and an automatic detection of spots was performed. Every different spot observed on the gels correspond to each of the studied proteins. Each gel was manually edited to correct for obvious errors on the automatic detecting process. Next, pairing of automatically detected spots was executed, and again obvious errors produced during the automatic procedure were manually corrected. An intra- and inter-individual reproducibility analysis was performed. Two groups of gels were established for each fraction: peri-infarct and contralateral regions. Finally a differential analysis of the spots between both regions was performed, considering a significant difference when the peri-infarct/contralateral expression ration differed by a factor of, at least, 3 (peri-infarct/contralateral ratio >3 or <.333).

4.2.2.3. Mass spectrometry analysis

Protein spots that satisfied the selection criteria (peri-infarct/contralateral expression ratio >3 or <.333) were manually cut from preparative gels. Obtained proteins were reduced, alkylated and digested with trypsin according with the protocol established by Shevchenko et al.[231] Briefly, proteins were washed twice in water and the spots were stirred for 15 minutes with acetonitrile and dried in a SpeedVac for 30 minutes. The samples were then reduced with DTT 10mM in ammonium bicarbonate 25mM for 30 minutes at 56ºC, and subsequently alkylated with iodoacetamide 55mM in ammonium bicarbonate 25mM for 20

minutes in the dark. Finally, samples were digested with 12.5ng/µl trypsin (Roche Molecular Biochemicals) in 25 mM ammonium bicarbonate 25mM (pH 8.5) at 37ºC overnight.

After digestion, the supernatant was recovered and loaded onto a MALDI plaque, leaving it to dry at room temperature. Next, 0.4µl matrix in 50% acetonitrile was added, an again allowed to dry at room temperature. MALDI-TOF MS analysis was performed in a Proteomics Analyzer MALDI-TOF/TOF mass spectrometer (Applied Biosystems). Protein identification from the obtained masses was performed……

4.2.3. COFRADIC (COmbined FRActional DIagonal Chromatography) electrophoresis

In order to confirm the results obtained by 2D-eletrophoresis, a second proteomic technique was used, also based on liquid chromatography coupled with mass spectrometry (HPLC-MS). The COFRADIC technique for methionine peptides allowed us to compare the protein expression between peri-infarct and contralateral zones in all the fractions (membrane, soluble and insoluble fractions) for one animal. Protein samples were digested and resulting peptides were separated twice by HPLC, applying an methionine oxidation step in between. Every peptide was then analyzed and identified by mass spectrometry.

Samples were first desalinated in order to be processed by HPLC, using NAP-10 desalination columns (GE) and Guanidine-HCL 2M buffer. Six columns were emptied by decantation and equilibrated with 15 ml Guanidine-HCl 2M buffer. Next, 1ml of each sample (the three fractions for both peri-infarct and contralateral region samples) was introduced in each column and allowed to fall by gravity. 1.5 ml Guanidine-HCl 2M buffer was then added and the eluted protein sample was then recovered. Samples were then concentrated on a SpeedVac until a volume of 1ml was achieved.

Once desalinated, samples were reduced and alkylated with TCEP and iodineacetomide consecutively. Briefly, each sample was incubated with 26µl TCEP-HCl solution (45mg TCEP-HCl, 200µl 2M guanidine-HCl and 60µl NaOH) for 15 minutes at 37ºC in the dark. Afterwards samples were also incubated with 40µl iodineacetomide solution (27mg iodineacetomide, 200µl 2M guanidine-HCl buffer) for 10 minutes at 37ºC. When the reduction and alkylation processes were finished, the samples underwent another desalination step in NAP-10 columns following the protocol described above, except that in this case the used buffer was 1M TEAB (Fluka).

Next, protein concentration was calculated using the Bradford technique, and samples were incubated for 5 minutes at 99ºC. Proteins were then digested with 2.5µg endoproteinase-lysine C (Roche) per 500µg of protein at 37ºC overnight. In this step all proteins get digested in lysine residues. After digestion an isotopic label was introduced by serine, threonine and N-terminus peptide residue propionylation. This allows the differentiation between peri-infarct and contralateral peptides. Briefly, each sample was incubated with 10mM NHS-propionic acid in 50% acetonitrile for 2h at 30ºC. In this step, the NHS-propionic acid used was synthesized at prof. Kris Gevaert's laboratory (Gent University, Belgium) using ^{12}C for peri-infarct region peptides, and ^{13}C for contralateral region peptides, allowing us to differentiate peptides from each of those regions. The excess of NHS-propionic acid was removed by incubating the samples with 60µl 1M Glycine for 10 minutes at 30ºC. Finally serine and threonine residues were depropylated by a 99ºC incubation step for 1h. Samples were then dried on a SpeedVac and solved in 10% acetic acid for further use on a HPLC system.

Samples were then injected into a HPLC (Agilent chemstation for LC and LC/MS) in a 2.1mm reverse phase column at 80µl/minute flux, using as mobile phase A (10mM ammonium acetate in 2% acetonitrile) and 10mM ammonium acetate in 70% acetonitrile as mobile phase B, following the next protocol:

Step	% B	Time [minutes]
1	0	0
2	0	10
3	100	110
4	100	115
5	0	120
6	0	140

Table 1. fractions of the HPLC protocol

Peptide fractions were collected in 1 minute fractions from 20 to 80 minutes. Afterwards different fractions distributed within 15 minutes were mixed and dried in a SpeedVac and then diluted in 1% acetic acid. Then they were loaded again into the HPLC for further separation, following exactly the same protocol described above. In each sample, 20µl of a 3% H_2O_2 was added in order to oxidize the methionine residues. The fractions were recovered between 12 and 6 minutes sooner than proteins eluted in the previous phase (this peptides correspond to the ones containing methionine).

4.2.3.1. Mass Spectrometry

Samples belonging to the second chromatography were dried in a SpeedVac and solved in 10µl H2O2 for its use into LC-MS. Samples were loaded into a HPLC connected to a mass spectrometer. The HPLC column had a 0.3mm diameter and the flux was 20µl/minute. The column was situated in line with a PicoTip needle that introduced the sample into the mass spectrometer. The acquisition started 20 minutes after the HPLC gradient had commenced. Acquisition was adjusted so only ions with two charges were selected for the fragmentation analysis. After the LC-MS analysis a list of molecular weights was generated, and Mascot computer program was used in order to check the UniProt database.

4.2.3.2. Protein Identification

The LC-MS spectra obtained were exported into a Mascot compatible file format with the next parameters:

- Mass tolerance: 10 ppm
- Peptide tolerance: 10 ppm
- MS/MS tolerance: 0,5 Da
- Taxonomy: Rattus
- Database: SwissProt
- Enzyme: Lys-C
- Maximum missed cleavages: 1
- Fixed modifications: Acetylation N-term
- Variable modifications: acetylation N-term, carbamidomethyl, carbamidomethyloxide, gln-pyro-glu.
- Modification for quantization: propionyKfix

Furthermore a second search was made, in which no N-terminal modifications were considered (neither acetylation nor pyro-glu).

4.2.3.3. Quantification and validation

Every obtained spectrum was quantified in Mascot Distiller, considering that the correlation between experimental and calculated data was never lower than 97%, and that the standard error between samples was never over 0.16.

Finally, proteins that presented statistically significant differences in expression levels in the peri-infarct zone, respect to the contralateral region, were manually validated using the Rover computer program.

For the differential analysis between peri-infarct and contralateral regions, only those proteins identified by at least two different peptides were considered. Moreover, such peptides have had to belong exclusively to the identified

protein. Hence, peptides that could belong to more than one protein were not considered.

4.2.3.4. Results layout

Typically, in a HPLC-Mass spectrometry-based proteomic study, only proteins where a difference in expression is statistically significant ($p<0.05$) is considered. Besides such restriction, we have added an additional exclusion criterion, considering only those proteins in which the difference in expression between peri-infarct and contralateral regions was at least 3-fold.

4.2.4. Target validation

4.2.4.1. Western-Blot

In order to validate the results obtained in the proteomic study, the expression of selected proteins was evaluated by western-blot in both uni-dimensional and bi-dimensional approaches. Two animals were used for each experiment. For those, surgery and sample homogenized and sub-fractioning (membrane, soluble and insoluble) were performed as described above.

For uni-dimensional western-blot studies, a 1:1 dilution with Laemli buffer solution (Bio-Rad) was applied to the samples. 40µg of protein was loaded in each well of the gel (SDS-PAGE 10% acryl amide). Proteins were separated by a 100V constant current.

For bi-dimensional western-blot studies, samples were treated as described above, and 40µg of protein were loaded in 11 cm pH 3-10NL gradient IPG strips, together with 200µl of rehydration buffer. Proteins were separated by their isoelectric point within the strips by a Protean IEF Cell system (Bio-Rad) using a 50V current for 12 hours, 500V for 15 minutes and 8000V until 35000 Vh was reached.

Between the run of the first and second dimension processes, an equilibration step was performed using SDS buffer, which applied a negative charge to the protein. IPG strips were submerged in DTT equilibration buffer (50mM tris, 6M urea, 30% glycerol, 2% SDS, DTT 10 mg/ml) for 15 minutes. Next, they were introduced in equilibration buffer with iodineacetomide (50mM Tris, 6M urea, 30% glycerol, 2% SDS, iodineacetomide 25mg/ml) for another 15 minutes.

Once the equilibration process was finished the second dimension process was performed. In this process, proteins were separated by molecular weight using vertical electrophoresis in acryl amide gels. Briefly, an IPG strip was situated at the top of an acryl amide gel "Criterion XT Precast gel" (Bio-Rad, Hercules, CA) and filled with a sealing solution (0.5% agarose in electrolyte 1X with bromophenol traces). Separation was undertaken with electrolyte 1X (50mM Tris, 384 mM Glycine, 0.2% SDS) in both lower and upper chambers, applying a 2W/gel current for 15 minutes and 5W/gel current until the dye front reached the end of the gel. The temperature was set to 25ºC.

Once the proteins were separated (both uni- or bi-dimensionally), they were transferred to low fluorescence PVDF membranes (Millipore). In order to achieve this, a semi-dry system was used applying a 15V current for 45 minutes. Once transferred, PVDF membranes were blocked with a 5% dehydrated milk solution for 2 hours at room temperature. Next the membranes were washed for 5 minutes with TBST (0.1% TWEEN 20 in TBS buffer) three times, and then incubated overnight with a mouse monoclonal anti-HSP70 antibody (1:1000 abcam). The next day, the membranes were washed 3 times again with TBST and the membranes were incubated for 5 minutes with a rabbit anti-actin secondary antibody (1:3000 abcam). Finally, band detection was achieved using an anti-mouse Cy3-labeled antibody (1:3000, GE) and an anti-rabbit Cy5-labelled antibody (1:3000, GE) for 2h in the dark at room temperature. Pictures were acquired with an FXProPlus fluorescence scanner (Bio-Rad). Uni-dimensional western-blot

pictures were analyzed with QuantityOne software, whereas bi-dimensional western-blot pictures were analyzed using PDQuest software, both from Bio-Rad.

4.2.4.2. Immunohistochemistry

Brain sections were cut in 20µm slices with a cryostat and the slices were dried in an oven at 37ºC and stored at -20ºC for their posterior use. The slices were then first rehydrated in PBS and incubated with 0.3% H_2O_2 for 15 minutes in order to block endogenous peroxidase activity. After three 5 minute washes in PBS, slices were incubated in 2% normal serum in 0.2% Triton X-100 PBS for 2 hours, in order to block unspecific antibody binding sites. Next, a mouse primary monoclonal antibody against the decided antibodies (e.g. GFAP (abcam), HSC70 (abcam) and HSP72 (Enzo Life Sciences) was used (1:50) for 1 hour and then washed three times with PBS for 5 minutes. Afterwards a 1 hour incubation with a biotinylated horse anti-mouse IgG antibody, rat adsorbed (1:200, Vector Laboratories) was performed, followed again by a 5-minute wash applied three times. Next a 1:100 dilution of both avidin-DH and a biotinylated peroxidase (Vector Laboratories) was made and used for incubation for one hour with the slices. After three 5-minute washes with PBS, samples were incubated with a 2% diaminobenzidine solution (Dako Diagnósticos, S.A.) for 2 minutes. After another three step 5-minute wash, samples were dehydrated in ethanol water solutions of increasing concentration (50%-100%), and cleared with xylol (Panreac). Afterwards slices were mounted with entellan (Merck) and stored at room temperature for further use.

Double immunofluorescence

Together with the immunohistochemistry protocol described above, double immune fluorescence techniques were performed on 20 µm rat brain slices. Brain slices were first rehydrated in PBS and incubated with 10% normal serum in 0.2% Triton X-100 PBS for 2 hours in order to block unspecific antibody binding sites. Next a mouse primary monoclonal (e.g. HSP72) or

polyclonal (e.g. NeuN, GFAP or CD31) antibodies against selected targets were used (1:50) for 1 hour, and then washed three times with PBS for 5 minutes each. Afterwards, 1 hour incubation with a mixture of biotinylated horse anti-mouse IgG antibody, rat adsorbed (1:200, Vector Laboratories) and DyLight 488 Goat Anti-Rabbit IgG antibody (1:200, Vector Laboratories, Burlingame, CA) was performed, followed again by a 5-minute wash applied three times. Next, a 1:100 dilution of both avidin-DH and a biotinylated peroxidase (Vector Laboratories) was made and used for incubation for one hour with the slices. After three 5-minute washes with PBS, slices were mounted with Vectashield mounting medium with DAPI (Vector Laboratories) and stored at 4ºC temperature for further analysis.

4.2.4.3. HSP72 temporal profile expression

To evaluate the temporal profile expression of HSP72 on an ischemic brain we used a transient ischemia model since, due to a larger infarct, it allowed us to better discriminate between ischemic core and peri-infarct region in order to better quantify the positive staining for HSP72. Nine animals were sacrificed after reperfusion at the next time points: 6 and 12 hours and 1, 2, 3, 5, 7, 10 and 14 days after reperfusion.

Immunohistochemistry analysis

A representative slice corresponding to the middle of the infarct was selected for each time point. The slice selected corresponded approximately to bregma +0.5. First, an overview of the slice was made to subjectively estimate the degree and location of HSP72 expression. Then, 4 pictures were taken at 20X following the pattern described in a template (Figure 12). After picture acquisition cells were counted for each area and the results were represented as number of cells per mm2.

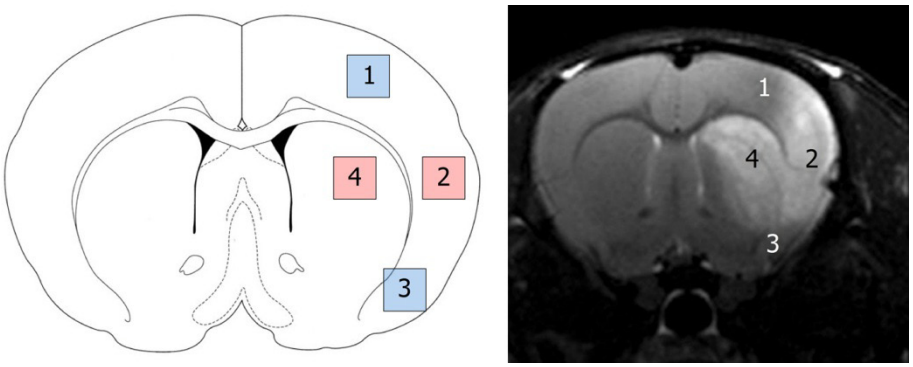

Figure 12. Rat brain coronal slice located approximately in the stereotaxic coordinates bregma + 0.5 (according to Paxinos and Watson anatomic atlas) that corresponds roughly with the middle of the infarct. Four pictures were taken per slices (at 20X). On the right, an MRI picture representative of that region can be seen. Zones 1 and 3 corresponded to the peri-infarct area, whereas zones 2 and 4 are located in the ischemic core.

4.3. LIPOSOME SYNTHESIS AND CHARACTERIZATION

4.3.1. Synthesis of base liposomes

Most liposomes used in our studies have a common structure (further modified in specific studies). In this section we describe the synthesis of such base liposomes.

Liposomes were prepared by the lipid film hydration method, followed by extrusion. For that procedure we used 1,2-distearoyl-sn-glycero-3-phosphocholine (DSPC), cholesterol, GdDTPA-bis-stearyl amide (Gd-BSA), 1,2-distearoyl-sn-glycero- 3-phospho ethanolamine N-[methoxy (polyethylene glycol 2000] (PEG 2000-DSPE) and 1 ,2-dipalmitoyl-sn-glycero-3-phospho ethanol-amine-N-(lissamine rhodamine B sulfonyl) (rhodamine-PE), all from Avanti Polar lipids. The synthesis started by solving those components at a molar ratio of 1.10:1:0.75:0.15:0.1 (typically 100 µmol total amount of lipids) in a mixture of chloroform and methanol (6:1 v/ v). The mixture of lipids was then evaporated to dryness by rotary evaporation at approximately 30°C and a

reduced pressure of 200 mmHg, and further dried under flow of N_2. The lipid film formed in this way was then hydrated in an appropriate volume of HEPES buffered saline (HBS) at pH 7.4 (typically 7 ml). The resulting lipid suspension underwent consecutive extrusion through single polycarbonate membrane filters (Whatman) with a pore diameter of 400nm (2 times), 200nm (4 times) and 100nm (8 times) at 65°C (over the critical temperature for these liposomes) to a final size of approximately 100nm.

4.3.2. Synthesis of immuno-liposomes

For targeting studies, base liposomes were modified to vectorize them with antibodies against selected proteins (mainly HSP72). For that, 1 ,2-distearoyl-sn-glycero-3-phosphoethanolamine-N - [maleimide- (poly(ethy lene glycol)) 2000] (Mal-PEG2000-DSPE, Avanti Polar lipids) was added to the conventional DSPC, Cholesterol, Gd-BSA, PE2000-DSPE and rhodamine-PE mixture and solved in a mixture of chloroform and methanol (6:1 v/ v) at a molar ratio of 0.075:1.10:1:0.75:0.075:0.1. The mixture of lipids was then evaporated to dryness by rotary evaporation at approximately 30°C and reduced pressure of 200 mmHg, and further dried under flow of N_2 for 1 hour. The resulting lipid film was then hydrated in an appropriate volume of HEPES buffered saline (HBS) at pH 6.7 (typically 7 ml) and submitted to consecutive extrusion through single polycarbonate membrane filters (Whatman) with a pore diameter of 400nm (2 times), 200nm (4 times) and 100nm (8 times) at 65°C (above the critical temperature of liposomes) to a final size of approximately 100nm.

4.3.2.1. Conjugation of anti-mouse HSP72

Monoclonal antibodies against human HSP72 (Enzo, clone C92F3A-5) were coupled to liposomes by covalent thioether linkage to the distal end of Mal-PEG2000-DSPE chains. First, an azide-free antibody preparation was obtained by centrifugation

of the original antibody solution three times on a Vivaspin concentrator with a 30kD MW cut-off filter in the presence of 2 ml HBS (pH 6.7). Both, the presence of sodium azide and a pH higher than 6.7, can disrupt the thioether bondage.

Next, HSP72 antibodies were modified with N-succinimidyl S-acetylthioacetate (SATA, Sigma-Aldrich) by a 45 minutes incubation period on a roller bench. The optimized molar ratio Antibody:SATA of 1:80 was used, . After incubation, the excess of SATA was removed by centrifugation three times on a Vivaspin concentrator with a 30kD MW cut-off filter in the presence of 4 ml HBS (pH 6.7). Subsequently, the SATA-reacted antibody underwent deacetylation by incubation with a hydroxylamine solution (at 1:10 v/v hydroxylamine solution-Antibody solution) for 60 minutes at room temperature on a roller bench. The activated antibody solution was added to the liposome suspension at a ratio of 50 µg protein/µmol lipid, to form covalent thioether bonds.

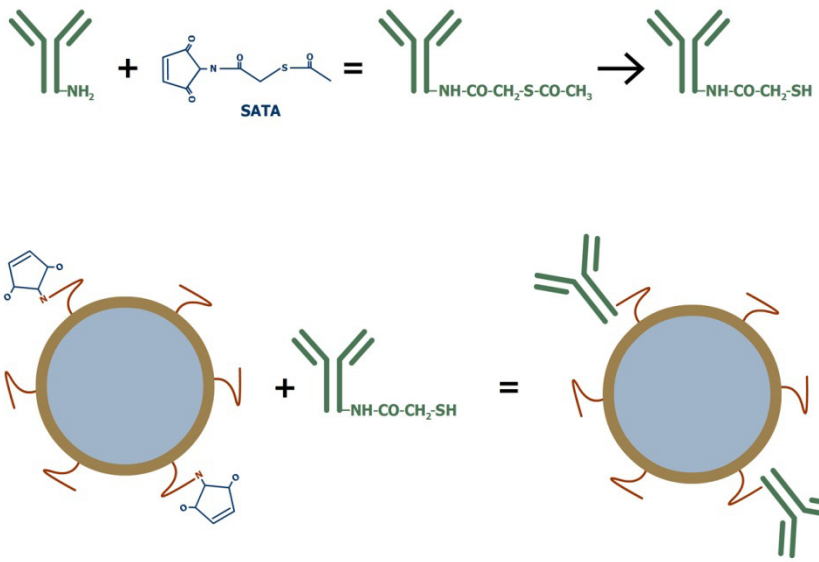

Figure 13. Schematic representation of the 2 step attachment of the antibody to lissome surface, via a thiol-maleimide reaction.

This preparation was stored overnight at 4ºC under N_2 atmosphere. Uncoupled antibody was separated from immunoliposomes by centrifugation at 65,000 rpm for 45 min. Pellets were then suspended in HBS pH 7.4 and stored at 4ºC until use.

4.3.3. Citicoline encapsulation in liposomes

For the study of the therapeutic action of theranostic agents a set of studies were done with citicoline doped liposomes (tagged or not against HSP72 protein), prepared as follows.

Citicoline was incorporated into the liposomes by adding it to the rehydration buffer in that step of the preparation of liposomes, as described above. To optimize the amount of drug, liposomes were prepared, adding 0, 40, 65 or 100 mg/ml of citicoline during the lipid film rehydration process. 50 µmol of lipids were prepared according to the described protocol for base liposomes. After the synthesis liposomes were centrifuged twice at 4ºC, 11000 rpm for 16 hours to remove free citicoline. The pellet obtained was suspended in 4 ml of HBS at pH 7.4. The encapsulation efficiency (EC, volume of citicoline hydrating solution encapsulated per mol of lipids) and drug content (DC, weight of citicoline (%) with respect to total weight of components: citicoline + liposomes) were obtained:

[cit] hidration /mg·ml^{-1}	Liposome Yield	EC (mM^{-1})	DC (%)	mg_cit /ml	umol_cit /umol_lipid
0	52%	0	0	0	0
40	50%	1.6	8	0.45	1.4E-01
65	29%	1.8	13	0.44	2.3E-01
100	2%	3.2	31	0.09	7.0E-01

Table 2.Overall results from the encapsulation tests (EC, volume of citicoline hydrating solution encapsulated per mol of lipids, DC, weight of citicoline (%) with respect to total weight of components: citicoline + liposomes)

Although the highest encapsulation efficiency was achieved when using 100 mg of citicoline (DC=31%), the best yield in liposome synthesis (50%) was obtained when using 40 mg of citicoline (Though DC was only 8% in this case) Data is presented in figure 14.

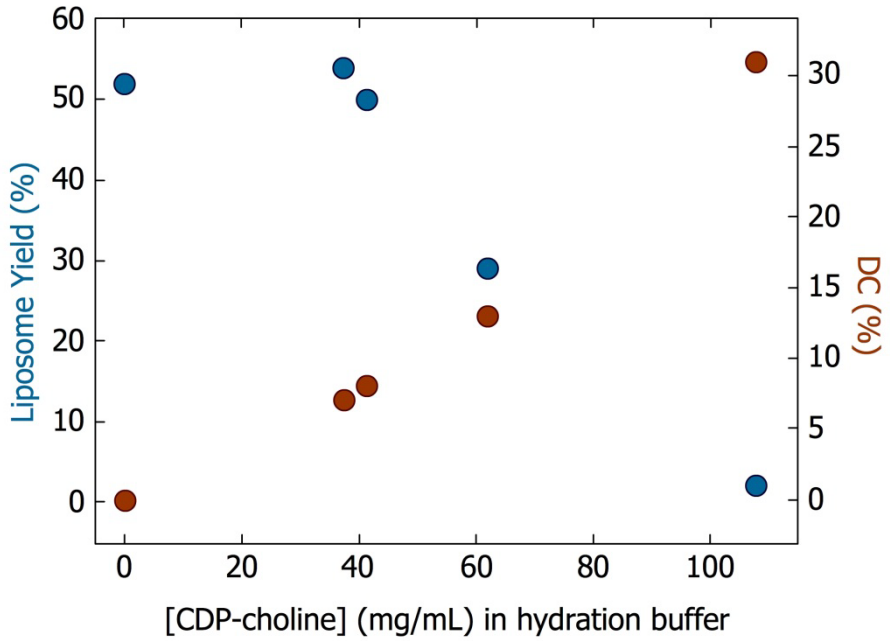

Figure 14. Graph comparing liposome yield and drug content (DC) related to the citicoline concentration used during liposome synthesis.

Since an 8% of 50% (4% of load) is much better than a 2% of 31% (0.6% of load), we decided to use 40 mg of citicoline per ml of liposome solution for the synthesis of therapeutic agents.

4.3.4. CHARACTERIZATION OF LIPOSOMES

4.3.4.1. Lipid concentration

The lipid concentration in liposome suspensions was indirectly assessed by determining the amount of phosphates from DSPC

and PEG2000-DSPE using the method proposed by Rouser[232] (non-significant traces of rhodamine-PE lipid were not considered for phosphate determination). Samples of liposome suspensions containing a variable concentration of phosphate, ranging 10-80nmol, were evaporated to dryness, and phospholipids were subsequently destructed to inorganic phosphate by adding 0.3ml of 70% perchloric acid, incubating the mixture for 45min at 180°C. Afterwards, 1ml of demineralized water, 0.5ml of hexa-ammonium-molybdate (1.25% w/v) and 0.5ml of ascorbic acid (5% w/v) were added to each sample, which were placed in boiling water for 5 minutes. During this incubation inorganic phosphate is converted to phospho-molybdate acid, which is reduced by ascorbic acid to a molecule with a strong absorbance at 797nm, measured after cooling the samples to room temperature. A representative calibration line obtained can be seen in figure 15.

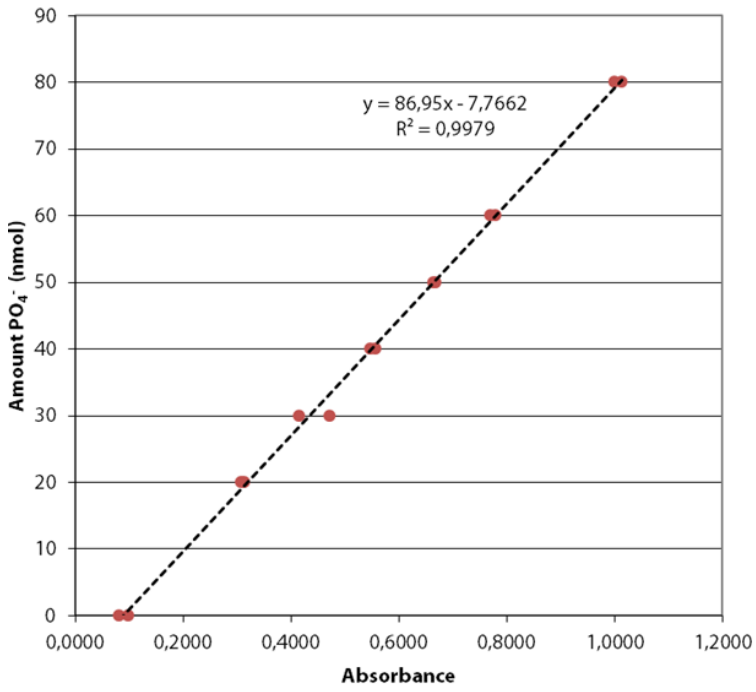

Figure 15. Graphic showing the phosphate calibration curve used for the phosphate determination of paramagnetic liposomes.

From the calibration plot, the amount of phosphate for all samples was obtained and, after correcting for the whole amount of lipid and the dilution used, the final lipid concentration in liposomes was obtained. In every batch synthesized, more than 24 µmol lipid per ml was obtained. Finally all liposome's suspensions were diluted to obtain exactly 24 µmol lipids per ml solution.

In the case of citicoline doped liposomes we have to consider that citicoline present two phosphate groups, hence it interferes with lipid phosphate determination. To characterize the lipid content in liposomes encapsulating citicoline, first the liposome drug content is determined by UV spectroscopy as described below (figure 16). Then the concentration is multiplied by two (since citicoline has two phosphate groups) and the result is subtracted from the total lipid content determined by Rouser phosphate determination of liposomes.

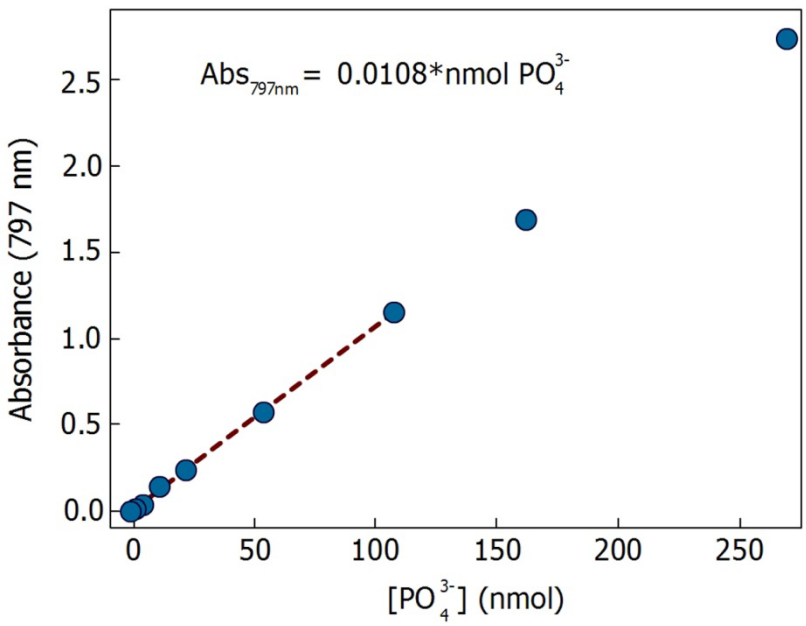

Figure 16. Phosphate determination for different concentrations of citicoline.

4.3.4.2. Liposome size

Average size and size-distribution of the liposomes was determined by dynamic light scattering (DLS) techniques. Dynamic light scattering (also known as photon correlation spectroscopy or quasi-elastic light scattering) is a technique that is usually employed to determine the size distribution profile of small particles in suspension

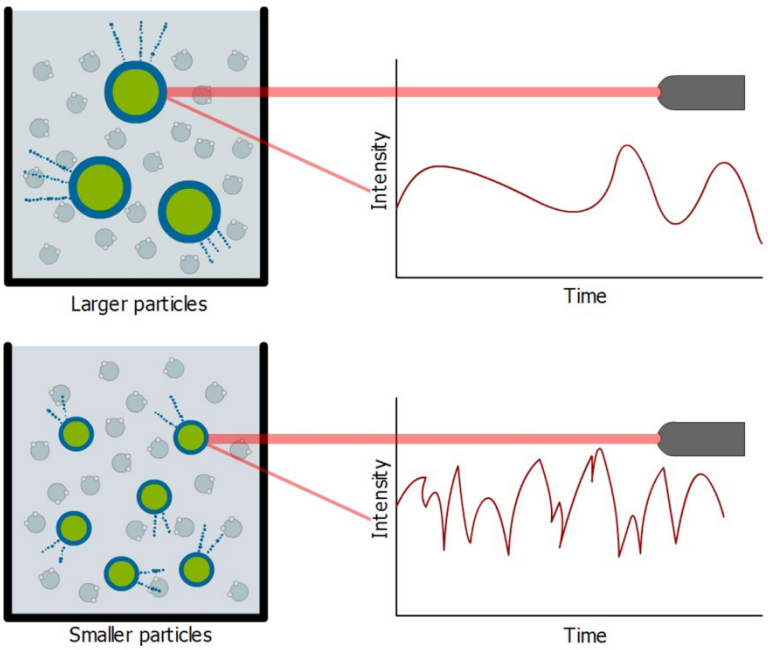

Figure 17. Schematic representation of how the DLS process works.

Projecting a monochromatic light beam, such as a laser, onto a solution with small particles in solution that follow a Brownian motion causes a Doppler shift on the wavelength, when the light hits the moving particle. Such shift is related to the size of the particle. Measuring the diffusion coefficient of the particle and using the autocorrelation function it is possible to compute the sphere size distribution and give a description of the particle's motion in the medium (figure 17).

4.3.4.3. MR properties (relaxivity) of liposomes

Cellular relaxation rates of loosely packed pellets were measured at room temperature on a 9.4T MR-scanner (Bruker) with a horizontal bore magnet. A bird-cage volume coil of 35mm was used for sending and receiving. PCR tubes containing the cell pellets were placed in a custom made holder (4 samples at a time) that was filled with water to facilitate shimming. For T1 measurements, data were obtained with an inversion recovery FLASH sequence within a slice of 1 mm planned through the pellets, with a time of 15 seconds between subsequent inversion pulses. After each 180° pulse, the magnetization recovered to its equilibrium value in a TI dependent way during which 60 images were acquired using a FLASH sequence after different inversion times TI (TI ranging from 72.5ms to 4792.5 ms). The flip angle was 15°, TR=4 ms, TE=2 ms, NA=4, FOV=30x30mm and matrix size=128x128 pixels. The average signal intensity in a region of interest was calculated with Mathematica 6.0 and plotted against the TI. Subsequently, the fit in the following equation was calculated:

$M=A-B*e^{-T1/T'1}$,

with T'1 being the observed T1, A=M0 as detected at the longest TI and B=A+M0·

However, since the FLASH acquisition causes saturation of the longitudinal magnetization the actual T1 is slightly higher and given by the following equation:

$T1=(B/A-1)*T'1$

Longitudinal relaxation rates were calculated as 1/T1.

4.3.4.4. Determination of protein content

In the case of liposomes vectorized with antibodies, it is necessary to determine the amount of proteins attached to liposomes' surface. Antibody coupling to liposomes was

assessed by protein determination using a modification of the Lowry protocol.[233] Two sets of solutions were prepared for the obtaining of a calibration line, using a range of IgG isotype control antibody concentrations and a fixed amount of non-conjugated liposomes (5mM lipid). Three sets of samples were then prepared with liposome samples, adjusting the lipid concentration in the samples to the same level as the one used in the calibration line. The calibration line obtained can be seen under figure 18

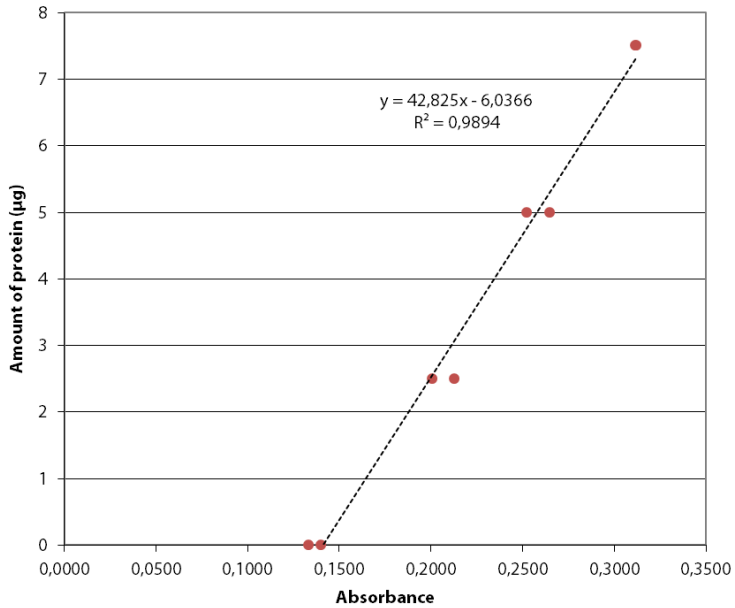

Figure 18. Calibration line plot used to determine the amount of protein coupled to liposomes.

After determining the amount of protein for both IgG and antibody (mainly anti-HSP72) coupled liposomes, the coupling efficiency was calculated assuming no antibody loss during synthesis. An average of 70% efficacy was found for the different batches of liposomes synthesized.

4.3.4.5. Determination of citicoline content

For those liposomes doped with citicoline, drug content was determined by UV spectroscopy due to the property of citicoline to absorb UV light at 271.5 nm. First a calibration curved was used using citicoline concentration ranging from 0 to 0.55 mM (in HBS). Liposomes encapsulating the drug were first dissolved in SDS 5mM in order to disrupt their membranes and release their content. Samples were then placed in 96 UV-transparent microplates (BD) and absorbance was measured at 271.5 nm using a Synergy 2 Multi-Mode Microplate Reader (Biotek). A typical result can be seen in figure 19.

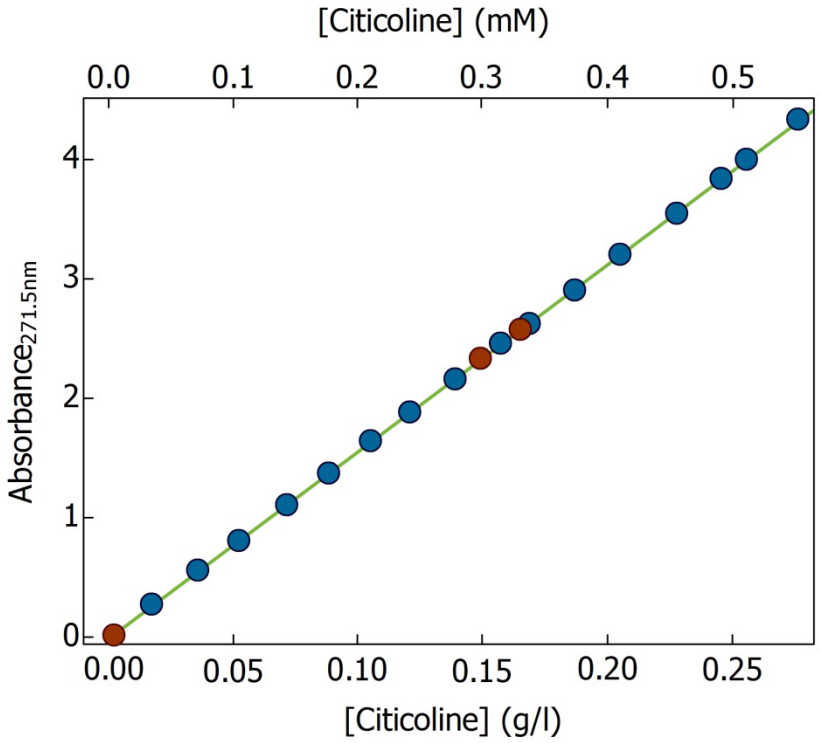

Figure 19. Linear trend line representing different citicoline concentrations. The red dots represent liposomes dissolved in SDS 5 mM.

4.4 *IN VITRO* STUDIES

4.4.1. Cell cultures

In vitro studies of interaction between cells and liposomes were performed in rat astrocytes and endothelial cells. Primary rat astrocyte cell cultures were obtained following the protocol described for McCarthy et al.[234] with few modifications.[235] Briefly, neonatal rat brains were harvested and digested with an enzyme system (Accutase® Sigma-Aldrich) and pass through a 70 µm filter (Filcons). $6x10^4$ cells/cm^2 were seeded in T75 flasks, the low cell density prevented oligodendrocyte proliferation.[236]

Rat Brain Microvascular Endothelial Cells (RBMVEC) from Sprague-Dawley rats were obtained from Cell Applications (Cell Applications Inc.). Cells were thawed and seeded in T75 fibronectin coated flasks (BD Biosciences). Clonetics® EGM® Endothelial Cell Growth Medium (Lonza Walkersville Inc.), supplemented with EGM-MV SingleQuot Kit Suppl. & Growth Factors CC-4143 (Lonza Walkersville Inc.), has been used to support the growth and expansion of RBMVEC in a low serum environment. Both astrocytes and RBMVEC were maintained in an incubator at 37ºC with a humidified atmosphere containing 95 % air/ 5% CO_2.

4.4.2. Cell stress studies

Molecular recognition processes between stressed cells (expressing HSP proteins) and base and targeted liposomes were performed using a stress model performed as follows. First, two sets of cells were incubated in 96-well plates until they reached 80-90% confluence. Then, one plate was incubated at 45ºC for 15 minutes whereas another plate was left at 37ºC. Afterwards, both plates were placed again in an incubator at 37ºC for a recovery period of 6 hours. After such period, the culture medium was removed, and cells were incubated with 15mM liposome suspensions (in culture medium) for 30 minutes or 1

hour. After the incubation period, three 5 minute washing steps were performed to remove unbound liposomes and cells were taken under the microscope to observe the fluorescence intensity (liposomes contain rhodamine). Finally, cells were harvested with acutase solution, introduced in eppedorf tubes, and washed three times by centrifugation at 3000 rpm for 5 minutes. After the last centrifugation step, the supernatant was removed and the tubes with cell pellets were studied under the NMR system as described above, to determine the relative gadolinium content (proportional to the amount of liposomes incorporated by the cells.

4.5 *IN VIVO* THERANOSTIC APPROACH

Both targeted and untargeted liposomes were evaluated in a rat stroke model for their efficacy identifying the peri-infarct zone and reducing the ischemic brain lesion after citicoline encapsulation.

4.5.1. Diagnostic function

To determine the targeted liposome capacity to accumulate within the peri-infarct zone in a permanent rat model of stroke the next experiment was performed. The study consisted of three groups: vehicle, untargeted liposome and targeted liposome. Rats were injected 30 minutes, 6, 12, 18, 24 and 30 hours after permanent MCA occlusion with a 1 ml suspension of either HBS pH7.4 (vehicle), untargeted liposomes (control group) and targeted liposomes against HSP72. T2WI and T1WI were acquired one day before surgery and 1, 3 and 7 days after surgery. DWI maps were acquired immediately after the MCA occlusion to assess the initial infarct size (figure 20).

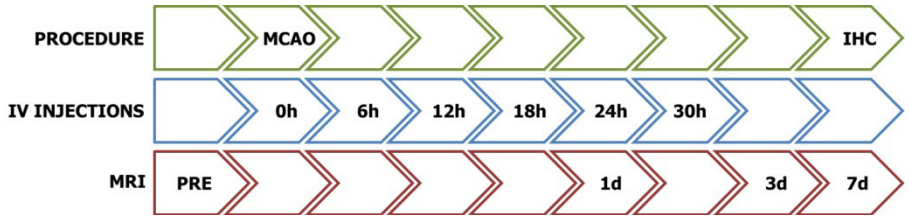

Figure 20. Experimental setup for the evaluation of the diagnostic function of HSP72 targeted liposomes in a rat brain ischemia model.

The presence of liposomes in the brain was also assessed by fluorescence 7 days after the occlusion. When the MRI acquisition was finished, animals were transcardially perfused with 100 ml serum saline. The brain was removed, cut into 3 mm coronal slices and introduced in a 20 % sucrose solution (in PBS) for 1 hour at 4ºC. Afterwards brain slices were placed in plastic block templates, filled with O.C.T. (sakura) and frozen in 2-methilbutane pre-cooled in liquid N_2. The blocks were stored at -80ºC. To check for fluorescence signal, blocks were cut in 20 µm brain slices and analyzed under a fluorescence microscope.

4.5.2. Therapeutic function

Finally, targeted liposomes therapeutic function was also evaluated on a rat permanent brain focal ischemia model. For this purpose citicoline as a neuroprotective drug was administered free intraperitoneally and intravenously, and bound inside targeted and untargeted liposomes intravenously. The study consisted of the following groups:

- Vehicle (n=4): administered with 6 IV injections (1ml HBS pH 7.4 each) over the first 30 hours after the MCA occlusion.
- Untargeted empty liposomes (n=4): administered with 6 IV injections (1ml of a 24 µmol lipid/ml solution of untargeted liposomes each) over the first 30 hours after the MCA occlusion.

- Free citicoline IP (n=4): administered with 1 IV injections (1ml in HBS pH 7.4 for a total citicoline content of 500 mg/kg) over the first 30 hours after the MCA occlusion.
- Free citicoline IV (n=4): administered with 6 IV injections (1ml in HBS for a total citicoline content of 48 mg/kg) over the first 30 hours after the MCA occlusion.
- Untargeted drug bound liposomes (n=4): administered with 6 IV injections (1ml of a 24 µmol lipid/ml solution of untargeted liposomes encapsulating a total citicoline content of 48 mg/kg) over the first 30 hours after the MCA occlusion.
- Targeted drug bound liposomes (n=4): administered with 6 IV injections (1ml of a 24 µmol lipid/ml solution of HDP72-targeted liposomes encapsulating a total citicoline content of 48 mg/kg) over the first 30 hours after the MCA occlusion.

The experimental setup can be seen in figure 21. The animals were subjected to 6 ml IV injections (in the jugular vein with the exception of the free citicoline group which only received 1 IP injection). The injections occurred 30 minutes and 6, 12, 18, 24 and 30 hours after the occlusion. The infarct size follow-up was performed first, immediately after the occlusion, by a DWI sequence and 1, 3 and 7 days after ischemia induction. Finally the animals were transcardially perfused with 100 ml serum saline, and their brains processed as described above under the theranostic approach section to detect the presence of liposome-induced fluorescence.

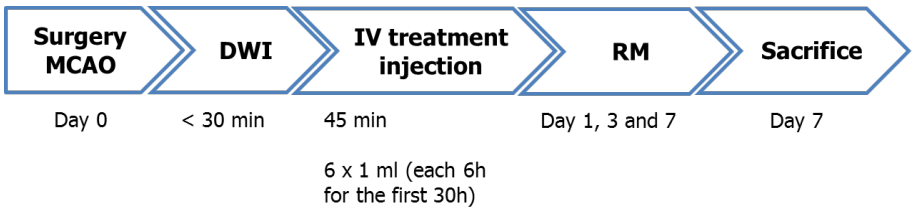

Figure 21. Flowchart representing the protocol followed for each animal studied.

The results are expressed as mean ± SD. An ANOVA test was performed to determine the presence of possible statistically significant differences. A student t-test intergroup analysis was done to check for differences between groups.

5. RESULTS

5.1 LIPOSOME DESIGN

5.1.1 Sizes and morphology of liposomes.

All liposomes were synthesized by extrusion of all their components through membranes of a pore size of 100 nm, as described in the methods section. A first step on their characterization was the measurement of their size distribution, generally performed by two different methods.

In first place we used dynamic light scattering (DLS) methods, as described. Typically, DLS was performed using 5µl liposome suspensions (1mM of lipids) diluted in 500µl of HBS at pH 7.4 and 23ºC. A size distribution graph form one of the samples can be seen in figure 22.

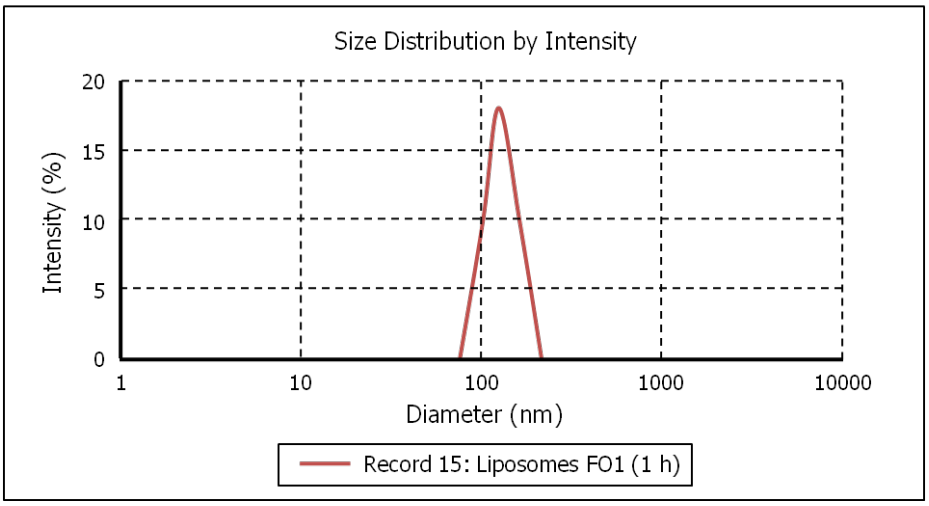

Figure 22. DLS graph representing the size distribution of a liposome suspension (mean 129.8 nm and width 24.2 nm).

In most of our studies the average particle size obtained for base liposomes extruded through 100 nm filters was ranged between 129 and 137 nm (depending on the batch), whereas in the case of targeted liposomes the diameter reached up to 144 nm. Typical size distribution widths were around 25 nm, for freshly prepared liposomes.

The stability of liposomes was also followed by DLS studies. In figure 23, we show the evolution of size populations of liposomes for a period of 96 hours. Te original size distribution obtained with freshly prepared liposomes decreases with time, as new populations of larger sizes (due to aggregation of liposomes) take place.

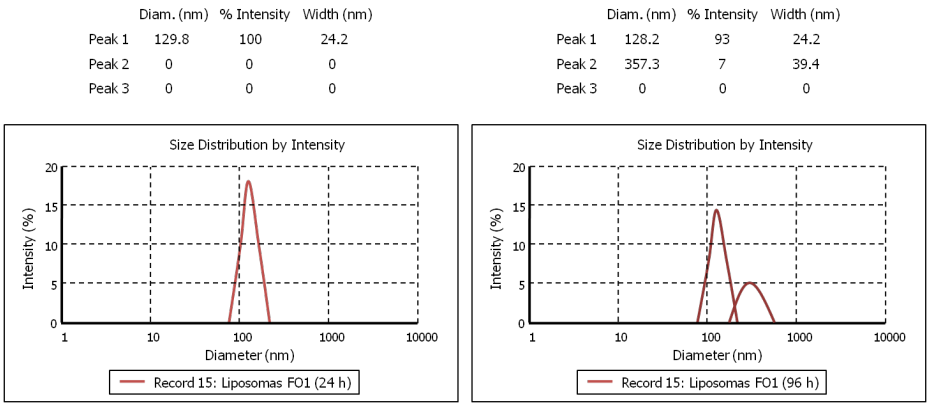

Figure 23. Changes in liposome size with time. Liposomes start to aggregate at long times after their synthesis.

Liposomes preserved at 4ºC have a good stability and only a minor fraction of them (ca. 7% on the plot presented in figure 2) correspond to large aggregates, during the first 4 days post preparation. Most liposomes remain free and with their original size after that period.

Alternatively, liposome shape and size characterization was also determined by optical analysis, using cryo-TEM microscopy images. A representative picture of a frozen sample of liposomes is presented in figure 24.

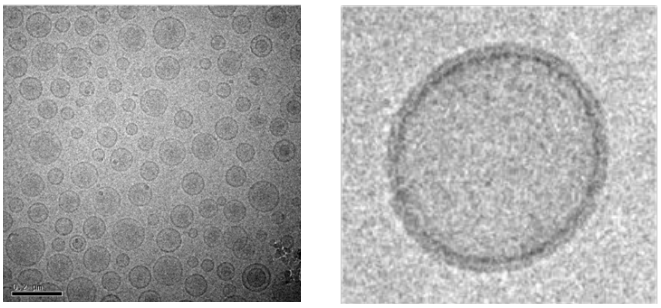

Figure 24. Cryo-TEM image of a frozen liposome suspension (left) and detail of a single liposome (right). Notice the detail of the phospholipids' double-layer.

Using ImageJ software liposome micrographs were processed for the calculation of the diameter and circularity of prepared liposomes (Figure 25).

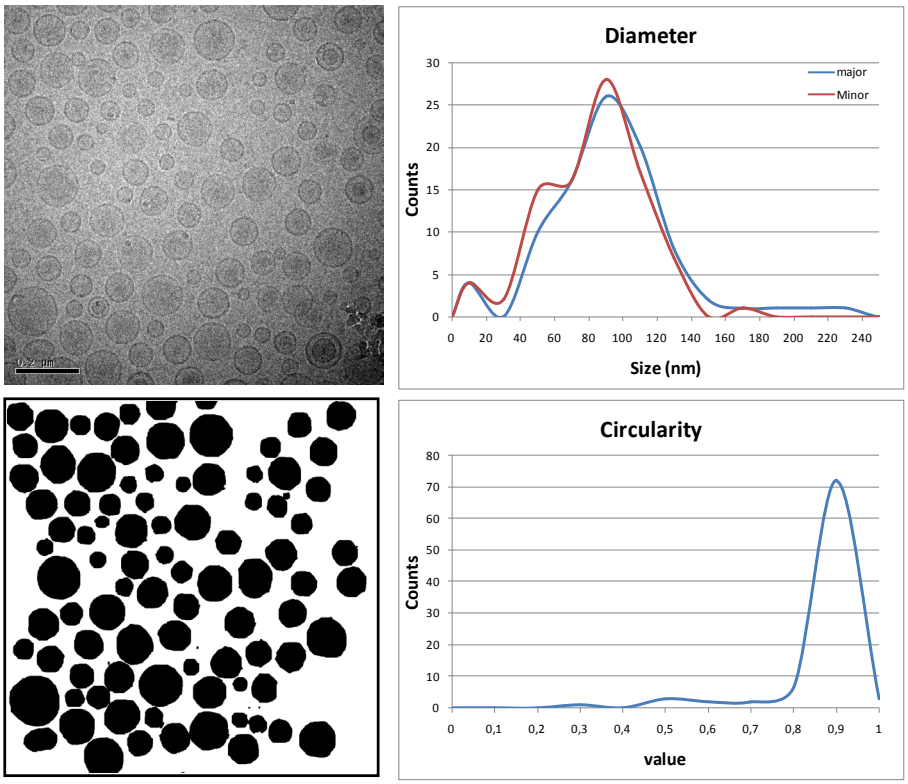

Figure 25. Liposome cryo-TEM picture analysis to determine both particle diameter and circularity. Gray-scale pictures were transformed in binary images, and further analyzed with imageJ.

Size distribution was centered in ca. 100 nm of diameter. Circularity, defined as the ratio between the two major perpendicular radii of the particles, was determined. A mean circularity of 0.9 demonstrated that liposomes present a highly circular shape on 2D micrographs.

We should mention that DLS diameters are always larger than those obtained from cryo-TEM micrographs, since the first ones represent hydrodynamic diameters in solution (the radius of the nanoparticle plus all water molecules that drags on its movements on the solvent) while the second ones are obtained in solid state samples (frozen samples). Nevertheless, differences are minor, and confirm the validity of the membranes used for extrusion of liposomes, for the preparation of nanoparticles around 100 nm of diameter.

5.1.2 Detection of liposomes by fluorescence.

Fluorescence microscopy was used to assess the effectiveness of the fluorescent labeling of liposomes, which incorporate rhodamine-PE in their structure. Microscopy pictures of a solution of regular liposomes synthesized at our laboratories is presented on figure 26.

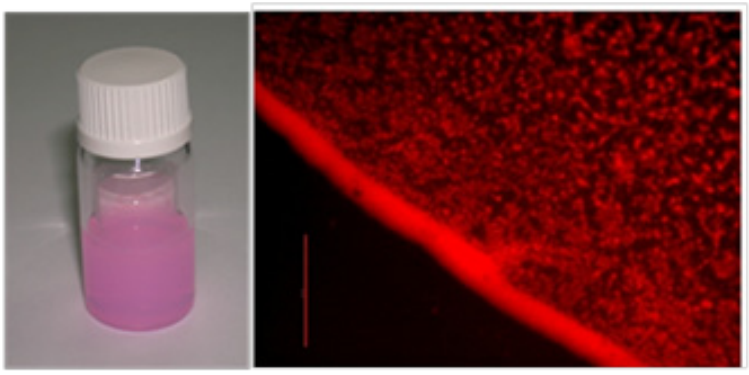

Figure 26. (Left) liposome solution with its characteristic pink color, due to the presence or rhodamine within their structure. (Right) Drop of liposomes under a fluorescence microscope.

5.1.3 Detection of liposomes by MRI.

Liposomes also contain a gadolinium chelate in their structure, and therefore are susceptible to be detected in T1 weighted MR images. To demonstrate this fact, a 20 μl of a liposomes solution (concentration 10 mM) was injected intra-parenchymally to an animal, and T1-weighted images were acquired (figure 27)

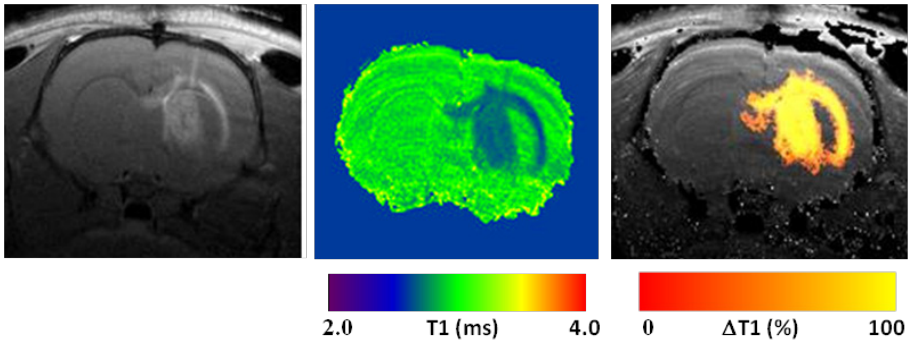

Figure 27. Liposomes injected on a rat brain and detected by MRI. (A) T1-weighted image. (B) T1 map. (c) Map of change in T1 values, expressed as (%) of the minimum T1 detected.

5.1.4. Cell culture transfection

We tested the capacity of liposomes to be incorporated into cells, in a series of transfection experiments.

Primary rat astrocytes were cultured and exposed to different concentrations of liposomes. Using poly-D lysine 12-well plates, 700.000 cells were plated in every well, except the last one that performed as a control. Different liposome concentrations were applied to each well, as it is represented in figure 28. After 24 hours of incubation, supernatant liposome-loaded medium was removed from cell wells, further washed three times with HBS. Plates were visualized under the microscope.

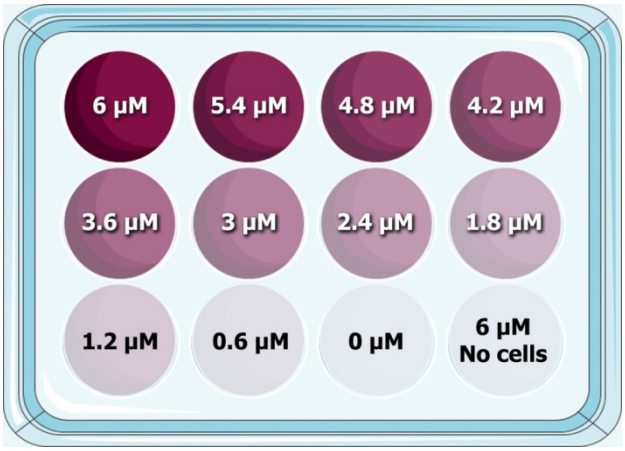

Figure 28. Schematic representation of a culture plate (700.000 cells in each well) treated with rising liposome concentrations.

As we can see on figure 29, Astrocytes incorporated the liposomes in the cytoplasm, without the need of a lipofecting agent, but such process required a long incubating time (24 h).

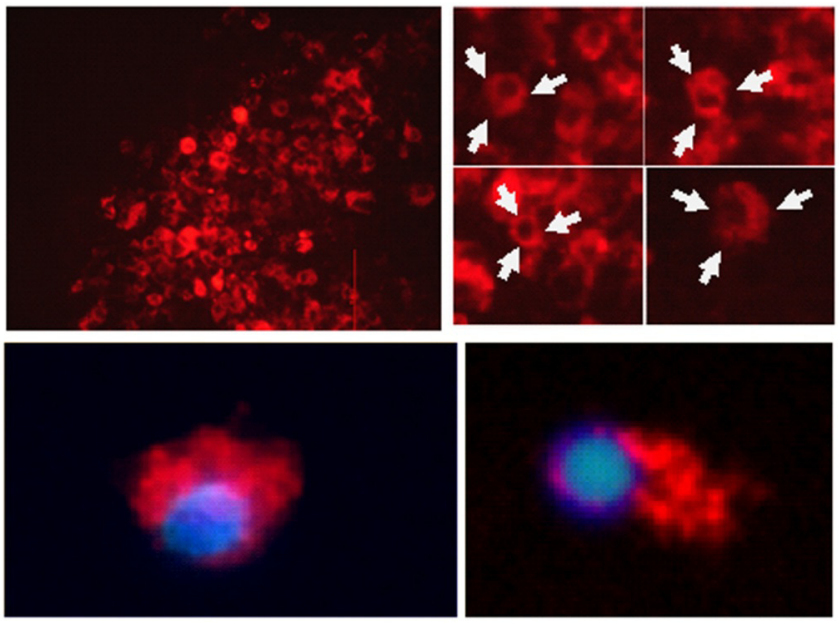

Figure 29. Fluorescence microscopy pictures showing the incorporation of liposomes (red) in the cytoplasm of cultured rat astrocytes. Cells' nuclei were stained with Hoescht (blue).

Fluorescence of each well was quantified using a plate reader, using plates from 3 different studies performed on the same way. In this way we quantified the efficiency of cell transfection at different concentration of liposomes (figure 30).

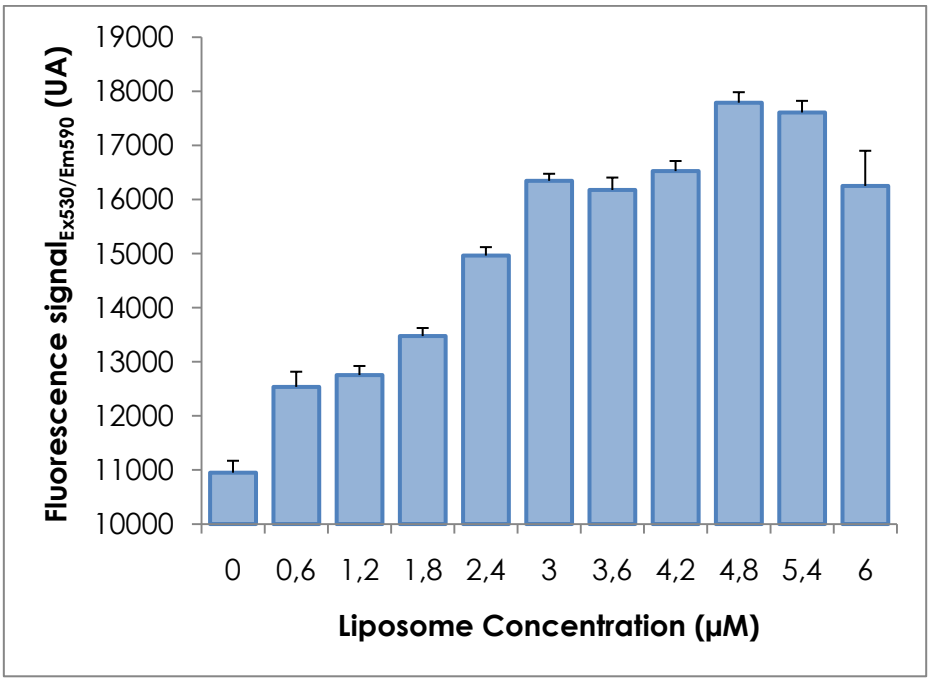

Figure 30. Fluorescence intensity of rat primary astrocytes in culture, incubated with different concentrations of rhodamine-labeled liposomes.

As we can see on figure 30, fluorescence increased almost linearly with the concentration of liposomes until it reached a plateau around a concentration of 3 to 6 µM of liposomes.

5.1.5. Magnetic Properties of liposomes

To characterize the magnetic properties of liposomes as T1 contrast agent we performed a series of relaxation studies on our MR system. On a typical experiment, 24 seriated dilutions of a liposomes solution ca. $1.0x10^{-4}$ mM were prepared. Gd

concentration in these solutions of liposomes was then calculated, and typically ranged 0.03 to 2 mM. Finally, T1 and T2 relaxation times, and corresponding relaxation rates (R1=1/T1 and R2=1/T2) were then calculated at 9.4 Tesla for each solution. A numeric example of these studies is presented in table 3.

[Gd](mM)	**2.09**	**1.67**	**1.34**	**1.07**	**0.85**	**0.68**	**0.55**	**0.44**	**0.35**	**0.28**	**.22**	**0.18**
T1 (s)	220	283	335	402	466	544	635	754	857	971	1110	1270
T2 (ms)	51.5	66.6	76.6	87.3	102	120	137	148	176	205	228	255
R1 (s^{-1})	4.54	3.53	2.99	2.49	2.15	1.84	1.57	1.33	1.17	1.03	0.91	0.79
R2 (s^{-1})	19.4	15.0	13.1	11.5	9.80	8.33	7.30	6.76	5.68	4.88	4.39	3.92

[Gd](mM)	**0.21**	**0.17**	**0.13**	**0.11**	**0.08**	**0.07**	**0.05**	**0.04**	**0.03**	**0.03**	**0.02**	**0.02**
T1 (s)	1560	1650	1780	1930	2170	2230	2320	2440	2630	2650	2720	2780
T2 (ms)	301	333	366	379	424	454	477	471	505	567	576	526
R1 (s^{-1})	0.64	0.61	0.56	0.52	0.46	0.45	0.43	0.41	0.38	0.38	0.37	0.36
R2 (s^{-1})	3.32	3.00	2.73	2.64	2.36	2.20	2.10	2.12	1.98	1.76	1.76	1.90

Table 3. Relaxivity measurements of different solutions of liposomes. Concentrations refer to gadolinium present in them.

Plots of relaxation rates versus concentration of gadolinium, and their corresponding linear regressions, are represented in figure 31. Relaxivity values for the contrast agent were calculated from the slope of the linear plots, resulting **r1=1.98 $mM^{-1}s^{-1}$** (r^2=0.996) and **r2=8.38 $mM^{-1}s^{-1}$** (r^2=0.988). Similar values were obtained for successive batches of liposomes prepared in the same way.

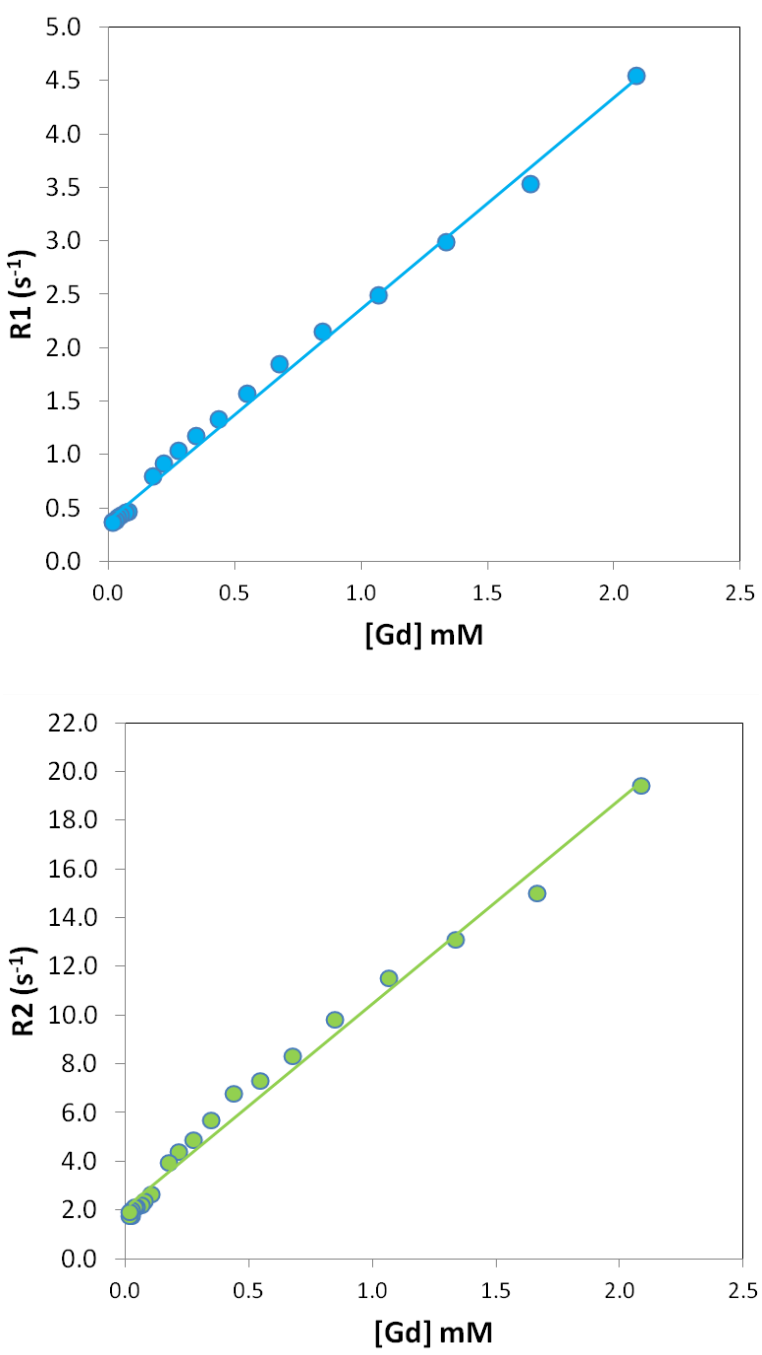

Figure 31. R1 and R2 relaxation rates values for different solutions of liposomes, adjusted to linear regression.

5.1.6. In vivo visualization of liposomes

Next step on this research was to calculate the minimum concentration of liposomes (gadolinium) required to be able to detect them *in vivo*. This step is necessary to estimate the amount of liposomes that should be administered in *in vivo* studies, in order to be able to detect liposomes in the brain, in future studies.

In a first set of experiments we determined the relaxation rates of an ischemic rat brain. Thus we obtained values for normal and ischemic brain tissues, together with the vehicle used to prepare liposomes solutions (Hepes 20 mM) and a solution of gadolinium doped liposomes (~10 mM). For that, a series of T1 weighted images were acquired with different repetition times, to fit them to a saturation-recovery scheme. The relaxation rates found for all the studied systems were:

Sample	Rat brain	Ischemic tissue (6h post MCAO)	Vehicle (Hepes 20 mM)	Liposomes (10 mM)
T1 (ms)	3212 ± 345	3944 ± 387	3200 ± 300	140 ± 4
R1 (s^{-1})	0.31	0.26	0.31	7.1

Table 4. Relaxation rates for different brain tissues and samples.

As we can see, there is a difference of 0.5 s^{-1} for the value of the relaxation rate of ischemic and normal brain tissues. Although there is certain variability on the relaxation times and rates observed for different animals, the difference between ischemic tissue and healthy tissue remains pretty constant ~ 0.5 s^{-1}, as we observed on successive studies.

We designed a second study in which we arbitrarily decided that, if a difference on relaxation rates of 0.5 s^{-1} is good to generate a detectable contrast between ischemic and normal brain tissue, the injection of liposomes on the brain should contain such amount of them that induces a relaxation rate of $R1_{tissue}$ + 0.5 s^{-1}, in order to be able to visualize the liposomes in the rat brain.

Thus, we prepared a solution of liposomes in Hepes (10 mM) that contained an amount of [Gd]=0.22 mM. From that solution we prepared a series of dilutions, and we determined their longitudinal relaxation times (from which relaxation rates were calculated). Finally we plotted the relaxation rates of such solutions versus their content on gadolinium (figure 32).

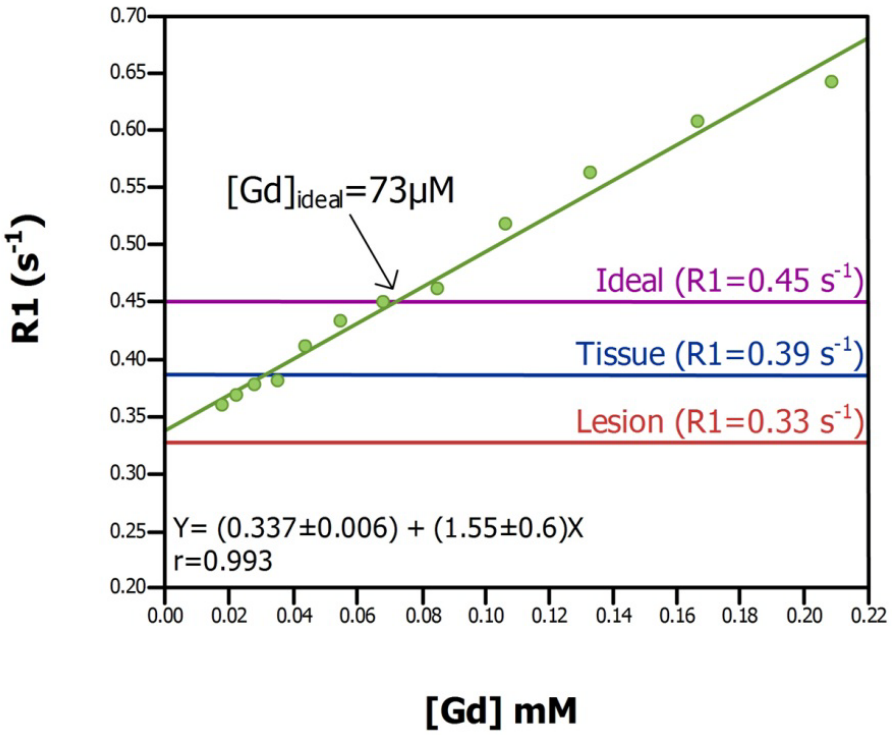

Figure 32. Relaxation rates of a series of solutions of liposomes of different concentration containing different concentrations of Gd. The relaxation times of ischemic tissue, normal brain tissue, and an arbitrary value of R1normal tissue + 0.5 s^{-1}.

Thereafter, relaxation rates of ischemic (0.33 s^{-1}) and normal (0.39 s^{-1}) brain tissues were measured on a rat, and an arbitrary value of 0.45 s^{-1} ($R1_{normal\ tissue}$ + 0.5) was chosen as "minimal [Gd] required for good contrast between liposomes / brain tissues", as shown in figure 32.

From this study we concluded that, for the sort of liposomes prepared on our laboratories, we should reach a concentration of them in the brain parenchyma that carry a concentration of gadolinium of, at least, [Gd]=73 μM, in order to induce a relaxation rate of 0.45 s^{-1}, in order to be distinguished from normal, and therefore form ischemic brain. To test this hypothesis we decide to perform 4 intraparenchymal injections of contrast agent on the brain of the animal, using a concentration of 70 μM of Gd for two of them (one in ischemic and one in normal tissue), and a concentration of 18 μM of Gd (4 times lower than the arbitrary threshold value selected) for the other two, as depicted on figure 33.

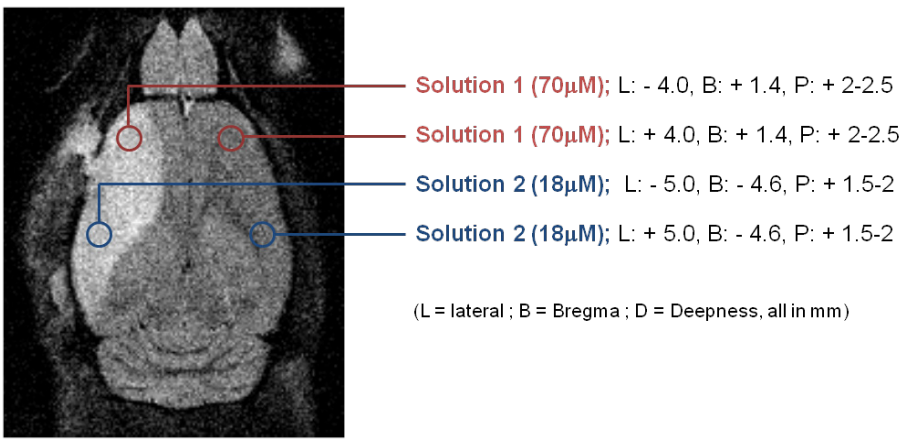

Figure 33. T2-weighted coronal MR image of a rat with a cerebral ischemia, a overlaying the schematic representation of the four liposome injection sites.

Following the injection of the solutions of liposomes, T1 and R1 maps of the brain were obtained, as presented on figure 34.

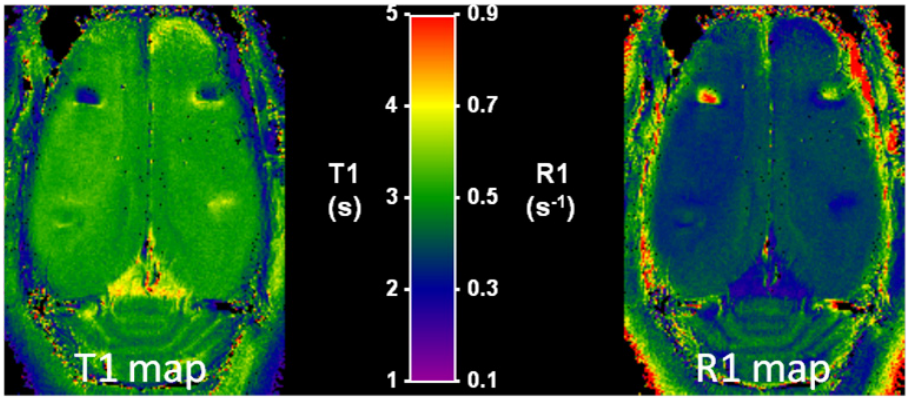

Figure 34. T1 and R1 of an ischemic animal, following the injection of two solutions of liposomes (containing [Gd]=70 M and [Gd]=18 M, respectively). Only solutions above the selected threshold of [Gd] are clearly visible on the maps.

As we can see on figure 34, both solutions containing an amount of gadolinium reaching the arbitrarily selected threshold of [Gd]=73 μM are visible on both, the ischemic and healthy tissue, as areas or reduced T1 / increased R1 values. Those solutions under the selected threshold are not identified so easily. We finally proceed to calculate the T1 and R1 values of the 4 injection spots in the maps, and compare them with the expected theoretical values for the solutions, calculated from the relaxivity plot presented in figure 32. Results (presented in table 5) confirm a good agreement between calculated and experimentally measured values.

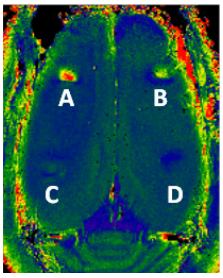

R1 (s^{-1})	Spot A	Spot B	Spot C	Spot D
Calculated	0.45	0.45	0.36	0.36
Measured R1	0.50	0.42	0.38	0.35

Table 5. Relaxivities measurements of for different brain tissues and samples.

5.2. PERI-INFARCT TARGET IDENTIFICATION

This work aims to vectorize liposomes to target the peri-infarct region. Therefore, a second phase on our studies consisted on the search for molecular markers of such zone, so they can be used as targets, using both 2D electrophoresis and COFRADIC techniques, as described under the methods section.

For these studies, brain samples from ischemic rats (infarct, peri-infarct and contralateral, healthy, tissue samples as describes in under the methods section) were sub-fractioned in three different fractions of proteins; membrane proteins, soluble and insoluble protein fractions. Sub-fractioning of samples was achieved by using a commercially available kit, as described before. Sub-fractioning allowed for an increment in the resolution of the study (less proteins per fraction involve a better discrimination among them), and also allowed us to focus on membrane targets, as cell membrane is the first contact site that nanoparticles will reach when interacting with cells over-expressing those proteins. It is obvious that if the selected target would be located at the nucleus of the cell, liposomes would have to be transfected into cell cytoplasm, before any molecular recognition process could take place, between cell target and liposome vector. A description of the results obtained by both techniques, as well as the validation of these results by Western-Blot and immunohistochemistry is presented next.

5.2.1. Bi-dimensional electrophoresis

5.2.1.1. 2D-PAGE: membrane proteins fraction

An average of 962 spots was identified in electrophoresis gels of samples corresponding to the membrane fraction of proteins. The reproducibility on the preparation of gels from the peri-infarct region and the contralateral (healthy) tissue was assessed by a reproducibility plot (as shown in figure 35). This preliminary

step is necessary to ensure that gels are prepared in the same way, in order to compare their protein expression in the same conditions. In this sort of plot, mean spot intensity of all gels of the contralateral region is plotted in the X axis, against mean spot intensity of all gels of the peri-infarct region, in the Y axis. A slope of 1 on this plot indicates a good correlation between samples to be compared. The obtained regression line (slope = 0.967) and the corresponding correlation coefficient (0.921) were determined (figure 35), indicating a highly reproducibility degree of the technique, which in turn enables a comparative analysis to be made.

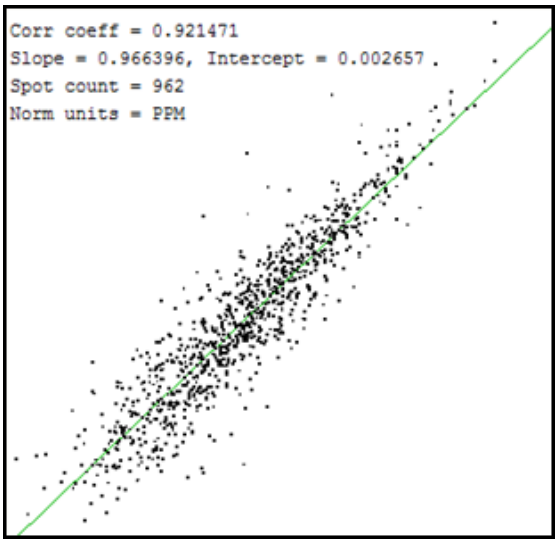

Figure 35. Interindividual reproducibility of samples of the membrane fraction of proteins. Mean spot intensity in gels of the contralateral region are shown in the X axis, whereas mean spot intensity in gels of the peri-infarct region are plotted in the Y axis. The green line represents the regression line of the scatter plot.

Two representative gels of proteins belonging to the membrane fraction of the contralateral and peri-infarct area tissue samples can be seen in figure 36.

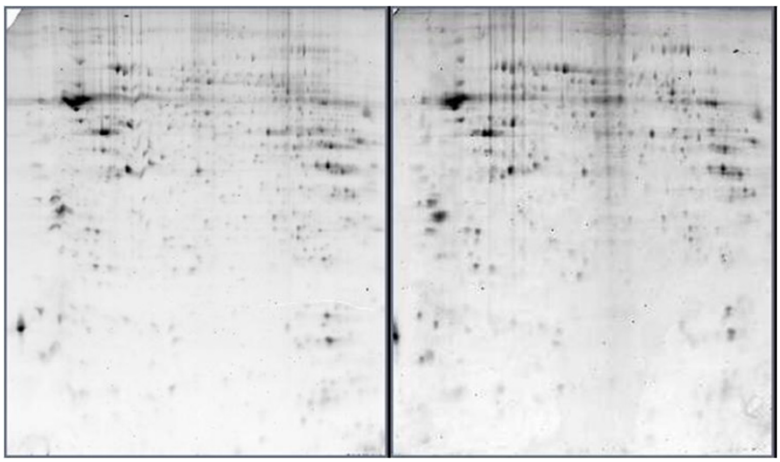

Figure 36. 2D electrophoresis gels of the membrane fraction of proteins. Each spot of the gels represent at different protein (or protein fraction) of the contralateral tissue (left) and the peri-infarct region tissue (right).

A qualitative analysis of all spots in the gels did not reveal a any protein expressed exclusively in either one of the tissues studied (contralateral or peri-infarct). These results do not discard the potential expression of a specific protein whose concentration remains below the detection limit of the technique.

A digital densitometer was used to scan the gels to quantify the intensity of the spots, directly related to the concentration of protein. This procedure allows the quantification of protein expression, and the analysis of statistically significant differences. Results corresponding to the quantification of the 4 differential spots found on our samples are presented in table 6.

The quantitative analysis revealed the presence of 4 spots in the gels, whose expression was at least 3-fold greater in the peri-infarct region than in the contralateral tissue (figure 37). Such threshold to consider a significant qualitative difference on protein expression between samples is generalized in 2D-PAGE studies.

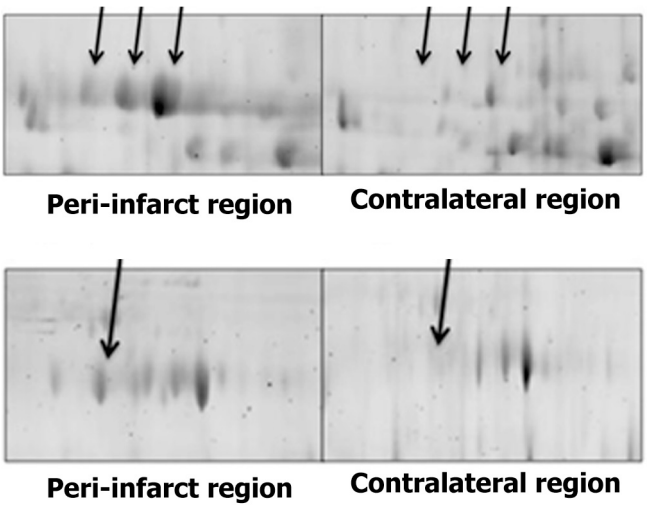

Figure 37. Fragments of 2D gels where the four qualitative differences in protein expression were found.

SPOT ID	Contralateral tissue Intensity (a.u.)	Peri-infarct tissue intensity (a.u.)	ratio
3813	279.8±134.9	2064.1±874.8	7.4
3901	1776.2±481.0	11326.3±2200.2	6.4
3908	503.3±257.1	5038.3±1237.7	10.0
6908	756.6±318.6	3116.2±1370.8	4.2

Table 6. Spot quantification for all four differential spots found on brain tissue gels. Results represent mean ± SD in arbitrary units.

The differential spots found, and generically named as 3813, 3901, 3908 and 6908 by the analysis software were isolated on preparative gels, and processed for mass spectrometry analysis, which allowed us to identify them. Spots 3813, 3901 and 3908 corresponded to **albumin**, whereas spot 6908 was identified as **serumtransferrin**.

5.2.1.2. 2D-PAGE: insoluble proteins fraction

Insoluble fraction 2D gel analysis produced an average of 1632 spots (figure 38), with a gel reproducibility of 0.92 (figure 39).

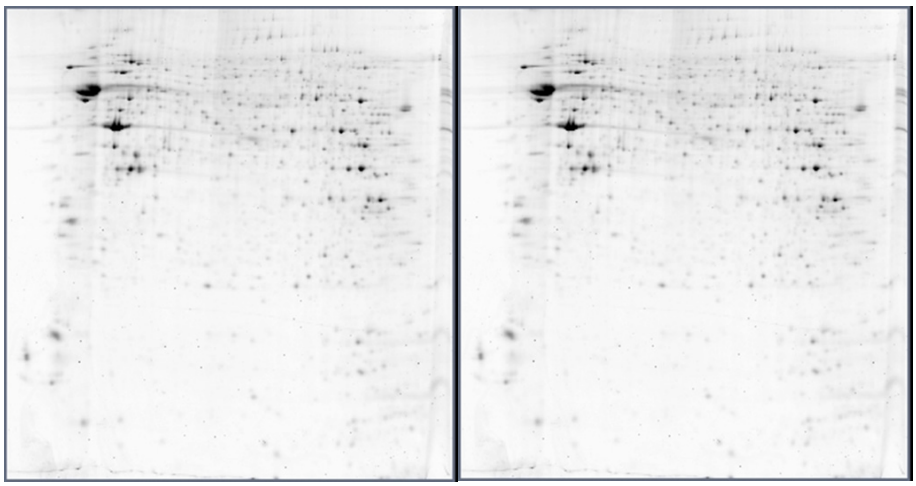

Figure 38. 2D gels of the insoluble proteins fraction of both contralateral tissue (left), and peri-infarct region tissue (right).

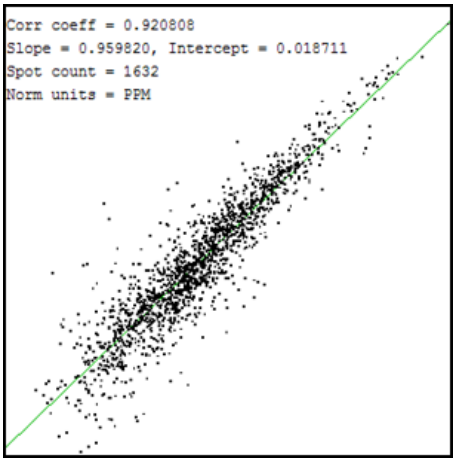

Figure 39. Interindividual reproducibility plot of the insoluble proteins fraction. Mean intensity of each spot on gels of the contralateral region (X axis) are plotted against those of the peri-infarct region (Y axis). The green line represents the regression line of the scatter points.

A qualitative analysis of the gels did not revealed any differential protein expressed exclusively in either one of the regions (contralateral or peri-infarct).

In the quantitative analysis of intensities we found 9 spots whose expression was statistically significantly different and at least 3-fold in the peri-infarct region (figure 40).

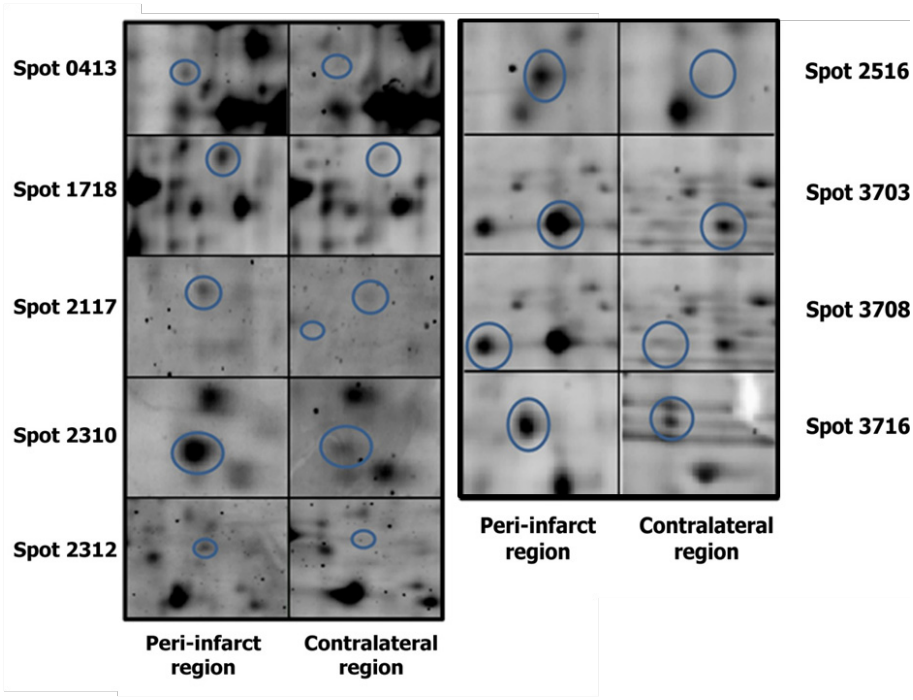

Figure 40. Gel fragments of the insoluble proteins fraction with at least 3-fold expression in the peri-infarct vs. contralateral region.

Results of the quantification of these spots after scanning the gels on a digital densitometer are presented in table 7.

SPOT ID	Contralateral tissue Intensity (a.u.)	Peri-infarct tissue intensity (a.u.)	ratio
S0413	10.5±19.8	128.3±46.4	12.2
S1718	27.2±37.2	442.6±179.9	16.3
S2117	35.1±32.5	188.6±68.1	5.4
S2310	29.8±29.4	317.4±126.5	10.6
S2312	12.2±11.3	48.4±20.7	4.0
S2516	77.7±46.2	341.8±98.7	4.4
S3703	325.6±301.6	1334.3±604.2	4.1
S3708	106.1±67.7	572.7±379.1	5.4
S3716	95.1±27.3	369.8±232.1	3.9

Table 7. Differential spot quantification of all nine spots described above. Results are showed as mean ± SD.

Differential spots were isolated and analyzed by mass spectrometry (see an example on figure 41). Identified proteins for each differential spot are presented on table 8.

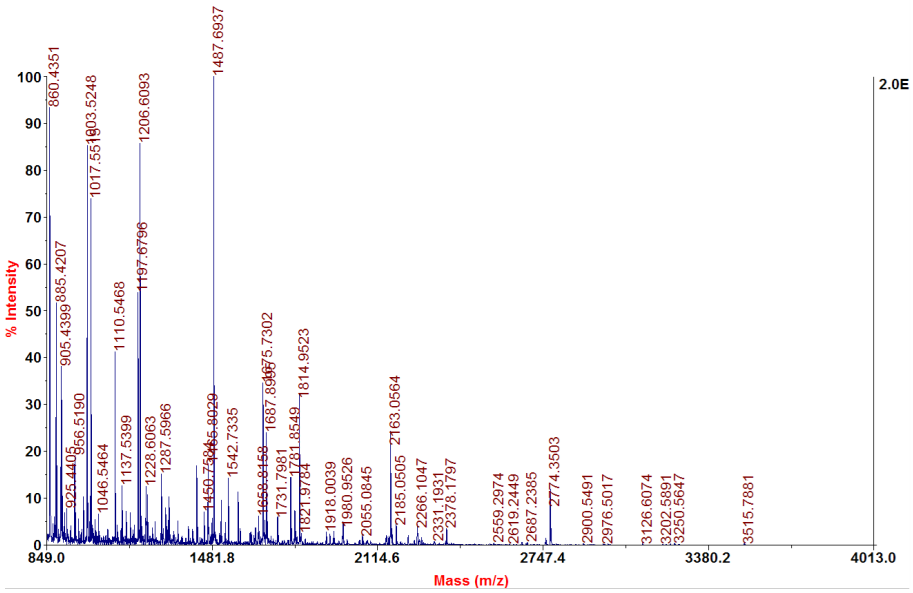

Figure 41. Mass spectrum of spot 3716.

SPOT ID	PROTEIN
0413	Eukaryotic translation initiation factor 2
1718	Tubulin beta 2C chain
2117	Heat Shock protein beta 1
2310	Heat Shock protein beta 1
2312	Prohibitin
2516	Actin cytoplasmic 1
3703	Serum albumin
3708	Serum albumin
3716	Heat Shock Protein 70 KDa

Table 8. Differential proteins of the insoluble fraction of peri-infarct region, as identified by mass spectrometry.

5.2.1.3. 2D-PAGE: soluble fraction

2D gel analysis of the soluble fraction of proteins produced an average of 814 spots (figure 42), with a gel reproducibility of 0.94 (figure 43).

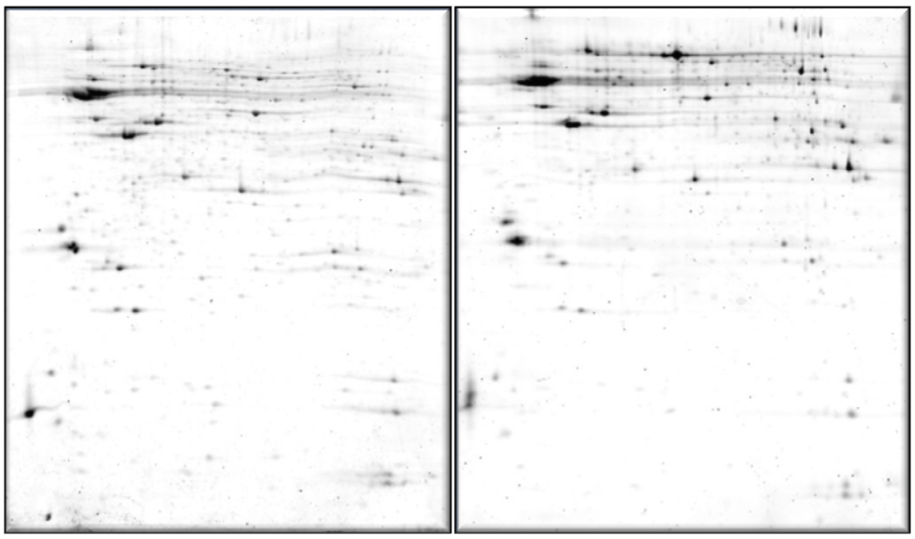

Figure 42. 2D gels of the soluble fractions of proteins at the contralateral (left) and peri-infarct (right) regions.

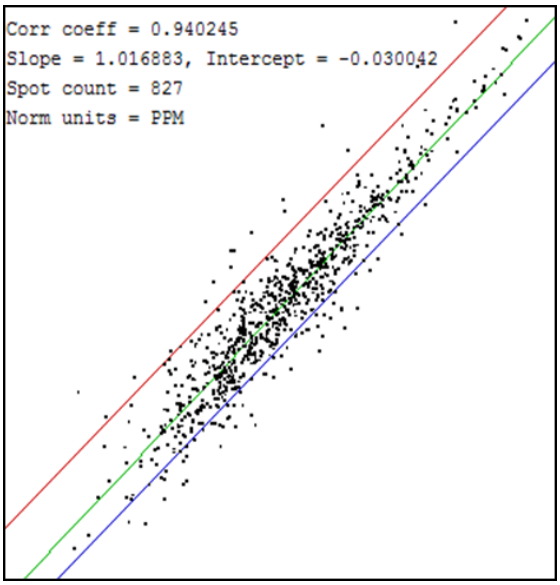

Figure 43. Interindividual reproducibility plot of the insoluble proteins fraction. Mean intensity of each spot on gels of the contralateral region (X axis) are plotted against those of the peri-infarct region (Y axis). The green line represents the regression line of the scatter points.

A qualitative analysis of the gels did not revealed any differential protein expressed exclusively in either one of the regions (contralateral or peri-infarct).

In the quantitative analysis of intensities we found 5 spots whose expression was statistically significantly different and at least 3-fold in the peri-infarct region (figure 44). Results of the quantification of these spots after scanning the gels on a digital densitometer are presented in table 9.

Differential spots were isolated and analyzed by mass spectrometry. Identified proteins for each differential spot are presented on table 10.

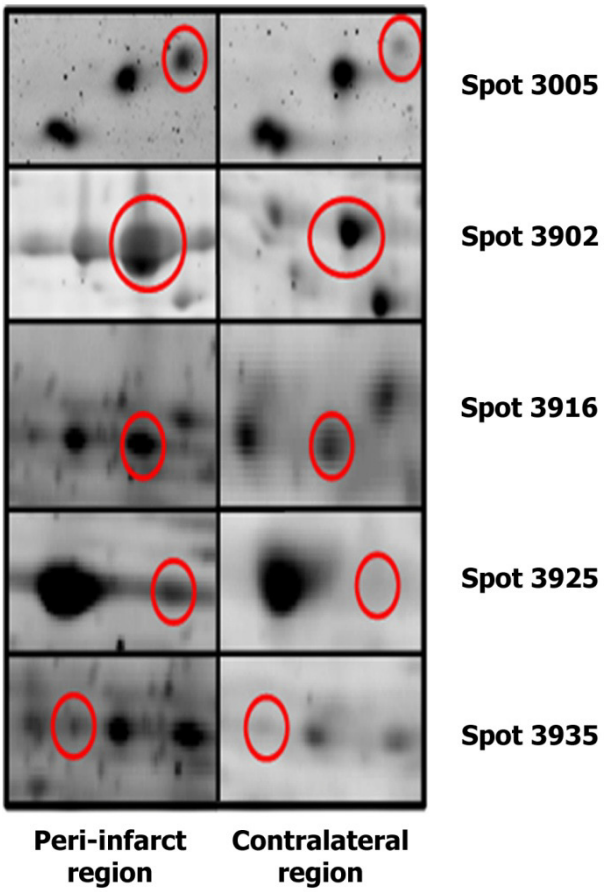

Figure 44. Gel fragments of the soluble proteins fraction with at least 3-fold expression in the peri-infarct vs. contralateral region.

SPOT ID	Contralateral tissue Intensity (a.u.)	Peri-infarct tissue intensity (a.u.)	ratio
3005	215.2±215.5	721.1±479.8	3.3
3902	3521.6±2553.3	11674.5±7673	3.3
3916	334.8±121.8	1121.1±811.2	3.3
3925	566.7±295.4	2989.7±1546.2	5.3
S2312	161.3±105.5	570.7±387.6	3.5

Table 9. Differential spot quantification of all nine spots described above. Results are showed as mean ± SD.

SPOT ID	PROTEIN
3005	Chain A, Rat Transthyretin Complex With Thyroxine (T4)
3902	Dihydropyrimidinase
3916	Dihydropyrimidinase-related protein 2
3925	Dihydropyrimidinase-related protein 2
3935	Dihydropyrimidinase-related protein 2

Table 10. Differential proteins of the soluble fraction of peri-infarct.

5.2.2. COFRADIC

In a parallel series of studies, tissue samples of the contralateral and peri-infarct regions of the brain of an animal were sub-fractioned in membrane, soluble and insoluble fractions and analyzed by the COFRADIC technique, as described on the methods section.

5.2.2.1. COFRADIC: membrane proteins fraction

1358 proteins of the membrane fraction were revealed by COFRADIC. 574 of those proteins were identified as membrane proteins according to the Uniprot database.

Differential analysis revealed 14 proteins expressed at least 3-fold in either the peri-infarct region or the contralateral side. One of those proteins was overexpressed in the contralateral region, whereas the rest were overexpressed in the peri-infarct region. Results of the quantitative analysis are presented on table 11.

Accession Number	Protein name	Peri-infarct/ Contralateral
Q02195	Keratinocyte growth factor	0,17
P19527	Neurofilament light polypeptide	3,38
P12839	Neurofilament medium polypeptide	3,69
P02680	Fibrinogen gamma chain	3,78
P06399	Fibrinogen alpha chain	3,41
P12346	Serotransferrin	4,44
P02770	Serum albumin	5,64
P04639	Apolipoprotein A-I	6,26
P02651	Apolipoprotein A-IV	6,41
Q63041	Alpha-1-macroglobulin	5,99
P09006	Serine protease inhibitor A3N	11,11
P17475	Alpha-1-antiproteinase	10,74
P05544	Serine protease inhibitor A3L	11,38
Q07439	Heat shock 70 kDa protein	20,63

Table 11. Quantitative differential analysis of protein expression of the membrane fraction between the peri-infarct and the contralateral regions.

5.2.2.2. COFRADIC: insoluble fraction

2070 proteins were identified in the insoluble fraction as described previously for the membrane fraction. In this case one protein was down-regulated and 20 were up-regulated in the peri-infarct region. Proteins and their expression ratios are presented in table 12.

Accession Number	Protein name	Peri-infarct/ Contralateral
Q10758	Keratin, type II cytoskeletal 8	0,21
P10362	Secretogranin-2	4,24
P62762	Visinin-like protein 1	4,79
Q63207	Coagulation factor X	5,57
P02680	Fibrinogen gamma chain	5,81
P63039	60 kDa heat shock protein, mitochondrial	6,30
P10354	Chromogranin-A	7,05
P12346	Serotransferrin	7,21
P06866	Haptoglobin	8,48
P21263	Nestin	9,07
P07150	Annexin A1	9,26
Q07439	Heat shock 70 kDa protein	11,56
P04639	Apolipoprotein A-I	11,61
Q5U2V4	Putative phospholipase B-like 1	22,94
P02651	Apolipoprotein A-IV	23,45
P02770	Serum albumin	23,58
P09006	Serine protease inhibitor A3N	27,01
Q8K4C0	Dimethylaniline monooxygenase	27,53
Q63644	Rho-associated protein kinase 1	70,73
Q01177	Plasminogen (EC 3.4.21.7)	288,49
P04276	Vitamin D-binding protein	370,45

Table 12. Quantitative differential analysis of protein expression of the insoluble fraction between the peri-infarct and the contralateral regions.

5.2.2.3. COFRADIC: soluble fraction

1984 proteins were identified in the soluble fractions. From this group of proteins, 39 showed different expression levels between peri-infarct and contralateral regions. All these proteins were up-regulated in the peri-infarct region (table 13).

Accession Number	Protein name	Peri-infarct/ contralateral
P70623	Fatty acid-binding protein, adipocyte	3,27
Q63416	Inter-a-trypsin inhibitor heavy chain H3	3,29
P12839	Neurofilament medium polypeptide	3,48
P19527	Neurofilament light polypeptide	3,61
P16884	Neurofilament heavy polypeptide	3,61
O35763	Moesin	3,74
P31232	Transgelin	3,78
Q5XFX0	Transgelin-2	3,85
Q07936	Annexin A2	3,99
P04961	Proliferating cell nuclear antigen	4,32
P51886	Lumican	4,34
P08649	Complement C4	4,49
P07150	Annexin A1	4,81
O08619	Coagulation factor XIII A chain	5,22
A7E3N2	Neutrophil cytosol factor 2	7,12
P14480	Fibrinogen beta chain	8,16
Q63041	Alpha-1-macroglobulin	8,26
Q6P734	Plasma protease C1 inhibitor	8,33

Table 13a. Quantitative differential analysis of protein expression of the soluble fraction between the peri-infarct and the contralateral regions (continues on next page).

Accession Number	Protein name	Peri-infarct/ contralateral
P06399	Fibrinogen alpha chain	8,52
P04639	Apolipoprotein A-I	8,75
P06866	Haptoglobin	8,78
P02651	Apolipoprotein A-IV	9,09
Q63556	Serine protease inhibitor A3M	9,18
P31211	Corticosteroid-binding globulin	9,58
P12346	Serotransferrin	9,72
P01026	Complement C3	10,03
P14046	Alpha-1-inhibitor 3	10,14
P13635	Ceruloplasmin	10,17
P20760	Ig gamma-2A chain C region	10,47
P05544	Serine protease inhibitor A3L	10,85
P01835	Ig kappa chain C region, B allele	10,94
P10959	Liver carboxylesterase 1	11,25
P02770	Serum albumin	11,84
P20759	Ig gamma-1 chain C region	11,91
P04276	Vitamin D-binding protein	12,59
P02680	Fibrinogen gamma chain	12,71
P09006	Serine protease inhibitor A3N	12,98
Q9WUW3	Complement factor I	14,82
Q07439	Heat shock 70 kDa protein	17,73

Table 13b. Quantitative differential analysis of protein expression of the soluble fraction between the peri-infarct and the contralateral regions.

Among all these proteins, HSP70 stands out with a peri-infarct/contralateral ratio above 10 (figure 45)

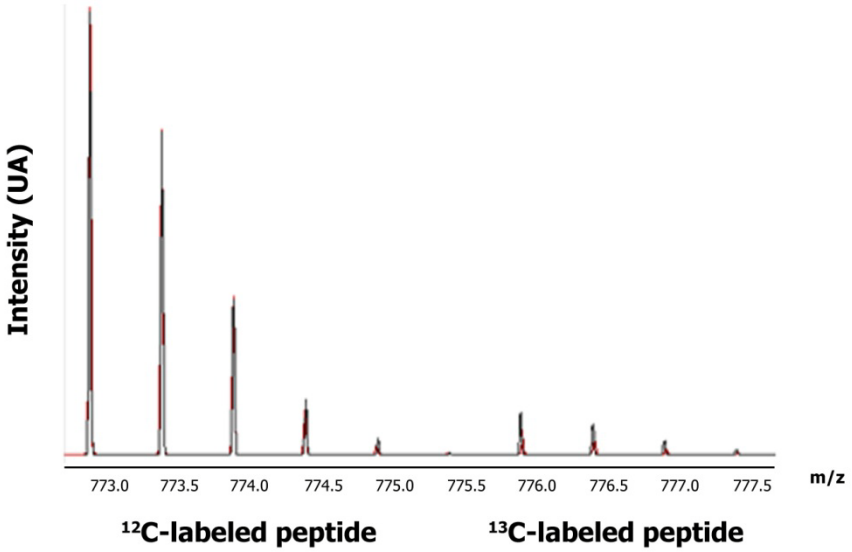

Figure 45. MS spectra showing one peptide of HSP70 from the peri-infarct (12C-labeled) and the contralateral (13C-labeled) regions. Peak intensity is proportional to the peptide quantity.

5.2.3. VALIDATION OF PROTEOMIC RESULTS

All differences on protein expression found by proteomic approaches were quantitative, and no qualitative differences were found. This fact does not discard the existence of specific proteins for the peri-infarct tissue, whose concentration remain under the detection limits of the aforementioned techniques.

It is noteworthy the particular case of the HSP70 family of proteins, cited as specific for the peri-infarct tissue by some authors (see discussion section for details), and the only one coincidental result for both proteomic approaches. Therefore, we decided to deep into the analysis of the expression of the HSP70 protein family by western-blot and immunohistochemical analysis.

5.2.3.1. Western-Blot analysis

No statistically significant differences were observed in a first analysis of HSP70 expression at peri-infarct and contralateral tissue samples by Western-blot (WB) studies (figure 46 left). We learn later that the antibody used on these studies was actually not able to differentiate between different members of the HSP70 family of proteins, and in particular between the inducible (HSP70i, HSP72) and constitutive (HSP70c, HSC70) forms of HSP70. We performed a new WB study in 2D in order to be able to distinguish between both forms (not separated in 1D WB studies).

When we performed a 2-dimensional western-blot analysis we observed one specific spot in for all protein fractions, which was only present in samples from the peri-infarct region, but not in the contralateral (control) tissue (figure 46 right). This spot was identified as the inducible form of the HSP70 protein, while the spot observed for both tissues (peri-infarct and control) was identified as constitutive HSP70.[183]

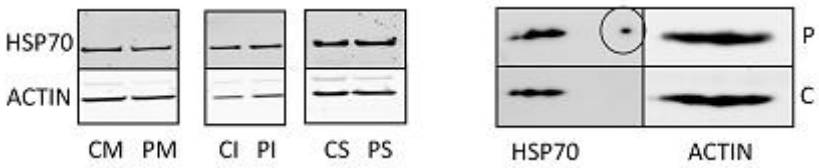

Figure 46. (Left) 1D Western-blot study of HSP70 proteins in sub-fractionated samples (CM, Contralateral membrane fraction; PM Peri-infarct membrane fraction; CI Contralateral insoluble fraction; PI Peri-infarct insoluble fraction; CS Contralateral soluble fraction; PS Peri-infarct soluble fraction), showing equal expression of HSP70 in peri-infarct and contralateral samples. Actin was used as load control. (Right) 2D Western-blot study of HSP70. At the peri-infarct region (P) there are two spots that correspond to the constitutive (the larger) and inducible (the smaller) forms of HPS70. The later (marked with a circle), is absent in the contralateral region (C).

Therefore, 2D WB studies indicated the existence of a minor fraction of HSP70 proteins, specific for the peri-infarct tissue.

5.2.3.2. Immunohistochemistry

Western-blot results were confirmed by immunohistochemical (ICH) studies. In these studies we used the same antibody used for WB studies (unspecific for different members of the HSP family) and a new antibody, specific for the inducible form of this protein. Figure 47 contains the results from the ICH studies with both forms, in consecutive brain slices.

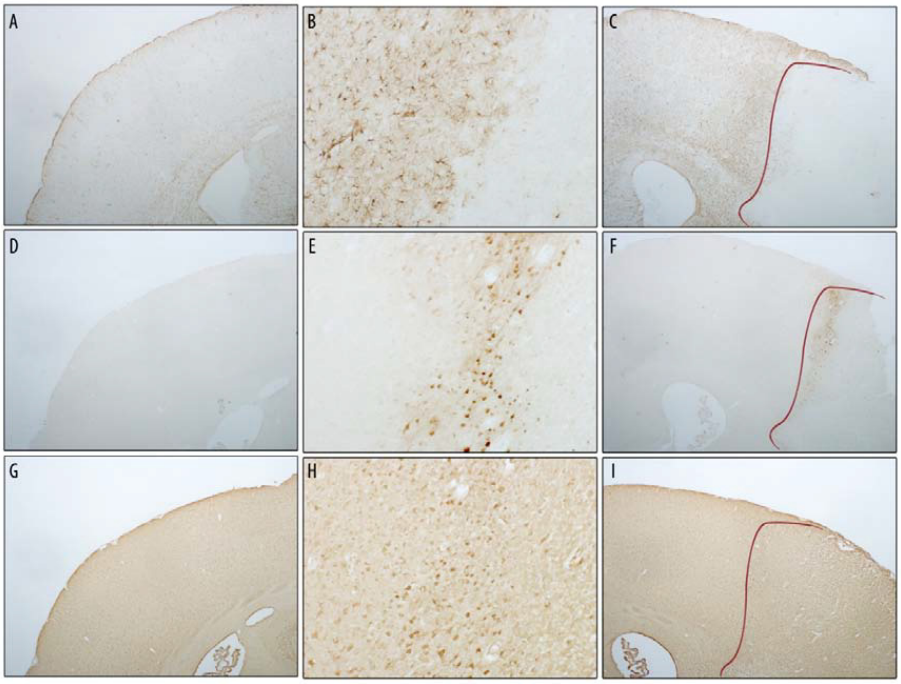

Figure 47. IHC micrographs of consecutive brain slices of 10 µm thickness, showing the contralateral (healthy) tissue at 2x (left column), the ipsilesional tissue at 2x (right column), and an amplification of the lesion border (red line) at 10x (central column). GFAP was used to stain the glial scar surrounding the ischemic lesion (A-C). Anti-HSP72 (or anti-HSP70i) was used to stain the inducible form of HSP70 protein (D-F), and anti-HSC70 (or anti-HSP70c) was used to stain the constitutive form of HSP70 protein.

The antibody specific for the inducible form of HSP70 was able to specifically stain a narrow band of cells at the border of the lesion, corresponding to the peri-infarct region, while the

unspecific antibody revealed the expression of constitutive HSP70 in both brain hemispheres, though a higher expression of the marker was found also at the peri-infarct region (figure 45 H). These results confirm those obtained by proteomic and western-blot studies.

To determine which type of cells of the peri-infarct region undergo an HSP70 up-regulation we performed a double immunofluorescence approach for the staining of GFAP (astrocytes) and FOX3 (neurons), using tissue samples corresponding to 48 hours after the induction of stroke. We firstly stained against astrocytes (GFAP) and HSP72. Upon merging both red and green channels, no positive double staining was perceived (figure 48).

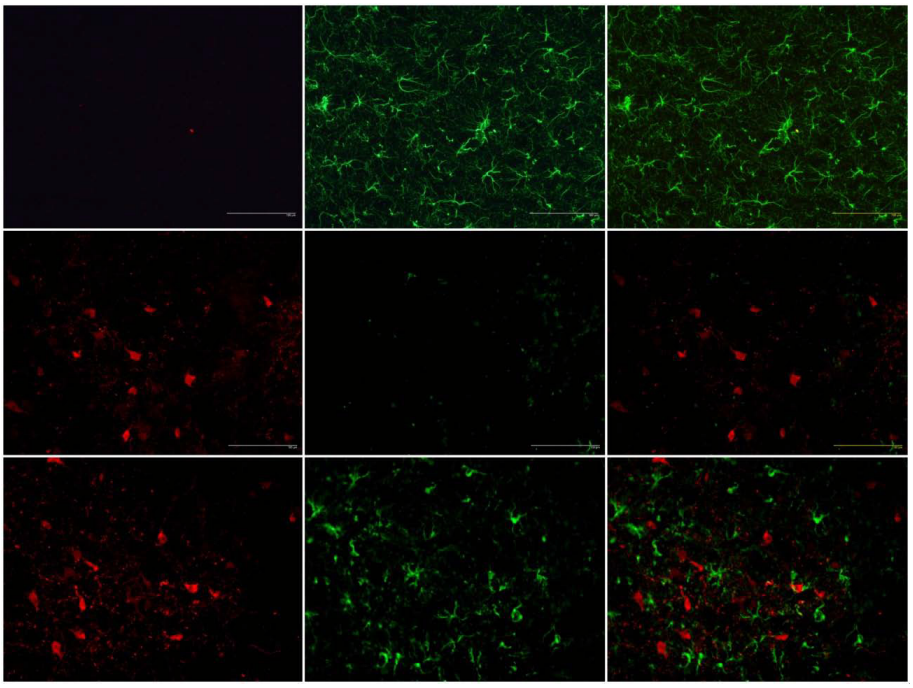

Figure 48. 10x double immunofluorescence images of brain tissue of the contralateral tissue (top row), of the infarct core (middle row) and tissue from the peri–infarct region (lower row). HSP72 (in red, 1st column) and astrocytes (in green, 2nd column) did not co-localized at merged images (3rd column).

In a second study we found a great number of HSP72 positive cells that were also FOX3 (neuron) positive. These results confirm that, at least 48 hours post ischemia, neurons of the peri-infarct region overexpress HSP72 (Figure 49).

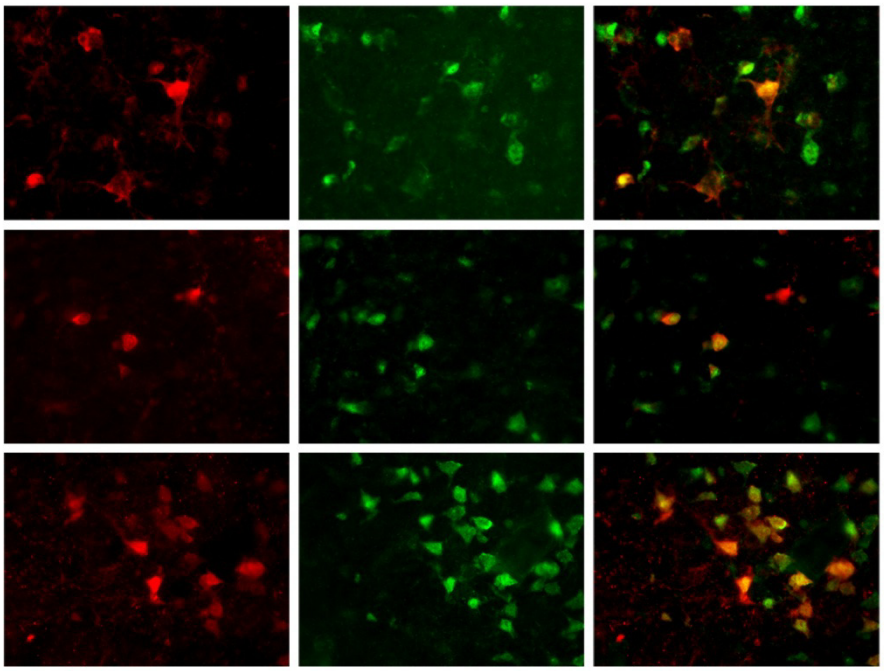

Figure 49. 40x double immunofluorescence images of the peri–infarct region of three different animals (top, middle and lower rows, respectively). HSP72 (in red, 1st column) and neurons (in green, 2nd column) were highly co-localized at merged images (3rd column).

5.2.3.3. HSP72 spatiotemporal dynamics

Once determined that the HSP72 protein is specifically overexpressed in the peri-infarct region following ischemia, we found necessary to characterize the temporal and spatial evolution of the up-regulation of this protein.

We performed a immunohistochemical analysis of protein expression in an animal model of focal transient (90 min)

ischemia. Nine time points were selected for the study, ranging from 6 h to 14 days from the induction of ischemia. An immunohistochemistry approach was taken using a semi-quantitative method to evaluate the degree of expression of HSP72 throughout the serial study. A group of animals was submitted to MCA occlusion and they were sacrificed at the different time points (4 animals per time-point). Brains were extracted and processed for ICH. A representative slice of each brain, corresponding approximately to bregma + 0.5, was selected, stained, and HSP72 positive cells were counted for 5 different regions of the lesion ore and the peri-infarct region, as described under the methods section. No positive expression of HSP72 was observed in the contralateral region. Results of this study are summarized on figure 50 and table 14.

Time	CELL DENSITIES (cell/mm²)				
	Peri-infarct region		Ischemic core region		Average
	Zone 1	Zone 3	Zone 2	Zone 4	
6h	14	14	320	20	92
12h	313	102	333	116	216
24h	136	231	156	41	141
48h	102	177	34	34	87
72h	102	150	61	14	82
5d	48	88	20	0	39
7d	41	68	0	0	27
10d	0	7	0	48	14
14d	41	0	0	0	10

Table 14. Densities of HSP72 positive cells in 10µm brain slices at different time points after induction of ischemia. Areas 1 and 3 correspond to peri-infarct tissue, whereas regions 2 and 4 represent the ischemic core. Results are plotted on figure 48 (note: see methods section for a detailed explanation of this study).

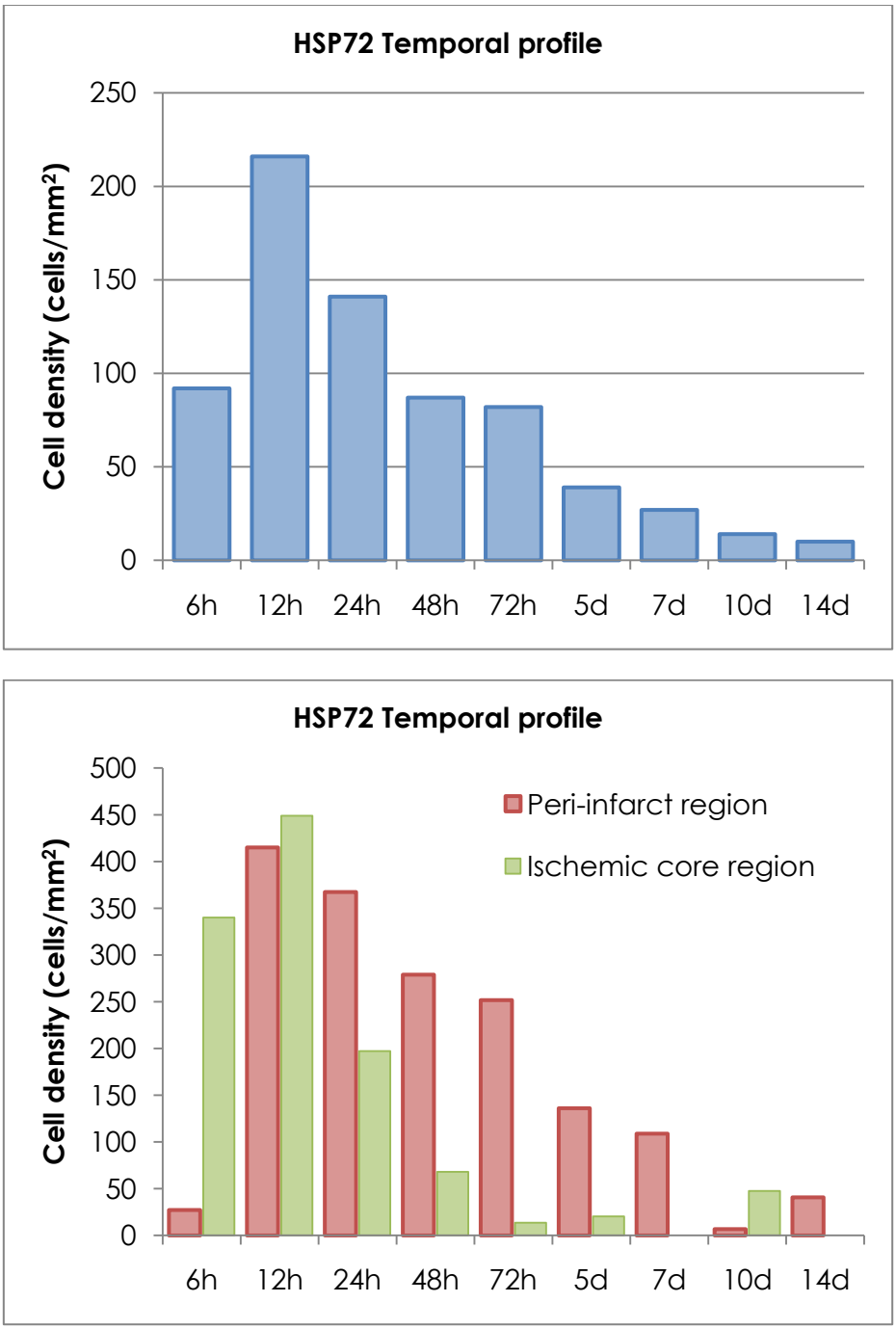

Figure 50. Temporal profile of the densities of HSP72 positive cells, quantified from 10µm brain slices. (Top) average of positive cells in all 4 regions analyzed. (Bottom) expression profile where peri-infarct and ischemic core regions are separated.

Our results indicate that HSP72 can be found as early as 6 hours after an ischemic event, although at this time point the expression is limited to the infarct core, and only a minimal positive staining can be seen at the peri-infarct region. Global expression of HSP72 peaks around 12 hours post ischemia and diminishes over time from that point, turning practically anecdotic by day 14. The expression of HSP72 is not restricted to the peri-infarct area but also includes the infarct core at early time points (6-24 hours). It is only from ca. 24 hours on that HSP72 becomes practically exclusive for the peri-infarct region. Data presented on figure 50 seem to indicate that 48 hours post ischemia is the most suitable time for the use of HSP72 as biomarker of the per-infarct tissue, since at this time point the expression of HSP72 at the peri-infarct region outweighs the one present at the ischemic core. The amount of cells that express HSP72 seems to be high enough to consider it an effective target for theranostics.

Using data presented in table 10 we constructed a density map of the expression of HSP72 post ischemia, overlying cell density maps (expressed in pseudocolor codified images) on a MRI image obtained from the fusion of MRI images obtained from the animals, prior their sacrifice. Density maps are presented in figure 51.

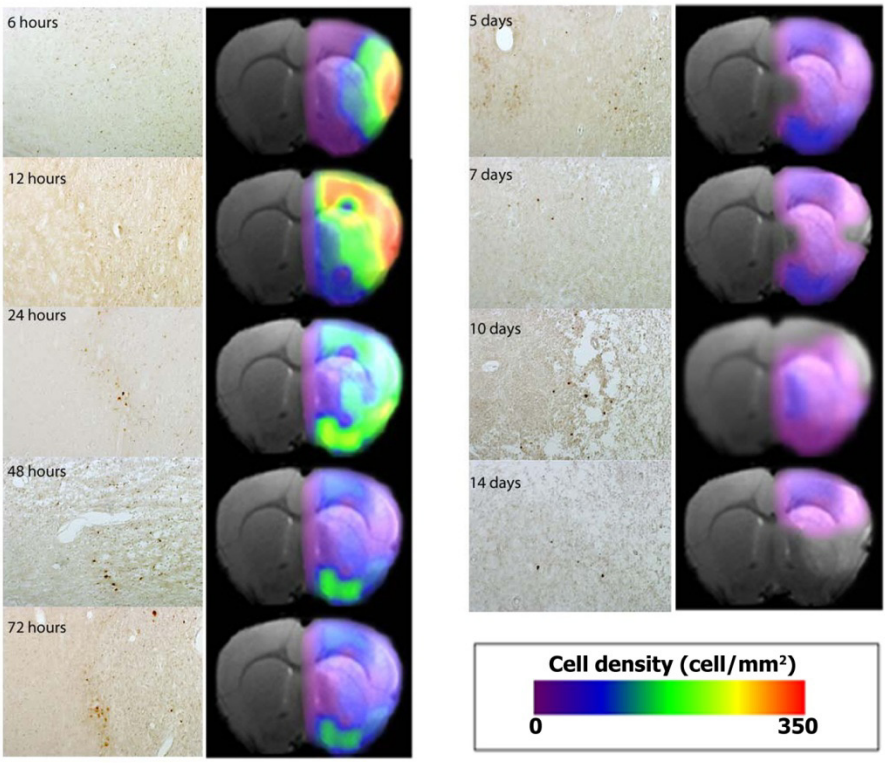

Figure 51. Pseudo-color maps representing densities of HSP72 positive cells at different time points after the induction of cerebral ischemia. Density maps are overlaid on MRI images. Side to side to maps, we present a representative IHC image (20x) of the lesion border.

5.3. *IN VITRO* MOLECULAR RECOGNITION OF TARGETS

The next step on our research, after developing a liposome-based theranostic agent and finding an specific target for it at the peri-infarct tissue, was the *in vitro* demonstration of the capacity of our targeted theranostic systems to interact with cells expressing the selected biomarker, in molecular recognition processes.

5.3.1. Astrocytes

In order to test the coupling efficacy of HSP72 targeted liposomes we performed a molecular recognition *in vitro* study with primary cultures of rat astrocytes. To induce HSP72 overexpression on cells we submitted them to a heat shock, as described elsewhere.[237] As described before, liposomes were labeled with rhodamine, a fluorescent dye that allowed us to visualize them under the microscope, and a gadolinium chelate, a MR contrast agent detectable by MRI. Two culture plats were prepared with astrocytes and upon achieving circa 80% of confluence, one was used as control cell culture, and a second one was submitted to a short thermal shock (15-30 minutes. After this period, both culture plates were allowed to rest for a period of 6 h on an incubator, and after that period cells on different wells were incubated with a) HSP72 targeted liposomes, b) untargeted liposomes or c) vehicle, as described under the methods section. Two incubation periods were tested (30 min or 1 hour), after which cultures where washed to remove the excess of liposomes not trapped by cells, and wells where observed under a fluorescence microscope. Fluorescence levels were roughly evaluated and data is presented on table 15 and figure 52.

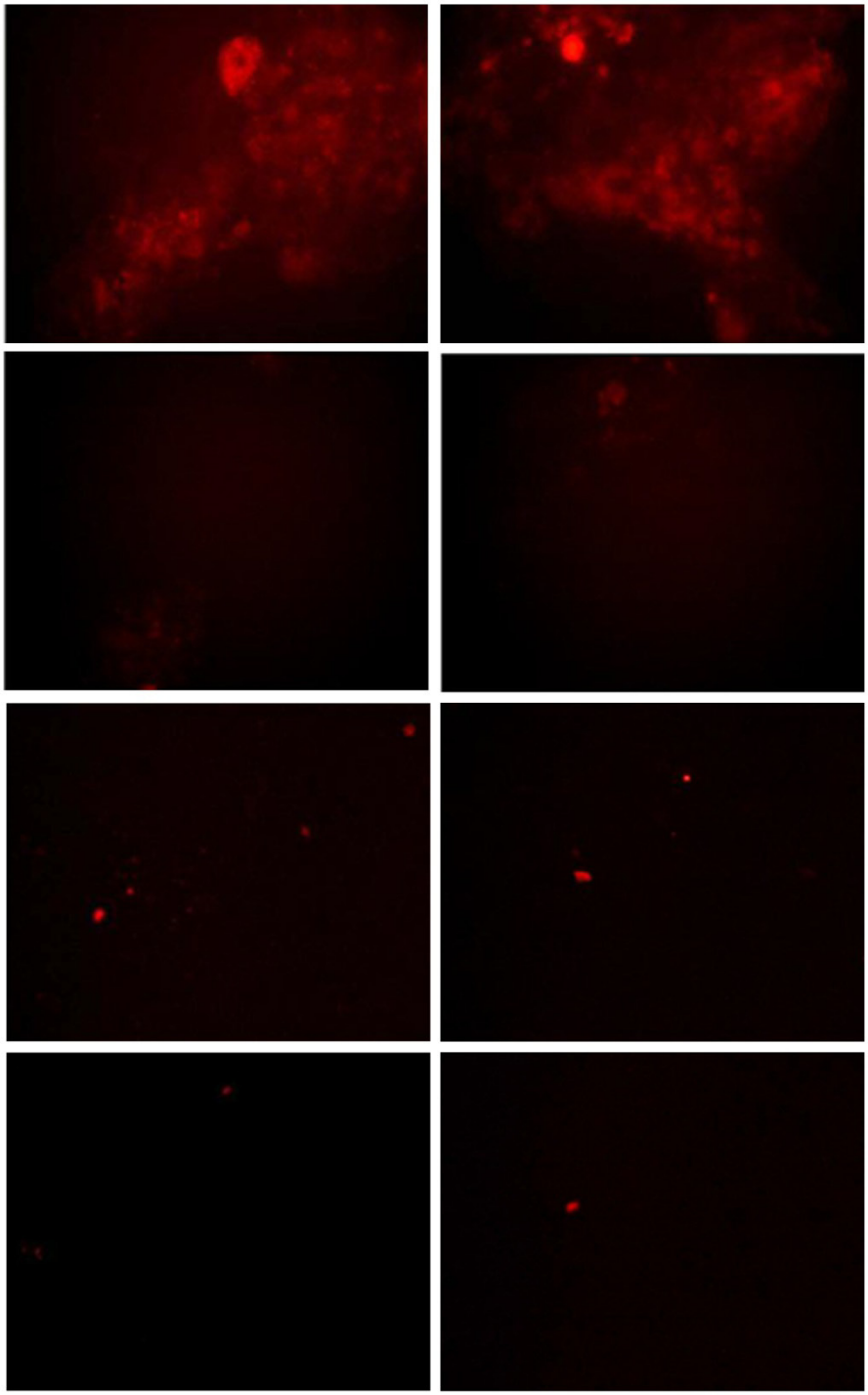

Figure 52. Astrocytes in culture transfected with HSP72 targeted liposomes (upper row), untargeted liposomes (middle row) or vehicle (lower row). Incubation time was 30 minutes (left column) or 1 hour (right column).

ASTROCYTES	LIPOSOMES	
	HSP72-targeted	Control
HSP72 (+)	++	-+
HSP72 (-)	+-	--

Table 15. Relative fluorescence in cultured astrocytes incubated with HSP72 targeted or (control) untargeted liposomes.

Transfection efficiency was not significantly affected by the incubation time, as observed in figure 52. Cells overexpressing HSP72 showed a strong fluorescence signal after incubation with targeted liposomes while a low (residual) fluorescence signal was detected when cells were incubated with untargeted liposomes instead. A residual fluorescence signal was also detected when control cells where incubated with both targeted and untargeted liposomes.

Once these experiments were finished, cells where harvested form plates and introduced in Eppendorf tubes, centrifuged, and supernatant was removed, leaving cell pellets on the tubes. Such tubes were introduced on our 9.4T MRI system and scanned following a saturation-recovery scheme, to obtain the longitudinal relaxation times (T1) of each cell pellet, which should be affected in cells transfected with gadolinium doped liposomes. Results of this study are presented on figure 53.

As we can see on figure 53, only the combination of HSP72 positive cells with HSP72 targeted liposomes led to a noticeable reduction of T1 relaxation time. Neither the combination of HSP72 positive and negative cells with untargeted liposomes, nor the combination of HSP72 negative cells with HSP72 targeted liposomes induced a significant reduction of T1 relaxation times with respect to cell culture media, used as control.

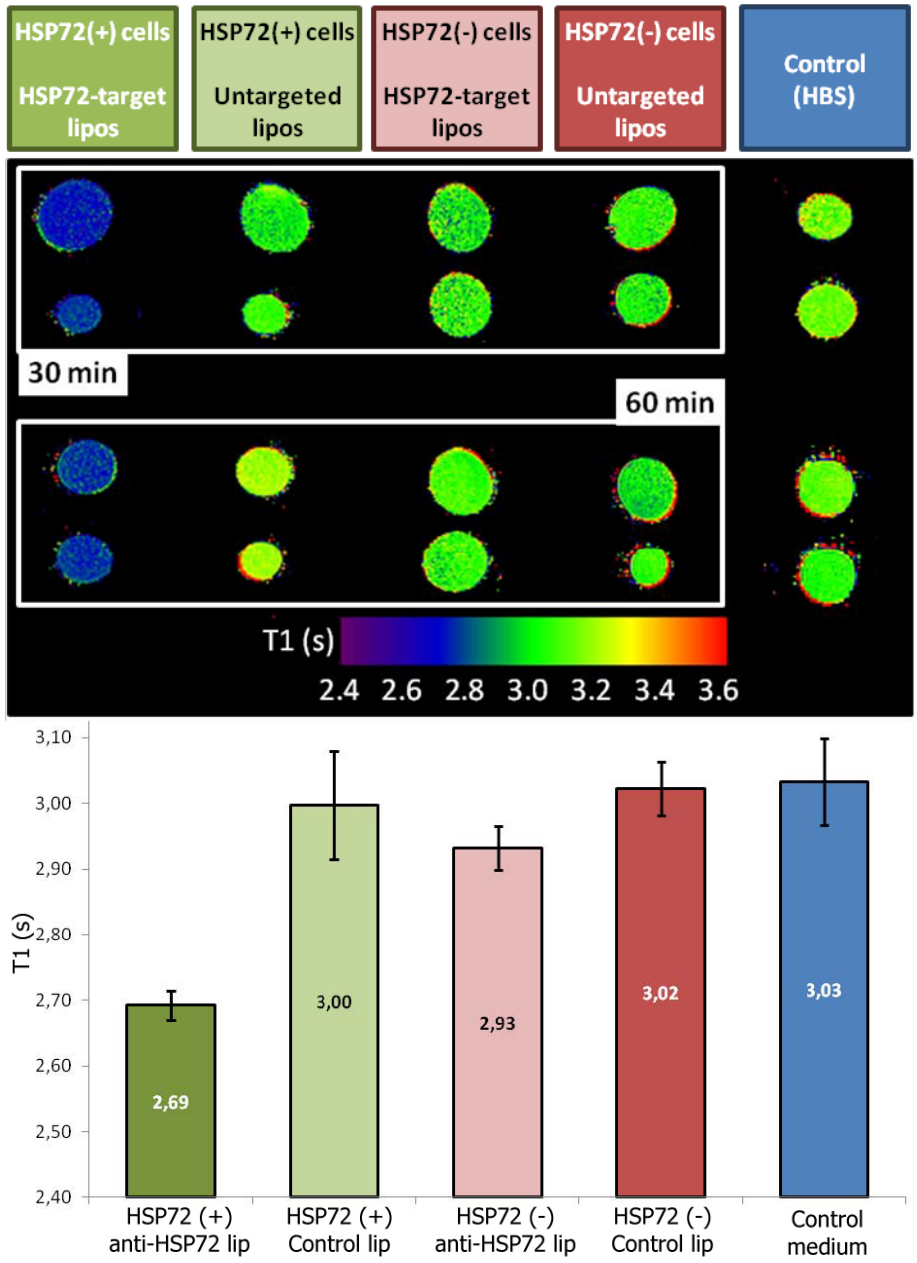

Figure 53. (Top) T1 maps (cross-sectional MR slice of 1 mm) of astrocyte's cell pellets. Incubation times are presented on the figure 52. (Bottom) quantification of the mean T1 values of cell pellets. Cells overexpressing HSP72 after a thermal shock and incubated with HSP72 targeted liposomes showed a noticeable reduction in T1 values respects with other combination of cells and untargeted liposomes, or HBS, used as control.

5.3.2. Endothelial cells

The first barrier the liposomes would face when they reach the brain will be the endothelial cells forming the brain capillaries. In order to test whether these cells are able to overexpress HSP72, and whether targeted liposomes will be greatly incorporated in these cells, we repeated the experiment described above endothelial cells. HSP72 overexpression was achieved by inducing a 15 minute thermal shock (45ºC). Cells were then left to recover for 6 hours as previously described for astrocytes, before transfecting them with a 15mM solution of either targeted or untargeted liposomes for 30 minutes or 1 hour.

In this case, cells were very sensitive to the addition of HBS solutions containing liposomes, and most of them were lifted from the plates, making not possible to observe them properly under the fluorescence microscope. In this case, cell cultures were directly transferred to Eppendorf tubes, centrifuged and the supernatant was removed. Cells were washed with HBS, centrifuged again, and this process was repeated for 3 times. Final cell pellets were send to the MRI system for the study of the relaxation times. Results are presented in figure 54.

All this experiments confirm the capacity of anti-HSP72 liposomes to target cells that overexpress this protein (such is the case of neurons of the peri-infarct region) and interact with them by molecular recognition processes, confirming the validity of the biomarker selected as target for out theranostic agents.

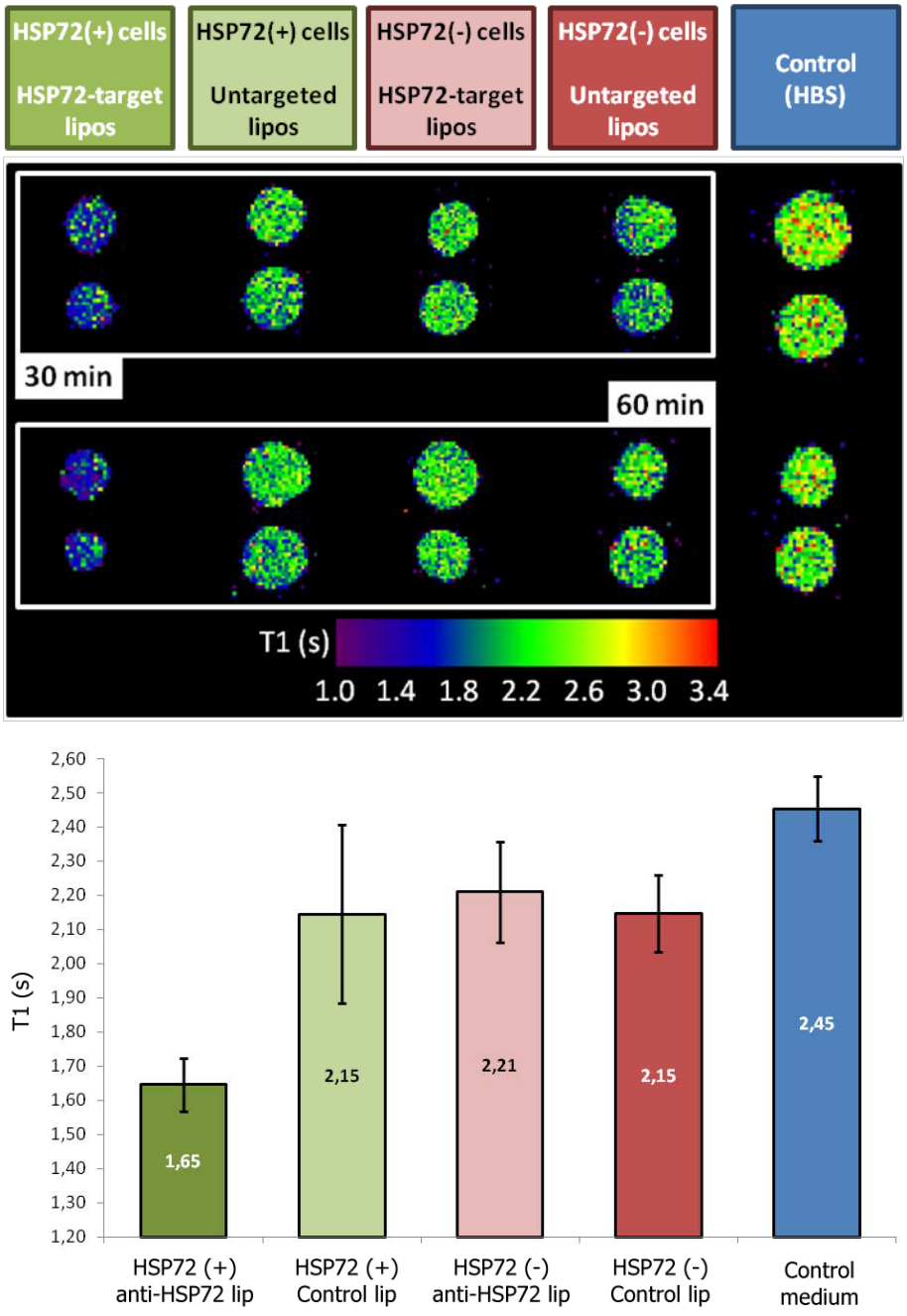

Figure 54. (Top) T1 maps (cross-sectional MR slice of 1 mm) of endothelial's cell pellets. Incubation times are presented on the figure 52. (Bottom) quantification of the mean T1 values of cell pellets. Cells overexpressing HSP72 after a thermal shock and incubated with HSP72 targeted liposomes showed a noticeable reduction in T1 values respects with other combination of cells and untargeted liposomes, or HBS, used as control.

5.4. *IN VIVO* MOLECULAR RECOGNITION OF TARGETS

The final stage of this research project aimed to demonstrate the theranostic capacity of the designed targeted liposomes.

5.4.1. Diagnostic function of targeted liposomes

We firstly tested the diagnostic capacity of the theranostic agent. We aimed to demonstrate that HSP72 liposomes will allow us to delimitate the peri-infarct region in an *in vivo* model of cerebral ischemia by using MRI, and confirm results *ex vivo*, by fluorescence microscopy.

5.4.1.1. MRI tracking of magnetoliposomes

In a first set of experiments a group of ischemic animals were injected with HSP72 targeted gadolinium doped liposomes, a second group was treated with untargeted liposomes, and a third group was treated with HBS, and used as control group. All animal were treated intravenously with 1 ml injections every 6 hours during 36 hours.

A set of T1 images of different repetition time (0.3, 0.6, 0.9, 1.5, 3, 6, 9 and 12 seconds) were acquired at 24, 48, 72 h and 7 days, Images were analyzed using IDL and Image-J. In a first step, the set of MR images were loaded into IDL and fitted on a pixel-by-pixel basis to a saturation-recovery equation:

$$S=Y_0 + S_0(1-\exp^{-TR/T1})$$

were TR is the independent variable, corresponding to the repetition time, S is the dependent variable, corresponding to the signal intensity of the fitted pixel, and the three fitting parameters are Y_0 (signal offset), S_0 (proton density) and T1 (longitudinal relaxation time or spin-lattice relaxation time).

Following the fitting of each set of images, three parametric images were constructed (corresponding to any of the fitting parameters) and stored for further analysis.

T1 maps (parametric images containing T1 values) were loaded on Image-J software for posterior analysis.

First, we used all images from all animals of the control group at 24 h post induction of ischemia (when lesion is fully developed) to calculate the normalized histograms of T1 pixel values that we could clearly identify as ischemic lesion, and pixels of the contralateral hemisphere, assumed to correspond to healthy tissue. Two main populations of T1 values were therefore characterized.

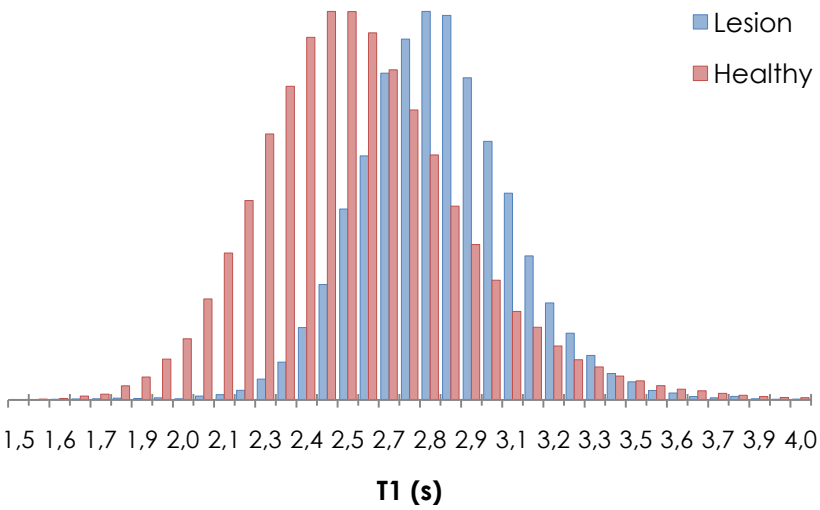

Figure 55. Cumulative histogram of T1 values of the ischemic lesion and the healthy contralateral tissue of multiple MRI slices of the brain of non-treated animals.

In the plot we can see a distribution of T1 values centered at T1 = 2.47 s (range of T1 values at half height: 2.25-2.73 s) corresponding to healthy tissue, and a second distribution of

values centered at T1 = 2.80 s (range of T1 values at half height: 2.53-3.07 s), corresponding to the ischemic lesion. Both populations can be distinguished on the images since the Raleigh criterion is satisfied. This criterion states that two different populations of pixels can be distinguished from each other if the crossing of the two distributions takes place at a height corresponding to the 80% of the minor of the maxima.

In our case we have decided to use an approximation to locate liposomes in the brain, consisting in the application of a cut-off filter for pixels with a T1 value higher than 2.25 s. This value corresponds to the value of T1 at half-height of the distribution of values for healthy tissue, considering that any value below 2.25 is abnormally low, and assuming that such effect is caused by the presence of contrast media (liposomes). Any value above 2.25 ms may be considered normal for healthy or ischemic tissue, and therefore will be cut away.

In our imaging protocol a set of 14 slices of 1 mm thickness are acquired to completely cover a rat brain (from the rhinal fissure to the edge of the cerebellum). Along this set of 14 image slices important differences on T1 values may be observed due to instabilities on the magnetic field, to failures on the fitting process (only sets of 8 images were used for the fitting) and to the fact that some tissue structures present different T1 values (the dentate gyrus of the hippocampus, for example, presents reduced T1 value as compared to the cerebral cortex). Thus, the center of the histogram and its shape are dependent on the user who analyzes the data, and may be narrower or wider depending on which portions of the images are selected to build it. We have selected the whole contralateral hemisphere of at least 7 slices per animal (the most rostral ones), avoiding the inclusion of the hippocampus and the ventricles (the first with reduced, and the second with increased T1 values).

The process performed on each image is summarized in figure 56.

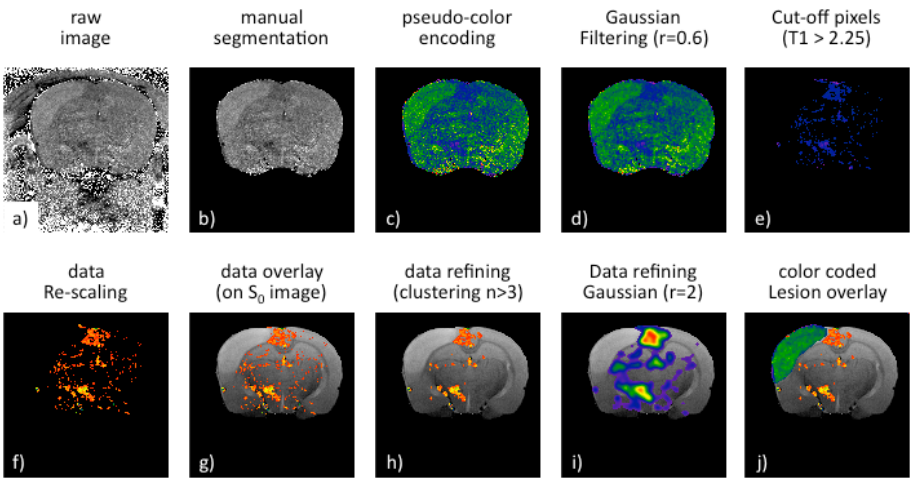

Figure 56. Image analysis performed for the location of gadolinium-doped liposomes. See text below for a detailed explanation.

First, raw T1 maps were taken (a) and manually segmented (b). A color code (5 color rainbow code: purple-blue-green-yellow-red) was used to enhance contrast between tissues with different T1 values (c). A Gaussian filter (radius=0.6) was applied to soften the image, which presents a noisy pattern due to individual pixels with aberrant fitting results (noise). Then, a cut-off filter was applied to remove pixels with values higher than 2.25 seconds (e). This value was selected as main criterion to consider the presence of liposomes. Then, images were re-scaled (minimum 0, maximum 2.25) to show high concentration of liposomes in yellow (very low T1) and reduced concentration of liposomes in orange-red (slightly low T1) (f). Data can be overlaid on the corresponding proton density image (S_0) (g). To reduce noise from the resulting image two alternative procedures can be performed. First, T1 data (f) can be refined by applying a clustering algorithm that deletes isolated pixels, or clusters of pixels of less than n=3 elements, considering them as noise (h). Alternatively, a Gaussian filter (radius=2) can be applied to (f), to remove noise (i). Finally, it is possible to color code the ischemic lesion to facilitate the visual identification of the lesion and the location of liposomes at its periphery (j). Following the described procedure, all images for all groups of animals were analyzed. Results are presented next.

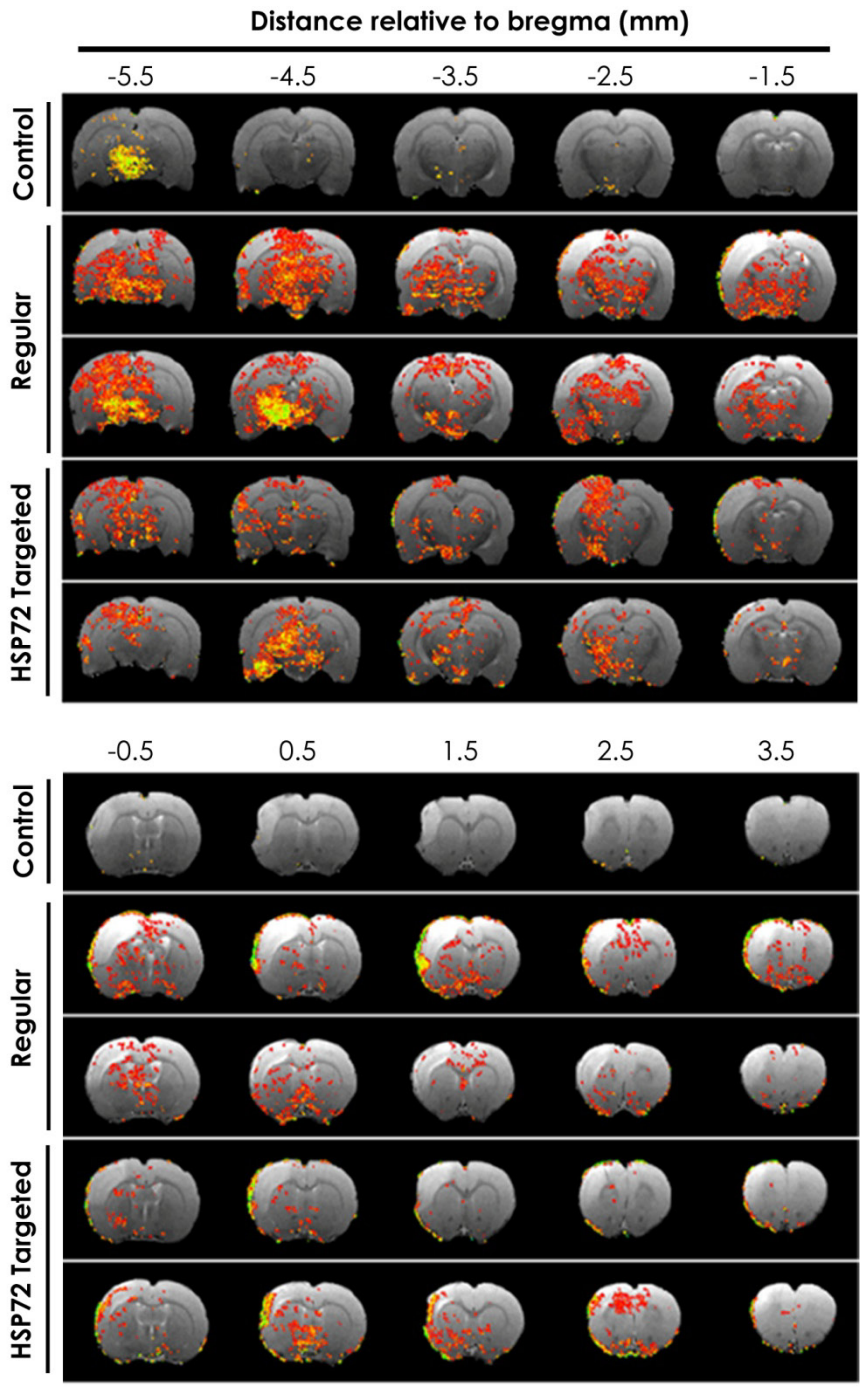

Figure 57. Distribution of liposomes (pixels with T1<2.25 ms) along the brain of a control animal (injected with HBS), two animals treated with regular (untargeted) liposomes, and 2 animals treated with HSP72-targeted liposomes. All images correspond to 3 days post induction of stroke .

The selection of images at day 3 for demonstration of proof of principle was performed based on figure 50, where we can see that the expression of HSP72 in the peri-infarct region is still noticeable, while it is almost negligible at the infarct core, for this time point.

For the control group, only a group of pixels are presented at the most caudal slice of the brain, and no presence of liposomes (pixels with T1 < 2.25 s) is detected in the brain of this animals. For animals treated with regular (untargeted) liposomes, liposomes (pixels with T1 < 2.25) are distributed along most of the brain, without preference for any region in particular. Finally, anti-HSP72 vectorized liposomes tend to accumulate in the periphery of the ischemic lesion, as correspond to the distribution of the HSP72 protein for this period of time.

In Figure 58 we present a representative slice of one animal of each group, where we can appreciate these facts in more detail.

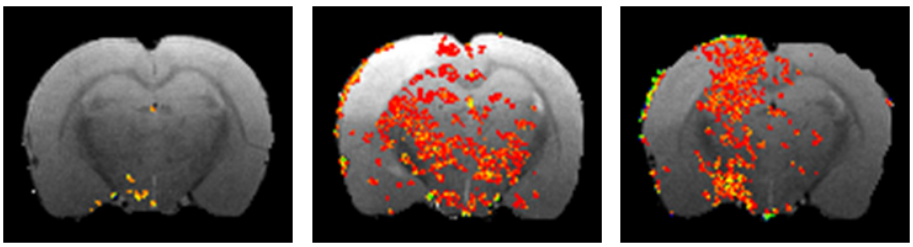

Figure 58. Ischemic animals treated with HBS (left), untargeted liposomes (middle) and HSP72-targeted liposomes (right).

In an attempt to quantify the uptake and distribution of liposome (pixels with T1<2.25 ms), we first counted the total amount of pixels with reduced T1 values for each animal group. Then, we calculated the percentage of such pixels that appear in the ipsilesional hemisphere, respect to the those located at the contra-lateral hemisphere, in order to estimate if pixels are

equally distributed along the whole brain (as may be expected for untargeted liposomes) or they are preferably located in the ipsilateral hemisphere (as may be expected for targeted liposomes. Finally, we calculated the mean value of T1 for all the groups, in an attempt to quantify the amount of liposomes taken in each group of animals (the lower the T1 value, the higher the concentration of liposomes). Results are presented next.

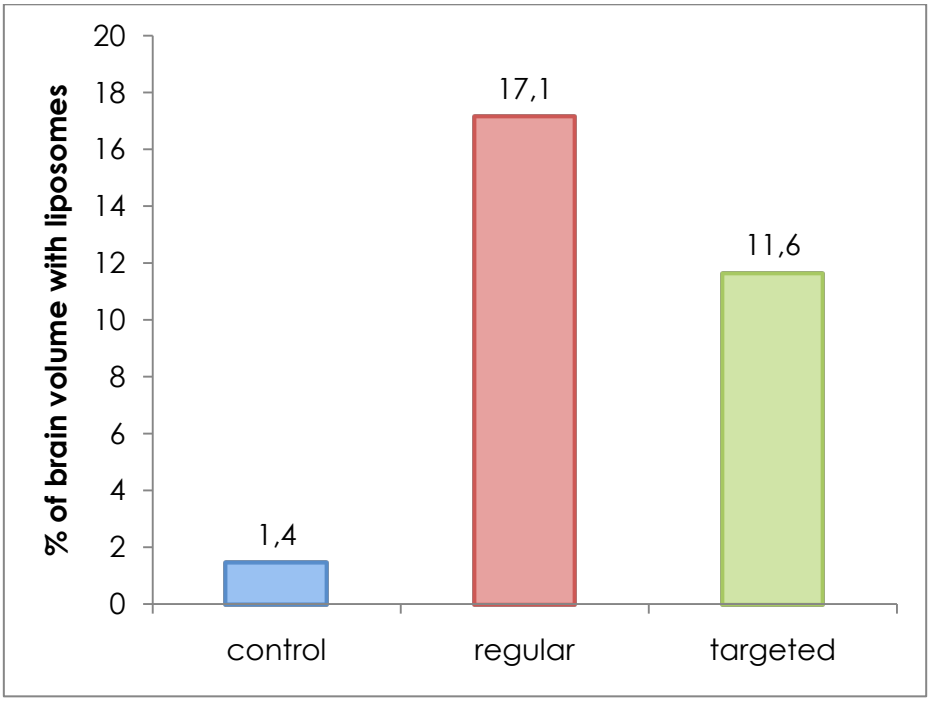

Figure 59. Percentage of brain volume occupied by liposomes (percentage of total volume with pixels with T1 < 2.25 s) for animals treated with HBS (control), untargeted liposomes (regular), or HSP72 targeted liposomes (targeted).

As we can see, the percentage of brain volume occupied by untargeted liposomes is higher than the volume occupied by targeted liposomes, indicating a higher uptake of the first ones by the brain. The amount of pixels in control animals is negligible.

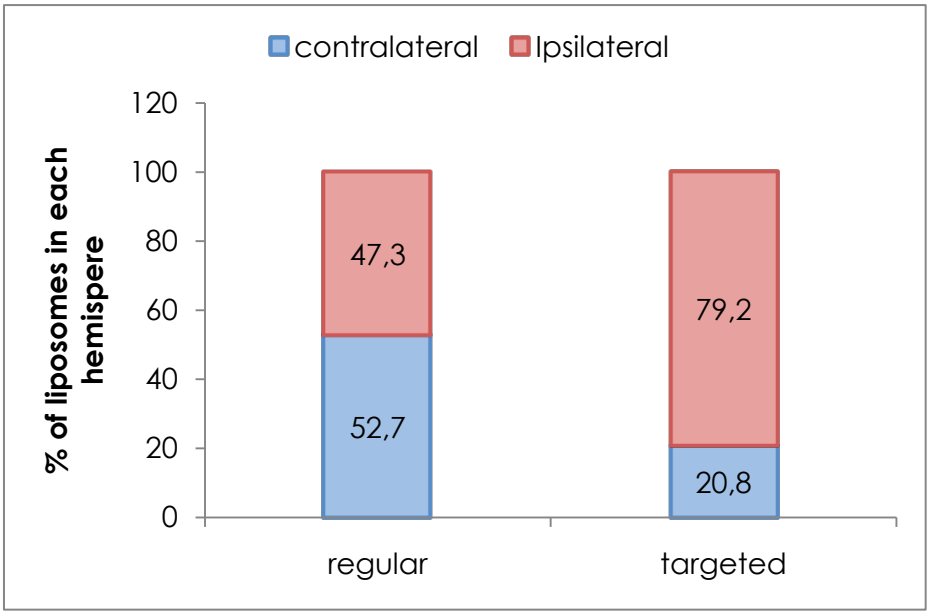

Figure 60. Distribution of liposomes on brain hemispheres. Regular (non-targeted) liposomes are equally distributed in both cerebral hemispheres, while targeted liposomes accumulate mainly on the hemisphere ipsilateral to the ischemic lesion.

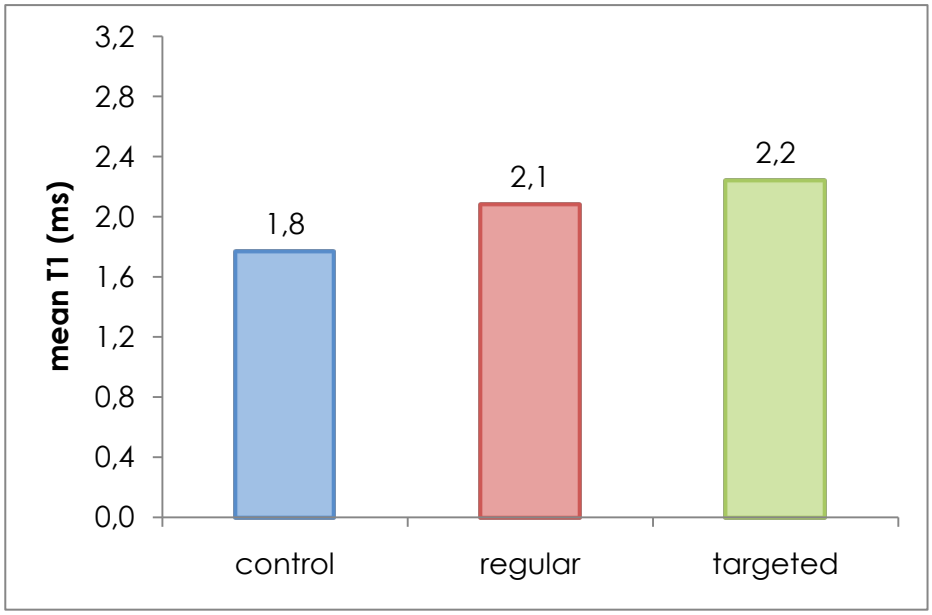

Figure 61. Mean T1 values of areas where liposomes are present for the control group (in this case low T1 values are assumed to be caused by noise and field instabilities), and regular (non-targeted) and HSP72-targeted liposomes. No significant differences were found for these two groups

Similarly to the procedure performed for images acquired at 72 h post ischemia, same set of images was acquired for each animal at days 1, and 7 post induction of focal ischemia.

To show the data from all groups in an easily interpretable way we constructed density maps for the distribution of liposomes on all animals for each group of treatments at all time points measured (1, 3 and 7 days). Images of all animals were co registered (using a bilinear algorithm and images including only pixels containing liposomes were added and divided by the number of elements used for its construction, expressing the results as density maps (% of animals on the group that presented liposomes in each pixel of the image). Density maps are presented on figure 60, along with images corresponding at individual time points (day 1, 3 and 7 post ischemia) for a representative animal of each treatment group (figure 63).

Figures 62 and 63 show that liposomes seem to accumulate preferentially at caudal regions of the brain. Untargeted liposomes are equally distributed on both hemispheres, while HSP72-targeted liposomes accumulate preferably at the hemisphere ipsilateral to the ischemic lesion.

Finally, data was analyzed to obtain the percentage of brain volume occupied by liposomes and the percentages of distribution of liposomes between both brain hemispheres for all time points. Results are presented on figures 64 and 65, respectively.

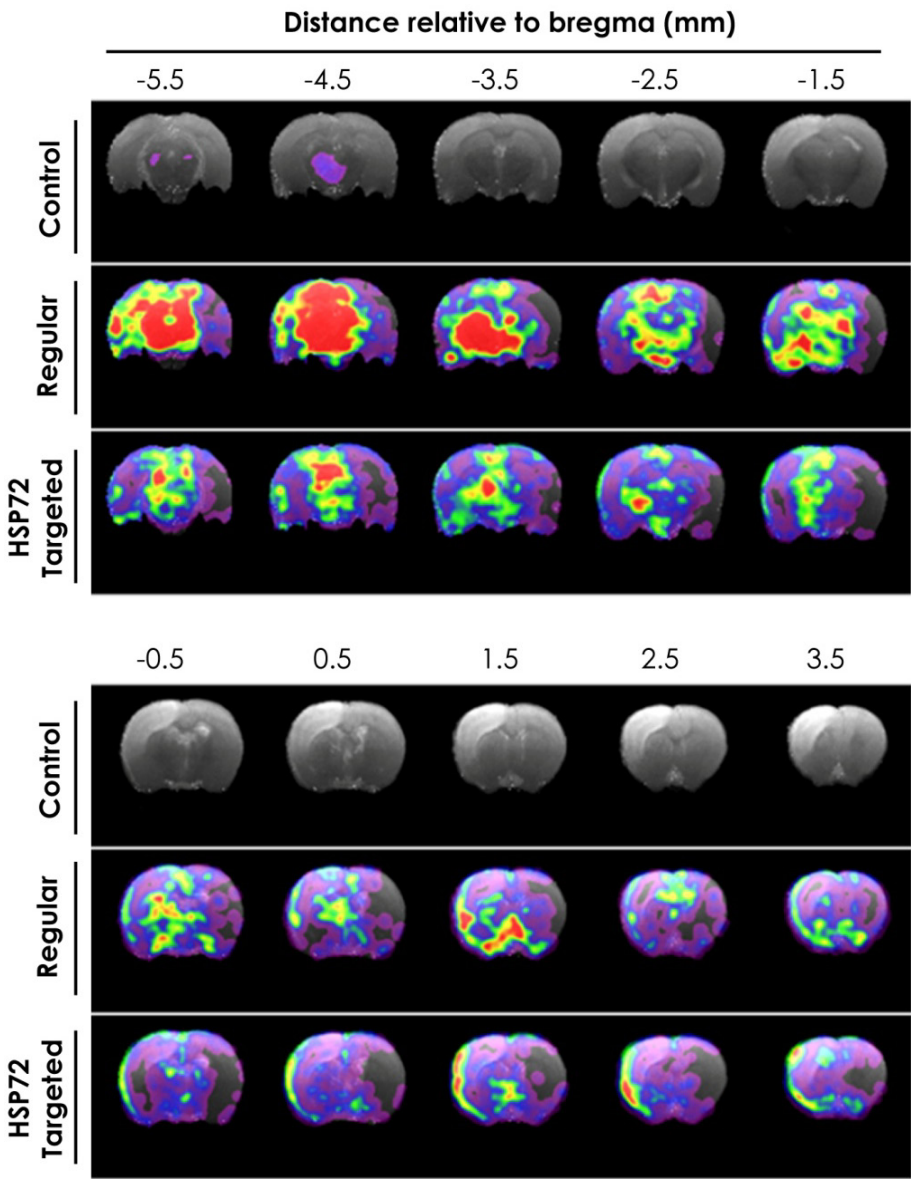

Figure 62. Density maps showing the distribution of liposomes for all animals treated with HBS (control), regular liposomes and HSP72 targeted liposomes.

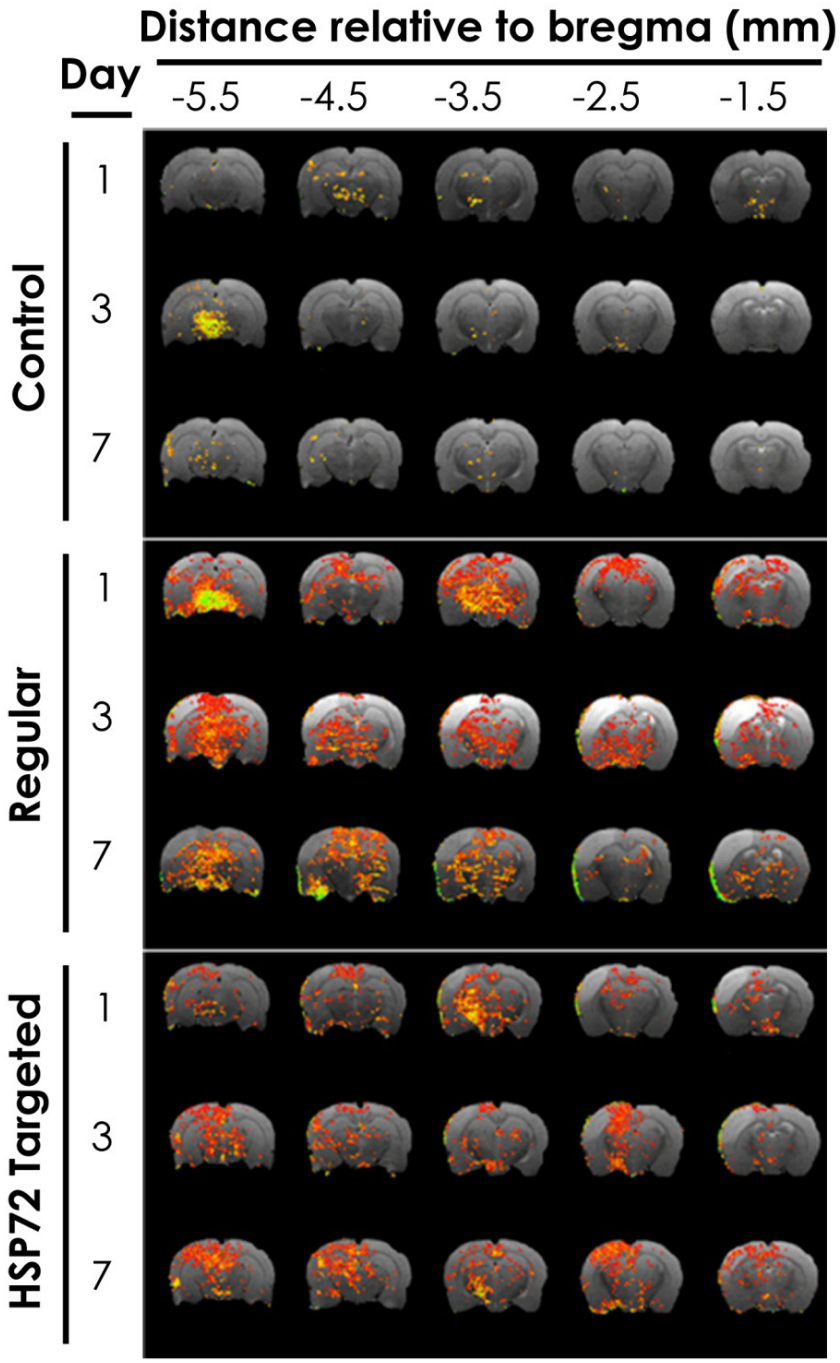

Figure 63a. Temporal evolution (days 1, 3 and 7 post MCAo) of the location of the liposomes for a representative animal of each of the treatment groups.

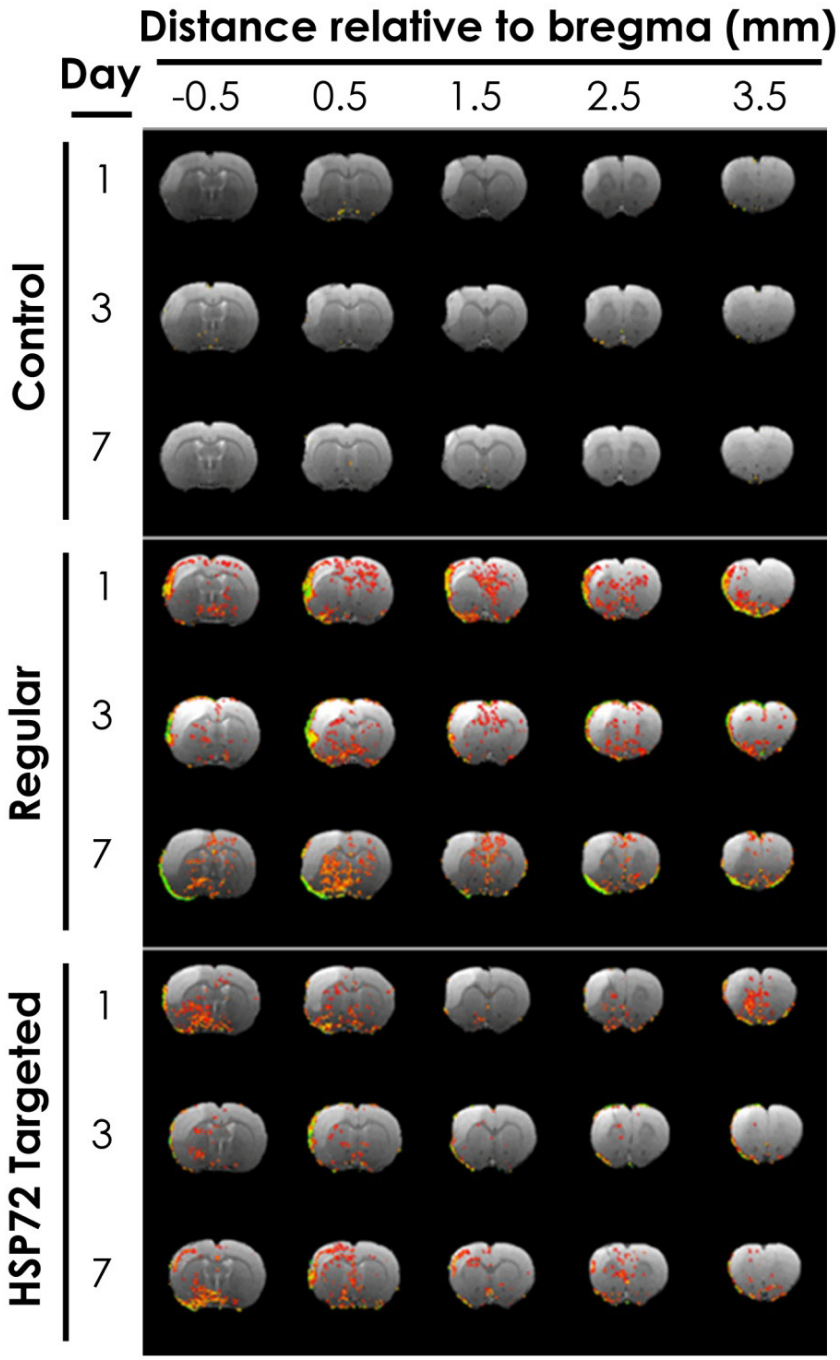

Figure 63b. Temporal evolution (days 1, 3 and 7 post MCAo) of the location of the liposomes for a representative animal of each of the treatment groups.

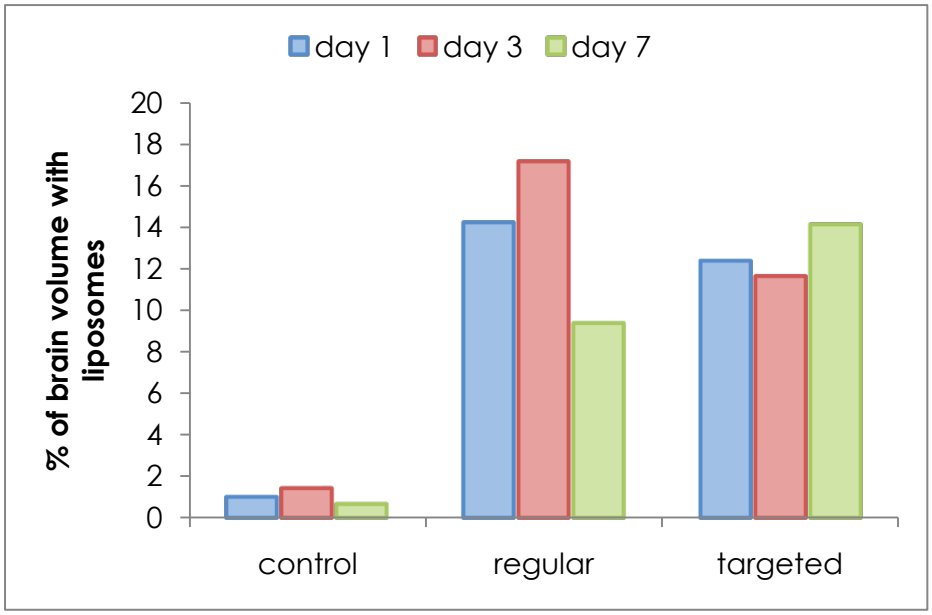

Figure 64. Percentage of brain volume occupied by liposomes (percentage of total volume with pixels with T1 < 2.25 s) at days 1, 3 and 7, for control animals, treated with untargeted liposomes (regular), or HSP72 targeted liposomes (targeted) .

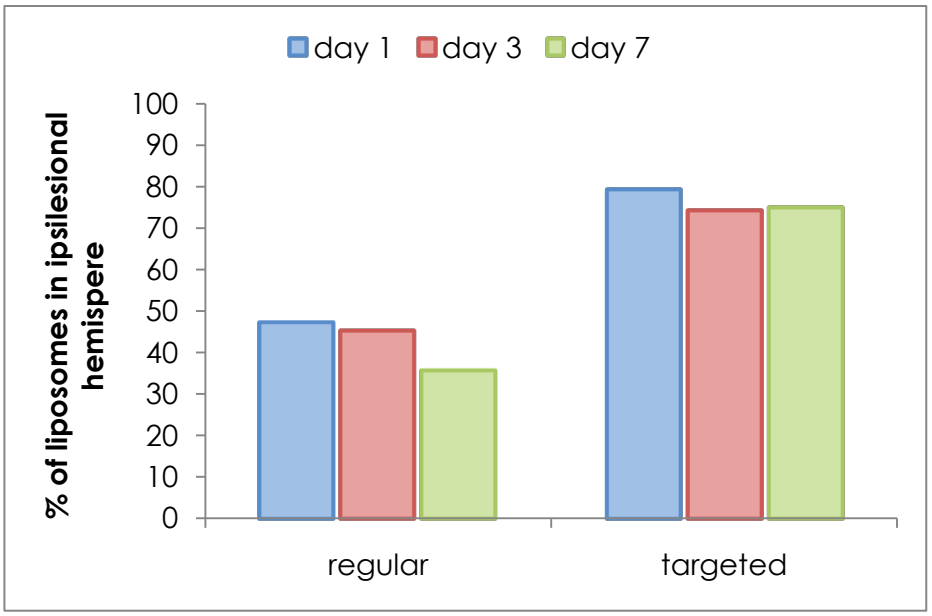

Figure 65. Percentage of liposomes present in the ipsilesional hemisphere (% of total liposomes in the whole brain) for regular (non-targeted) and HSP72-targeted (targeted) liposomes, at day 1, 3 and 7 post induction of focal cerebral ischemia.

5.4.1.2. Visualization by fluorescence microscopy

Seven days after MCA occlusion, animals were sacrificed and transcardially perfused with PBS (pH 7.4), their brains removed, and processed as described under the methods section. Several 10 µm slices were taken for each animal. Slices were fixated in NBF and rehydrated in PBS before mounting with a DAPI-containing medium. Rhodamine positive fluorescence was then evaluated under a microscope. A positive staining was found for all groups injected with liposomes, while no significant rhodamine fluorescence was observed for control animals. Red fluorescent signal (from the rhodamine present on liposomes) was only present in the area surrounding the infarct. Only a small amount of positive cells labeled (2-3 for each slice) was perceived at this time point.

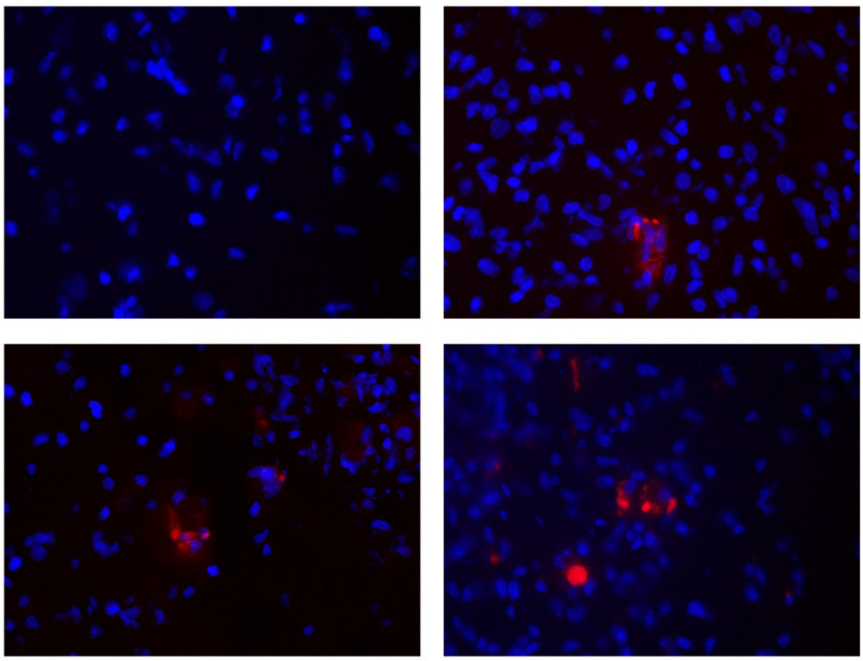

Figure 66. Fluorescence microscopy pictures taken from rat brains 7 days after MCAO. Images correspond to the peri-infarct area. (Top Left) Control animal. (Top right) animal treated with regular liposomes. (Bottom) images of two animals treated with HSP72-targeted liposomes. 7 days post ischemia (5 days post injection of liposomes) only a few elements are visible.

5.4.2. Therapeutic function of targeted liposomes

To test the efficacy of HSP72 targeted liposomes for the treatment of ischemic stroke a rat *in vivo* study was performed. Citicoline, a drug that has shown its capacity to induce a reduction in infarct size in previously published studies was selected to test the hypothesis that targeting of drugs toward the peri-infarct area induces an enhanced therapeutic effect, defined as a greater reduction in infarct volumes respect to other treatments. In our study we considered the following groups of treatment (n=6):

- Control 1 (saline)
- Control 2 (empty untargeted liposomes)
- Citicoline IP (intra-peritoneal injection of 500mg/kg)
- Citicoline IV (intravenous injection of 6x8mg/kg doses)
- Citicoline in untargeted liposomes IV (6x8mg/kg doses)
- Citicoline in HSP72 targeted liposomes IV (6x8mg/kg doses)

Each animal was submitted to the experimental protocol depicted in figure 67.

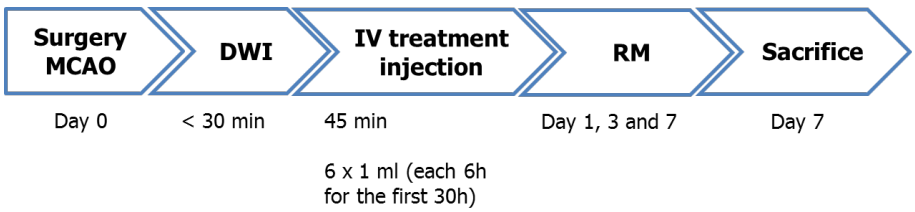

Figure 67. Flowchart representing the protocol followed for each animal studied.

5.4.2.1. Effects on ischemic lesion volume

Infarct sizes were measured on DWI MR images, immediately after surgery (t0), and on T2W MR images at days 1, 3 and 7 after induction of ischemia. Results are presented in table 16.

GROUP	Lesion volume (mm^3)			
	DAY 0	DAY 1	DAY 3	DAY 7
Vehicle	147.1 ± 44.9	215.1 ± 66.9	219.9 ± 77.2	183.2 ± 69.9
Citicoline IV	155.1 ± 41.2	223.2 ± 53.8	266.6 ± 52.9	142.1 ± 18.7
Citicoline IP	159.1 ± 14.7	244.4 ± 62.5	227.8 ± 64.8	147.5 ± 51.3
Control liposomes	147.8 ± 23.9	184.1 ± 17.2	196.4 ± 21.8	169.5 ± 20.9
untargeted liposomes	147.5 ± 15.0	153.7 ± 30.4	115.5 ± 64.1	81.9 ± 17.3
HSP72-targeted liposomes	145.6 ± 10.9	116.5 ± 18.2	105.7 ± 12.3	55.1 ± 16.2

Table 16. Infarct volumes (in mm^3) measured from MR images for all the study groups.

No statistically significant differences were found on infarct volumes of all groups at t0. Lesions had a tendency to grow at days 1 and 3, dropping later by day 7 (typical behavior on this animal model). In those groups were citicoline was used infarct volumes experiment a decrease from basal volumes at day 7, this phenomenon (not observed for both control groups) is more noticeable when citicoline is encapsulated in untargeted, and specially, in HSP72 targeted liposomes.

Figures 68 and 69 contains the plots of the results presented in table 16, and the statistical analysis of the results (ANOVA) is presented on table 17.

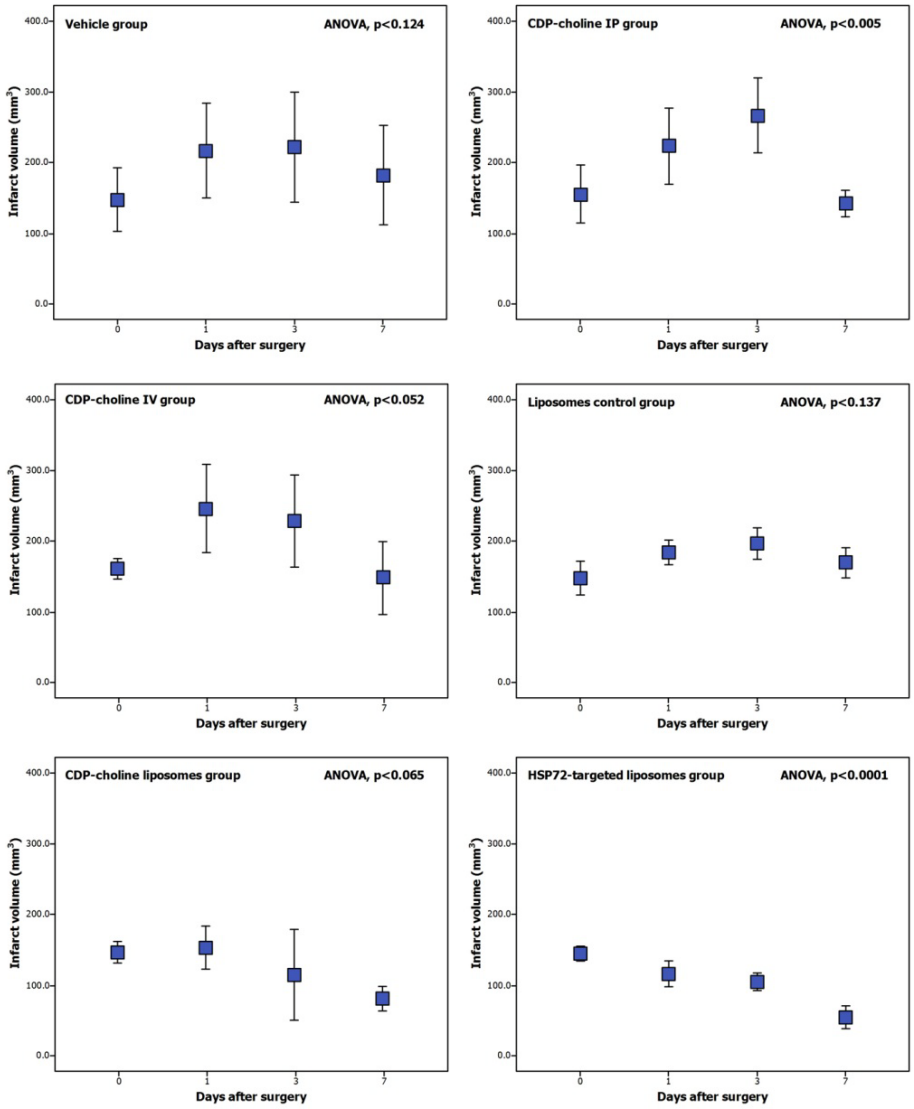

Figure 68. Graphical representation of the progression of infarct volumes for each group of the study.

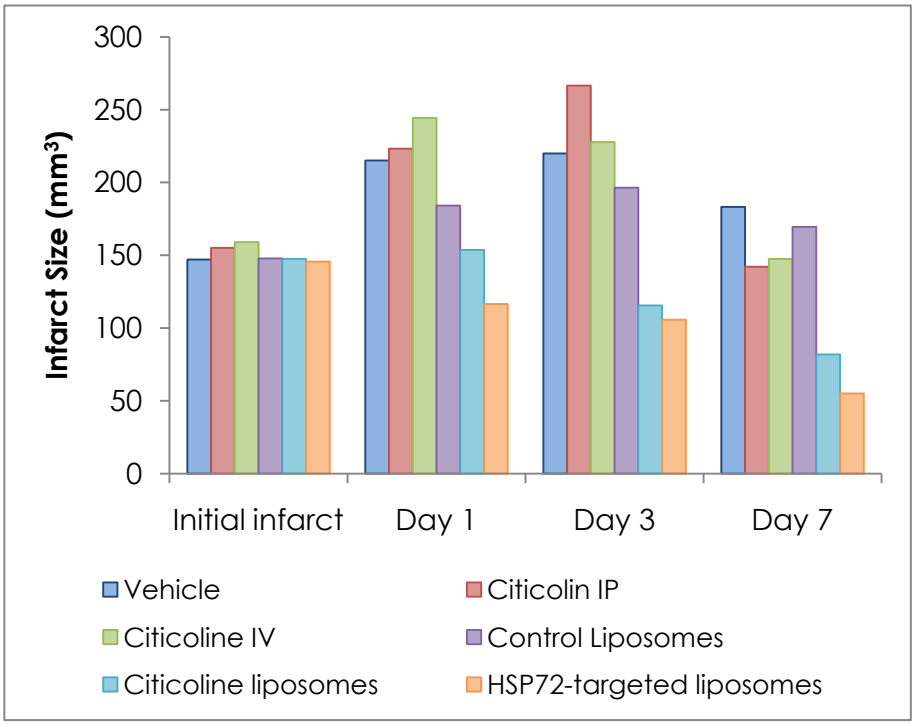

Figure 69. Graphical representation of the progression of infarct volumes for each group of the study.

GROUP	Student t-test p values			
	DAY 0	DAY 1	DAY 3	DAY 7
Vehicle				
Citicoline IV	0.920	0.504	0.239	0.012
Citicoline IP	0.231	0.683	0.483	0.230
Control liposomes	0.457	0.128	0.131	0.115
Untargeted liposomes	0.239	0.088	0.424	0.010 *
HSP72-targeted liposomes	0.167	0.030	0.014	0.009 *

Table 17. Student t-test values for each of the groups of the study. (*) statistically significant differences in infarct sizes. Difference between citicoline-containing untargeted and HSP72 targeted liposomes was also statistically different, p=0.032.

5.4.2.2. Effects on edema formation

Edema formation was also quantified for every treatment group.

GROUP	Edema (% ipsi-contralateral volumes)			
	DAY 0	DAY 1	DAY 3	DAY 7
Vehicle	3.6 ± 2.8	14.3 ± 3.8	13.2 ± 5.2	4.9 ± 3.9
Citicoline IV	1.5 ± 1.3	16.2 ± 2.4	18.2 ± 4.6	3.2 ± 2.7
Citicoline IP	2.7 ± 2.9	11.5 ± 5.2	12.7 ± 3.1	2.0 ± 2.8
Control liposomes	1.2 ± 0.5	14.0 ± 2.0	11.2 ± 2.4	3.3 ± 1.7
Citicoline liposomes	2.0 ± 2.2	12.0 ± 3.9	5.7 ± 8.1	1.5 ± 1.3
HSP72-targeted liposomes	1.5 ± 1.7	9.0 ± 0.8	6.7 ± 1.5	1.2 ± 1.9

Table 18. Edema formation (% of increase of ipsilateral hemispheric volume respect to contralateral hemispheric volume) measured from DWI and T2W MR images for all the study groups.

GROUP	Student t-test p values			
	DAY 0	DAY 1	DAY 3	DAY 7
Vehicle				
Citicoline IV	0.209	0.727	0.678	0.439
Citicoline IP	0.813	0.346	0.299	0.363
Control liposomes	0.059	0.611	0.177	0.121
Citicoline liposomes	0.514	0.682	0.026 *	0.042 **
HSP72-targeted liposomes	0.342	0.039	0.042 *	0.014 **

Table 19. Student t-test values for each study group. Edema formation was not significantly different between untargeted and targeted liposomes at day 3 (p=0.306) or 7 (p=0.512).

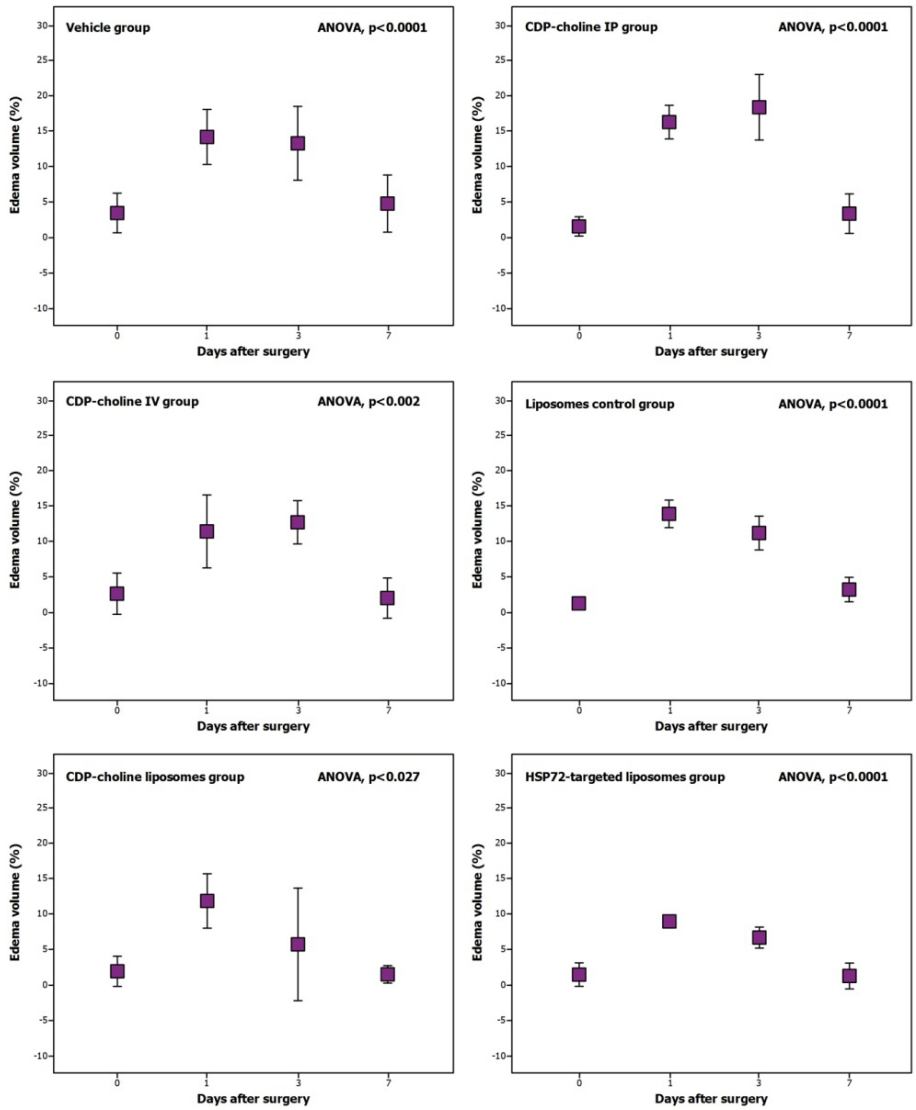

Figure 70. Graphical representation of the progression of edema volumes for each of the groups of the study.

The ANOVA test showed that only groups where citicoline was encapsulated showed a statistically significant difference in edema formation at days 3 and 7. No significant differences were found between targeted and untargeted liposomes at day 3 ($p=0.306$) or 7 ($p=0.512$) (Table 19).

6. DISCUSSION

6.1. Identification of peri-infarct tissue targets

In this study we have demonstrated that the inducible form of HSP70 protein (HSP70i or HSP72) but not its constitutive form (HSP70c or HSC70) is an specific biomarker for the delimitation and targeting of the peri-infarct region after brain ischemia. Several other proteins were found to be up-regulated at the peri-infarct region, including HSC70, but none of them was specific for such region.

Comparison of protein expression between peri-infarct and contralateral regions was performed using two different proteomic techniques, the most widespread one that is based on two-dimensional electrophoresis and mass-spectrometry (2d-PAGE), and a second technique based on COFRADIC. The analysis by two-dimensional electrophoresis showed the up-regulation of 11 proteins in the peri-infarct region for 6 different samples while COFRADIC technique revealed 72 up-regulated proteins in peri-infarct region. Comparison of results from both techniques showed only one coincidence corresponding to the HSP70 protein family. Other 10 proteins that were found up-regulated in the 2D-PAGE study have not been detected by COFRADIC, and 71 up-regulated proteins observed by the later technique were not found in 2D-PAGE. The obtaining of different results from both techniques is not surprising, and this fact has been already discusses in the literature, where it is described that proteomics based on liquid chromatography and mass spectrometry (COFRADIC) and proteomics based on gel electrophoresis frequently yield on different results, that must be considered complementary to each other rather than contradictory.[238] We started our search of such biomarker by the most robust result and thus, the family of HSP70 proteins, only common result in both techniques, was selected for further analysis by western-blot and by immunohistochemistry studies.

These techniques revealed that such election was correct, and studies performed in the other 10 targets found in 2D-PAGE studies (data not shown) demonstrated that they were not specific for the peri-infarct region, and were also expressed on healthy tissue (differences were quantitative and no qualitative).

6.1.1. HSP72

Validation by western-blot analysis revealed that only the inducible form of HSP70 (HSP72) was specifically up-regulated in the peri-infarct region, whereas expression of constitutive HSP70 was similar for both the peri-infarct and contralateral brain tissue. Immunohistochemistry studies with constitutive HSP70 showed light uniform expression all over the brain slices, whereas significant expression of HSP72 was only detected in the peri-infarct region. These results confirm that HSP72 is a specific biomarker of the peri-infarct area, while the constitutive form of this protein is not specific of such region.

There are previously reported studies that have shown the over-expression of HSP70 in ischemic brain tissue.[85, 239-240] however none of such studies have tackled a global analysis of protein expression of peri-infarct area, and focused only in particularly selected proteins. We believe that such global analysis had to be performed, since the definition of protein biomarkers based only on specific proteins can miss more potent biomarkers than those considered. Another published study shows a global analysis of protein expression in the ischemic penumbra, on an *in vitro* model, finding up-regulation of several heat shock proteins.[241] The fact that such study was performed in an *in vitro* model, may implicate that results could not be directly extrapolated to the *in vivo* situation, where protein expression under ischemic conditions may be rather different than in a cell culture. For the rest of the studies published on this field, some describe the up-regulation of HSP70 protein at the peri-infarct area, but none of them specify that it is only the inducible form the one that is specific of the peri-infarct region, creating some

confusion about this particular point. To our knowledge, this is the first study that, after performing a global analysis of more than 3000 proteins, expressed at ischemic brain tissue, clearly specifies that only the inducible form of HSP70, but none of the other members of the HSP70 family of proteins), is an specific biomarker of the peri-infarct tissue.

HSP72 has been confirmed as a powerful target for theranostics of stroke, focused on the peri-infarct region. In first place, our results show an up-regulation of this protein of more than 10-fold at the peri-infarct region compared to healthy tissue. In the second place, although HSP72 is not a membrane protein, it has been described that under several conditions, including ischemia, this protein is up-regulated and re-located at the external surface of cell membranes,[242-243] which is necessary for the participation of such cells in molecular recognition processes with theranostic agents.

We have tested the value of HSP72 as target for theranostics of peri-infarct tissue using an *in vitro* assay. Cells over-expressing HSP72 were incubated with lipid nanoparticles containing fluorescent probes and vectorized with antibodies against HSP72 in their surface. Only rat astrocytes subjected to a thermal shock participated in a molecular recognition processes with vectorized nanoparticles, whereas HSP72-targeted liposomes barely reacted with cells cultured in normal conditions.

The temporal expression profile of HSP72 expression after induction of ischemia shows that this protein is expressed as soon as 6 hours post ischemia, although at early time points its presence is not restricted to the peri-infarct region, but can be seen in the infarct core also. This may reveal the temporal and dynamic processes going on at a cellular level after a stroke. In those initial hours in the infarct core coexist both death cells and survived cells, but are surrounded by a stressing environment. It is not until 48 hours later that HSP72 expression remains only in cell of tissue surrounding the infarct core. By then, the glial scar has already been established, protecting the brain from the cellular debris products released by the infarct. At 72 hours after the

induction of ischemia, the expression of HSP72 is anecdotic at the lesion core, and only remains at the peri-infarct area, where decreased up to 14 days.

6.2. Design and synthesis of liposomes

In the present study we have devised a strategy to target the peri-infarct region, being able to identify it *in vivo*, for diagnostic purposes, and allowing us to concentrate the release of a therapeutic drug at this location.

There are several nanocarriers that have could been used as has enumerated in the introduction. We decided to use phospholipidic liposomes as base structure due to their biocompatibility and the simplicity of their synthesis in a small-scale laboratory. Liposomes are composed of either natural or synthetic amphiphilic lipids that can be sized to a defined diameter in the range of 50 to 500 nm, and they can be coated with polymers to increase stability and to prolong circulation half-life *in vivo*.[244] The use of PEGylated lipids is necessary because it reduces phagocytosis *in vivo*, and complement activation. [245] Due to their size, this type of particles are also able to accommodate large amounts of Gd-chelates, [246-248] which are widely used contrast agents for T1-weighted MRI. [249-251]

We decided to construct ca. 100 nm nanoparticles since the threshold upon which lipophilic particles are able to freely cross the BBB is around such value. Particles higher than 100 nm have difficulties to get through the BBB.[252] Since citicoline (or any therapeutic drug) is going to be incorporated to liposomes, smaller liposome sizes would significantly decrease the amount of drug transported by liposomes, decreasing its efficacy. Drug release is also affected by particle size. Smaller particles have larger surface/volume ratios, therefore, most of the associated drug would be at or near the particle surface, leading to fast drug release. Whereas, larger particles have large cores which allow more drug to be encapsulated and slowly diffuse out. [253] Smaller particles also have greater risk of aggregation during

storage of nanoparticle dispersion. It is always a challenge to formulate nanoparticles with the smallest size possible but maximum stability. Hence we have decided to use 100 nm pore filters during lipid extrusion, to get the liposome diameter around such value. At this size a good compromise between BBB passage and particle stability was reached.

Given the gadolinium content in our liposomes, we have established a threshold of $\Delta R1=0.06$ s-1 that allow us to differentiate between normal and ischemic tissue. This would imply that the liposome concentration at the peri-infarct region needs to be around 55μM to be able to visually localize them. Nevertheless, by measuring T1 values on T1 maps, we were able to estimate the liposome presence even when there were no differences on T1w images, observed with the naked eye.

6.3. *In vivo* theranostic function

6.3.1. Diagnostic capacities

MRI tracking of paramagnetic liposomes was achieved after the determination of T1 histograms of both healthy and damaged tissue. Besides these two populations, we should be able to see a third population of T1 values, corresponding to the series of pixels where the tissue contains the contrast agent (i.e. liposomes) that lowers T1 values. Although a solution of pure liposomes has a T1 value around 450 ms (as determined in *in vitro* experiments) the value of T1 for pixels that contain liposomes is not trivial, since T1 depends on the concentration of the contrast agent. Thus, portions of tissue with a high load of liposomes should present a T1 value widely lower than 2.47 s (the mean value determined for healthy tissue). On the other hand, portions of tissue with a small concentration of liposomes would present a T1 value slightly lower than that value. This fact complicates the localization of liposomes on the brain of treated animals. Ideally, this situation may be resolved by using a contrast agent with a high relaxivity (T1 very low), or by enhancing the uptake of

liposomes by brain cells, for example by enhancing its capacity to cross the BBB. Both situations would potentially facilitate the analysis of images and the identification of liposomes in the brain, so studies can be further optimized on the future.

A limitation of the image analysis performed is related to the acquisition of the histograms associated to healthy tissue, and the decision of using the T1 < 2.25 s cutoff filter for the discrimination of liposome-containing pixels. The use of a different selection criterion for the construction of the histograms may lead to different results than those presented on this manuscript.

After applying the T1 < 2.25 s cutoff filter, results are further refined to reduce noise using either a clustering algorithm or a Gaussian filter. Any of these steps have advantages and disadvantages that could be discussed. Most procedures are related to the quality of the fitting process. Fitting data to a 3-variable equation (saturation-recovery equation) with 8 values for the independent variable TR (8 images are acquired on each set) produces noisy results. The quality of T1 maps may be further optimized by the acquisition of more images with different repetition times, but this would require longer acquisition times (which is around 30 minutes with current experimental setup), or sacrifice spatial resolution, for the sake of time saving. We have already discussed that there are pixels of "normal tissue" that present values of T1 lower than 2.25, but applying a more restrictive filter will undoubtedly remove pixels with a low concentration of contrast agent (T1 values close to the cutoff filter). On the other hand, the reduction of noise by removing isolated pixels (pixel clustering) or by the application of a Gaussian filter will most probably affect to some pixels where liposomes are present, but in this way only regions of tissue with significant presence of liposomes are presented on the images, which consequently look "clearer".

After processing the images for all animal groups, the presence of signal at more caudal regions of the brain of the animals has been observed, regardless of the treatment used. Nevertheless

there is a significant presence of liposomes in all of brain slices of MRI images for the groups treated with paramagnetic liposomes. After performing a quantification of the presence of liposomes, the liposome distribution area for the untargeted liposomes was much higher than the HSP72-targeted liposomes, and liposomes were spread along both brain hemispheres. For targeted liposomes, presence was mainly detected at the brain hemisphere ipsilateral to the ischemic lesion. Nevertheless, after correcting for the amount of drop in T1 value, there was no significant difference between both groups. This could indicate that in both groups, the same amount of liposomes are able to cross the BBB, nevertheless in the group treated with HSP72-targeted liposomes, they tend to accumulate preferentially in the ipsilateral hemisphere, in the peri-infarct region.

6.3.2. *Therapeutic efficacy*

citicoline, either free or liposome bound, was used to evaluate the therapeutic potential of our liposome formulations.[254] citicoline has been successfully used in neuroprotective strategies in animal models of stroke. It has also been studied the liposome bound configuration for citicoline treatment in experimental studies. Fresta et al.[255] used a DPPC-liposome stabilized with ganglioside GM1 to improve circulation time in an animal model of brain ischemia based on the bilateral occlusion of the carotid arteries. They evaluate the survival rate in these animals and found a much higher survival rate in animals treated with citicoline-loaded liposomes.[255] Also Adibhatla et al.[256] used a similar type of liposome in an animal model of transient focal ischemia, founding a 62% reduction in infarct volume in animals treated with citicoline bound liposomes.[256] In our experimental setup, the infarct evolution in vehicle treated animals grew at day 1 and 3 compared to the basal infarct, and has the tendency to reduce at day 7, although it remains slightly larger than lesions detected by DWI. This is a normal pattern for this animal model.[257] A similar pattern was also found in the free citicoline treated groups, either IV or IP, and the control liposome

group. In contrast, in targeted-liposome encapsulated citicoline, this tendency was not appreciated. The infarct in this group was always lower than the observed in DWI images, at t=0. This indicates an enhanced effect in the treatment with citicoline bound to liposomes, with respect to free delivered citicoline. In the case of HSP72-targeted liposomes, an improved effect compared with untargeted liposomes was only appreciated at day 7. It should be appreciated that the number of animals per group was reduced (only 4 animals per group) and further studies should be carried in the future to add robustness to our study.

Further optimization of the diagnostic and therapeutic activity of our theranostic agent is possible by modifying the nature or structure of the base liposomes (for example, with double targeting to facilitate the crossing of the BBB after IV administration), by using an enhanced T1 contrast agent, by optimization of the encapsulating process and by using different therapeutic agents, etc.

In summary, we have provide prove of principle that theranostics of the peri-infarct tissue is possible, and truly enhances the diagnosis and therapeutic action of drugs for the treatment of stroke.

7. CONCLUSIONS

1. The peri-infarct region of the brain of ischemic animals presents a characteristic protein expression, with over-expression of particular molecular markers that allows its identification by molecular biology techniques.

2. We have identified 15 molecular markers of the peri-infarct region. Among them, the HSP72 or inducible HSP70 member of the Heat Shock Proteins family is the only truly specific one.

3. The spatiotemporal dynamics of expression of the HSP72 protein has been characterized by immuno-histochemistry techniques, showing a maximal expression at the peri-infarct region 12-24 h after the induction of ischemia, and continues up to 14 days post ischemia.

4. HSP72 protein is mostly expressed by neurons of the peri-infarct region, as demonstrated by immunofluorecence techniques.

5. It is feasible the synthesis of theranostic agents, with a phospholipid liposome based structure, that contain imaging probes for their detection by conventional imaging techniques, and able to carry drugs on their structure for their transport and controlled release at target tissues.

6. MRI techniques allow the detection of the gadolinium doped theranostic agents *in vivo*, either after their intraparenchymal or systemic injection in the rat.

7. Fluorescence microscopy techniques allow the detection of the Rhodamine doped theranostic agents *in vitro* and *ex vivo*, of cell cultures and brain tissue samples.

8. It is feasible to attach anti-HSP72 antibodies to the surface of the aforementioned theranostic agents, so they participate in molecular recognition processes at the peri-infarct region.

9. It is feasible to load the aforementioned theranostic agents with citicoline (a known therapeutic agent for stroke).

10. Constructed anti-HSP72 magnetoliposomes do effectively participate in molecular recognition processes with cells that overexpress HSP72 protein *in vitro*, allowing the identification (by MRI and fluorescence microscopy) of such cells,

11. Constructed anti-HSP72 magnetoliposomes have been detected *ex vivo* (by fluorescence microscopy) in tissue samples of the peri-infarct region of ischemic animals.

12. Constructed anti-HSP72 magnetoliposomes have been detected *in vivo* (by MRI) showing a preferential accumulation of the agent at the peri-infarct area of ischemic animals, as compared to animals treated with non-vectorized magneto-liposomes (controls).

13. Citicoline doped anti-HSP72 magnetoliposomes show an enhanced therapeutic action in ischemic animals (defined as reduced lesion volumes on MRI), as compared with animals treated with citicoline doped non-targeted liposomes and animals treated with non-encapsulated (free) citicoline.

7. CONCLUSIONES

1. La región peri-infarto del cerebro de animales isquémicos muestra una expresión proteica característica, en la que se encuentra la sobre-expresión de determinados marcadores moleculares, lo que permite su identificación mediante técnicas de biología molecular.

2. Hemos identificado 15 marcadores moleculares de la región peri-infarto. Entre ellos, la forma inducible de la proteína de choque térmico HSP70 o HSP72 ha sido la única que ha mostrado ser específica de esta región.

3. La dinámica espaciotemporal de expresión de la proteína HSP72 ha sido caracterizada por técnicas inmunohistoquímicas, mostrando una expresión máxima en la región peri-infarto entre las 12 y 24 horas tras la inducción de la isquemia. La HSP72 ha conseguido identificarse hasta 14 días tras la inducción de la isquemia.

4. Mediante técnicas de inmunofluorescencia, se ha revelado que la proteína HSP72 se expresa fundamentalmente en las neuronas de la región peri-infarto.

5. Ha sido posible la síntesis de liposomas como agentes teranósticos, a partir de una estructura fosfolipídica basal, que contienen tanto sondas de imagen que permiten su detección mediante técnicas de imagen convencional, así como son capaces de transportar drogas en su estructura para su posterior liberación controlada en los tejidos diana.

6. Las técnicas de MRI han permitido la detección de los agentes teranósticos marcados con gadolinio, bien tras su inyección intraparenquimal, o sistémica en ratas.

7. Técnicas de microscopía de fluorescencia han sido utilizadas para la detección de agentes teranósticos marcados con rodamina tanto *in vitro* (en cultivos celulares), como *ex vivo* (en muestras de tejido cerebral).

8. Ha sido posible la unión de anticuerpos frente a la proteína HSP72 en la superficie de los agentes teranósticos ya mencionados, de tal modo que estos participan en procesos de reconocimiento molecular en la región peri-infarto.

9. Ha sido posible la inclusión de citicolina (un agente cuya actividad neuroprotectora ha sido ampliamente demostrada) en los agentes teranósticos sintetizados.

10. Los magnetoliposomas anti-HSP72 construidos participan en procesos de reconocimiento molecular de forma efectiva en cultivos celulares con células que sobreexpresan la proteína HSP72, lo que permite su identificación mediante MRI y microscopía de fluorescencia.

11. Los magnetoliposomas anti-HSP72 construidos se han detectado *ex vivo* (mediante microscopía de fluorescencia) en muestras de tejido cerebral de la región peri-infarto de animales isquémicos.

12. Los magnetoliposomas anti-HSP72 construidos han sido detectados *in vivo* (mediante técnicas de MRI) y han mostrado una acumulación diferencial en el área peri-infarto de animales isquémicos, en comparación con animales tratados con magnetoliposomas no vectorizados (controles).

13. Los magnetoliposomas anti-HSP72 cargados de citicolina han mostrado un incremento en la acción terapéutica sobre animales con isquemia cerebral (entendiéndose ésta como una reducción en el volumen de lesión en MRI), comparado con animales tratados con liposomas no vectorizados, también cargados de citicolina, así como con animales tratados con citicolina no encapsulada.

8. REFERENCES

1. The World Health Organization MONICA Project (monitoring trends and determinants in cardiovascular disease): a major international collaboration. WHO MONICA Project Principal Investigators. J Clin Epidemiol. 1988;41:105-14.

2. Arboix A, Díaz J, Pérez-Sempere A, Álvarez-Sabín J. Ictus: Tipos etiológicos y criterios diagnósticos. Neurologia. 2002;17:3-12.

3. Feinberg WM, Albers GW, Barnett HJ, Biller J, Caplan LR, Carter LP, Hart RG, Hobson RW, 2nd, Kronmal RA, Moore WS, et al. Guidelines for the management of transient ischemic attacks. From the Ad Hoc Committee on Guidelines for the Management of Transient Ischemic Attacks of the Stroke Council of the American Heart Association. Circulation. 1994;89:2950-65.

4. Adams HP, Jr., Bendixen BH, Kappelle LJ, Biller J, Love BB, Gordon DL, Marsh EE, 3rd. Classification of subtype of acute ischemic stroke. Definitions for use in a multicenter clinical trial. TOAST. Trial of Org 10172 in Acute Stroke Treatment. Stroke. 1993;24:35-41.

5. Castillo J. Fisiopatología de la isquemia cerebral. Rev Neurol. 2000;30:459-64.

6. Back T. Pathophysiology of the ischemic penumbra--revision of a concept. Cell Mol Neurobiol. 1998;18:621-38.

7. Astrup J, Symon L, Branston NM, Lassen NA. Cortical evoked potential and extracellular K+ and H+ at critical levels of brain ischemia. Stroke. 1977;8:51-7.

8. Hansen AJ. Effect of anoxia on ion distribution in the brain. Physiol Rev. 1985;65:101-48.

9. Blank WF, Jr., Kirshner HS. The kinetics of extracellular potassium changes during hypoxia and anoxia in the cat cerebral cortex. Brain research. 1977;123:113-24.

10. Choi DW. Ionic dependence of glutamate neurotoxicity. J Neurosci. 1987;7:369-79.

11. Choi DW, Rothman SM. The role of glutamate neurotoxicity in hypoxic-ischemic neuronal death. Annu Rev Neurosci. 1990;13:171-82.

12. White BC, Sullivan JM, DeGracia DJ, O'Neil BJ, Neumar RW, Grossman LI, Rafols JA, Krause GS. Brain ischemia and reperfusion: molecular mechanisms of neuronal injury. J Neurol Sci. 2000;179:1-33.

13. Choi DW. Excitotoxic cell death. J Neurobiol. 1992;23:1261-76.

14. Schiene K, Bruehl C, Zilles K, Qu M, Hagemann G, Kraemer M, Witte OW. Neuronal hyperexcitability and reduction of GABAA-receptor expression in the

surround of cerebral photothrombosis. J Cereb Blood Flow Metab. 1996;16:906-14.

15. Banasiak KJ, Xia Y, Haddad GG. Mechanisms underlying hypoxia-induced neuronal apoptosis. Prog Neurobiol. 2000;62:215-49.

16. Grandati M, Verrecchia C, Revaud ML, Allix M, Boulu RG, Plotkine M. Calcium-independent NO-synthase activity and nitrites/nitrates production in transient focal cerebral ischaemia in mice. Br J Pharmacol. 1997;122:625-30.

17. Nogawa S, Zhang F, Ross ME, Iadecola C. Cyclo-oxygenase-2 gene expression in neurons contributes to ischemic brain damage. J Neurosci. 1997;17:2746-55.

18. Akins PT, Liu PK, Hsu CY. Immediate early gene expression in response to cerebral ischemia. Friend or foe? Stroke. 1996;27:1682-7.

19. Massa SM, Swanson RA, Sharp FR. The stress gene response in brain. Cerebrovasc Brain Metab Rev. 1996;8:95-158.

20. Koistinaho J, Hokfelt T. Altered gene expression in brain ischemia. Neuroreport. 1997;8:i-viii.

21. Kovacs Z, Ikezaki K, Samoto K, Inamura T, Fukui M. VEGF and flt. Expression time kinetics in rat brain infarct. Stroke. 1996;27:1865-72; discussion 72-3.

22. McDonald ES, Windebank AJ. Mechanisms of neurotoxic injury and cell death. Neurol Clin. 2000;18:525-40.

23. Jander S, Kraemer M, Schroeter M, Witte OW, Stoll G. Lymphocytic infiltration and expression of intercellular adhesion molecule-1 in photochemically induced ischemia of the rat cortex. J Cereb Blood Flow Metab. 1995;15:42-51.

24. Rami A, Agarwal R, Botez G, Winckler J. mu-Calpain activation, DNA fragmentation, and synergistic effects of caspase and calpain inhibitors in protecting hippocampal neurons from ischemic damage. Brain research. 2000;866:299-312.

25. Adams HP, Jr., del Zoppo G, Alberts MJ, Bhatt DL, Brass L, Furlan A, Grubb RL, Higashida RT, Jauch EC, Kidwell C, Lyden PD, Morgenstern LB, Qureshi AI, Rosenwasser RH, Scott PA, Wijdicks EF. Guidelines for the early management of adults with ischemic stroke: a guideline from the American Heart Association/American Stroke Association Stroke Council, Clinical Cardiology Council, Cardiovascular Radiology and Intervention Council, and the Atherosclerotic Peripheral Vascular Disease and Quality of Care Outcomes in Research Interdisciplinary Working Groups: the American Academy of Neurology affirms the value of this guideline as an educational tool for neurologists. Stroke. 2007;38:1655-711.

26. Dirks M, Niessen LW, van Wijngaarden JD, Koudstaal PJ, Franke CL, van Oostenbrugge RJ, Huijsman R, Lingsma HF, Minkman MM, Dippel DW. Promoting thrombolysis in acute ischemic stroke. Stroke. 2011;42:1325-30.

27. Donnan GA, Davis SM, Parsons MW, Ma H, Dewey HM, Howells DW. How to make better use of thrombolytic therapy in acute ischemic stroke. Nat Rev Neurol. 2011;7:400-9.

28. Lees KR, Bluhmki E, von Kummer R, Brott TG, Toni D, Grotta JC, Albers GW, Kaste M, Marler JR, Hamilton SA, Tilley BC, Davis SM, Donnan GA, Hacke W, Allen K, Mau J, Meier D, del Zoppo G, De Silva DA, Butcher KS, Parsons MW, Barber PA, Levi C, Bladin C, Byrnes G. Time to treatment with intravenous alteplase and outcome in stroke: an updated pooled analysis of ECASS, ATLANTIS, NINDS, and EPITHET trials. Lancet. 2010;375:1695-703.

29. Kakuda W, Lansberg MG, Thijs VN, Kemp SM, Bammer R, Wechsler LR, Moseley ME, Marks MP, Albers GW. Optimal definition for PWI/DWI mismatch in acute ischemic stroke patients. J Cereb Blood Flow Metab. 2008;28:887-91.

30. Rodríguez-Yáñez M, Sobrino T, Arias S, Vázquez-Herrero F, Brea D, Blanco M, Leira R, Castellanos M, Serena J, Vivancos J, Dávalos A, Castillo J. Early biomarkers of clinical-diffusion mismatch in acute ischemic stroke. Stroke. 2011;42:2813-8.

31. Ginsberg MD. Current status of neuroprotection for cerebral ischemia: synoptic overview. Stroke. 2009;40:S111-4.

32. Castillo J, Álvarez-Sabín J, Dávalos A, Díez-Tejedor E, Lizasoain I, Martínez-Vila E, Vivancos J, Zarranz JJ. Neuroprotección farmacológica en la isquemia cerebral: ¿es todavía una opción terapéutica? Neurologia. 2003;18:368-84.

33. Donnan GA, Davis SM. Neuroprotection: still achievable in humans. Stroke. 2008;39:525.

34. Hazell AS. Excitotoxic mechanisms in stroke: an update of concepts and treatment strategies. Neurochem Int. 2007;50:941-53.

35. Horn J, de Haan RJ, Vermeulen M, Limburg M. Very Early Nimodipine Use in Stroke (VENUS): a randomized, double-blind, placebo-controlled trial. Stroke. 2001;32:461-5.

36. Horn J, de Haan RJ, Vermeulen M, Luiten PG, Limburg M. Nimodipine in animal model experiments of focal cerebral ischemia: a systematic review. Stroke. 2001;32:2433-8.

37. Brea D, Castillo J. Neuroprotección y neurorrestauración. In: Martinez-Vila E, editor. El ictus isquémico en Atención Primaria: Profármaco; 2010. p. 57-73.

38. Muir KW, Lees KR, Ford I, Davis S. Magnesium for acute stroke (Intravenous Magnesium Efficacy in Stroke trial): randomised controlled trial. Lancet. 2004;363:439-45.

39. Ginsberg MD. Neuroprotection for ischemic stroke: past, present and future. Neuropharmacology. 2008;55:363-89.

40. Campos F, Sobrino T, Ramos-Cabrer P, Argibay B, Agulla J, Pérez-Mato M, Rodríguez-Gonzalez R, Brea D, Castillo J. Neuroprotection by glutamate oxaloacetate transaminase in ischemic stroke: an experimental study. J Cereb Blood Flow Metab. 2011;31:1378-86.

41. Teichberg VI. GOT to rid the body of excess glutamate. J Cereb Blood Flow Metab. 2011;31:1376-7.

42. Teichberg VI, Cohen-Kashi-Malina K, Cooper I, Zlotnik A. Homeostasis of glutamate in brain fluids: an accelerated brain-to-blood efflux of excess glutamate is produced by blood glutamate scavenging and offers protection from neuropathologies. Neuroscience. 2009;158:301-8.

43. Koziol JA. NXY-059 for acute ischemic stroke. N Engl J Med. 2006;354:2075-6; author reply -6.

44. Savitz SI, Fisher M. Future of neuroprotection for acute stroke: in the aftermath of the SAINT trials. Ann Neurol. 2007;61:396-402.

45. Serebruany V. NXY-059 for acute ischemic stroke. N Engl J Med. 2006;354:2075-6; author reply -6.

46. Hurtado O, Cárdenas A, Pradillo JM, Morales JR, Ortego F, Sobrino T, Castillo J, Moro MA, Lizasoain I. A chronic treatment with CDP-choline improves functional recovery and increases neuronal plasticity after experimental stroke. Neurobiol Dis. 2007;26:105-11.

47. Adibhatla RM, Hatcher JF, Larsen EC, Chen X, Sun D, Tsao FH. CDP-choline significantly restores phosphatidylcholine levels by differentially affecting phospholipase A2 and CTP: phosphocholine cytidylyltransferase after stroke. J Biol Chem. 2006;281:6718-25.

48. Ferro JM, Dávalos A. Other neuroprotective therapies on trial in acute stroke. Cerebrovasc Dis. 2006;21 Suppl 2:127-30.

49. Hurtado O, Pradillo JM, Fernández-López D, Morales JR, Sobrino T, Castillo J, Alborch E, Moro MA, Lizasoain I. Delayed post-ischemic administration of CDP-choline increases EAAT2 association to lipid rafts and affords neuroprotection in experimental stroke. Neurobiol Dis. 2008;29:123-31.

50. Zhang ZG, Chopp M. Neurorestorative therapies for stroke: underlying mechanisms and translation to the clinic. Lancet Neurol. 2009;8:491-500.

51. Martí-Fábregas J, Romaguera-Ros M, Gómez-Pinedo U, Martínez-Ramírez S, Jiménez-Xarrie E, Marin R, Martí-Vilalta JL, García-Verdugo JM. Proliferation in the human ipsilateral subventricular zone after ischemic stroke. Neurology. 2010;74:357-65.

52. Oudin MJ, Gajendra S, Williams G, Hobbs C, Lalli G, Doherty P. Endocannabinoids regulate the migration of subventricular zone-derived neuroblasts in the postnatal brain. J Neurosci. 2011;31:4000-11.

53. Le Belle JE, Orozco NM, Paucar AA, Saxe JP, Mottahedeh J, Pyle AD, Wu H, Kornblum HI. Proliferative neural stem cells have high endogenous ROS levels that regulate self-renewal and neurogenesis in a PI3K/Akt-dependant manner. Cell Stem Cell. 2011;8:59-71.

54. Wilkins A, Kemp K, Ginty M, Hares K, Mallam E, Scolding N. Human bone marrow-derived mesenchymal stem cells secrete brain-derived neurotrophic factor which promotes neuronal survival in vitro. Stem Cell Res. 2009.

55. Osredkar D, Sall JW, Bickler PE, Ferriero DM. Erythropoietin promotes hippocampal neurogenesis in in vitro models of neonatal stroke. Neurobiol Dis. 2010;38:259-65.

56. Arenillas JF, Sobrino T, Castillo J, Davalos A. The role of angiogenesis in damage and recovery from ischemic stroke. Curr Treat Options Cardiovasc Med. 2007;9:205-12.

57. Brea D, Sobrino T, Ramos-Cabrer P, Castillo J. Reorganización de la vasculatura cerebral tras la isquemia. Rev Neurol. 2009;49:645-54.

58. Sobrino T, Hurtado O, Moro MA, Rodríguez-Yáñez M, Castellanos M, Brea D, Moldes O, Blanco M, Arenillas JF, Leira R, Dávalos A, Lizasoain I, Castillo J. The increase of circulating endothelial progenitor cells after acute ischemic stroke is associated with good outcome. Stroke. 2007;38:2759-64.

59. Seevinck PR, Deddens LH, Dijkhuizen RM. Magnetic resonance imaging of brain angiogenesis after stroke. Angiogenesis. 2010;13:101-11.

60. Zacharek A, Chen J, Cui X, Li A, Li Y, Roberts C, Feng Y, Gao Q, Chopp M. Angiopoietin1/Tie2 and VEGF/Flk1 induced by MSC treatment amplifies angiogenesis and vascular stabilization after stroke. J Cereb Blood Flow Metab. 2007;27:1684-91.

61. Font MA, Arboix A, Krupinski J. Angiogenesis, neurogenesis and neuroplasticity in ischemic stroke. Curr Cardiol Rev. 2010;6:238-44.

62. Liu XS, Chopp M, Zhang RL, Hozeska-Solgot A, Gregg SC, Buller B, Lu M, Zhang ZG. Angiopoietin 2 mediates the differentiation and migration of neural progenitor cells in the subventricular zone after stroke. J Biol Chem. 2009;284:22680-9.

63. Liu XS, Zhang ZG, Zhang RL, Gregg S, Morris DC, Wang Y, Chopp M. Stroke induces gene profile changes associated with neurogenesis and angiogenesis in adult subventricular zone progenitor cells. J Cereb Blood Flow Metab. 2007;27:564-74.

64. Teng H, Zhang ZG, Wang L, Zhang RL, Zhang L, Morris D, Gregg SR, Wu Z, Jiang A, Lu M, Zlokovic BV, Chopp M. Coupling of angiogenesis and

neurogenesis in cultured endothelial cells and neural progenitor cells after stroke. J Cereb Blood Flow Metab. 2008;28:764-71.

65. Jiang Q, Zhang ZG, Ding GL, Zhang L, Ewing JR, Wang L, Zhang R, Li L, Lu M, Meng H, Arbab AS, Hu J, Li QJ, Pourabdollah Nejad DS, Athiraman H, Chopp M. Investigation of neural progenitor cell induced angiogenesis after embolic stroke in rat using MRI. Neuroimage. 2005;28:698-707.

66. Chopp M, Zhang ZG, Jiang Q. Neurogenesis, angiogenesis, and MRI indices of functional recovery from stroke. Stroke. 2007;38:827-31.

67. Parr AM, Tator CH, Keating A. Bone marrow-derived mesenchymal stromal cells for the repair of central nervous system injury. Bone Marrow Transplant. 2007;40:609-19.

68. Caplan AI, Dennis JE. Mesenchymal stem cells as trophic mediators. J Cell Biochem. 2006;98:1076-84.

69. Munoz JR, Stoutenger BR, Robinson AP, Spees JL, Prockop DJ. Human stem/progenitor cells from bone marrow promote neurogenesis of endogenous neural stem cells in the hippocampus of mice. Proc Natl Acad Sci U S A. 2005;102:18171-6.

70. Buhnemann C, Scholz A, Bernreuther C, Malik CY, Braun H, Schachner M, Reymann KG, Dihne M. Neuronal differentiation of transplanted embryonic stem cell-derived precursors in stroke lesions of adult rats. Brain. 2006;129:3238-48.

71. Pomper MG, Hammond H, Yu X, Ye Z, Foss CA, Lin DD, Fox JJ, Cheng L. Serial imaging of human embryonic stem-cell engraftment and teratoma formation in live mouse models. Cell Res. 2009;19:370-9.

72. Baharvand H, Mehrjardi NZ, Hatami M, Kiani S, Rao M, Haghighi MM. Neural differentiation from human embryonic stem cells in a defined adherent culture condition. Int J Dev Biol. 2007;51:371-8.

73. Bentz K, Molcanyi M, Hess S, Schneider A, Hescheler J, Neugebauer E, Schaefer U. Neural differentiation of embryonic stem cells is induced by signalling from non-neural niche cells. Cell Physiol Biochem. 2006;18:275-86.

74. England TJ, Abaei M, Auer DP, Lowe J, Jones DR, Sare G, Walker M, Bath PM. Granulocyte-Colony Stimulating Factor for Mobilizing Bone Marrow Stem Cells in Subacute Stroke: The Stem Cell Trial of Recovery Enhancement After Stroke 2 Randomized Controlled Trial. Stroke. 2011.

75. Hossmann KA. Cerebral ischemia: models, methods and outcomes. Neuropharmacology. 2008;55:257-70.

76. Hossmann KA. Viability thresholds and the penumbra of focal ischemia. Ann Neurol. 1994;36:557-65.

77. Ramos-Cabrer P, Campos F, Sobrino T, Castillo J. Targeting the ischemic penumbra. Stroke. 2011;42:S7-11.

78. Lo EH. A new penumbra: transitioning from injury into repair after stroke. Nat Med. 2008;14:497-500.

79. Kogure T, Kogure K. Molecular and biochemical events within the brain subjected to cerebral ischemia (targets for therapeutical intervention). Clin Neurosci. 1997;4:179-83.

80. Samdani AF, Dawson TM, Dawson VL. Nitric oxide synthase in models of focal ischemia. Stroke. 1997;28:1283-8.

81. Hossmann KA. Periinfarct depolarizations. Cerebrovasc Brain Metab Rev. 1996;8:195-208.

82. Lu XC, Williams AJ, Wagstaff JD, Tortella FC, Hartings JA. Effects of delayed intrathecal infusion of an NMDA receptor antagonist on ischemic injury and peri-infarct depolarizations. Brain research. 2005;1056:200-8.

83. Castellanos M, Sobrino T, Castillo J. Evolving paradigms for neuroprotection: molecular identification of ischemic penumbra. Cerebrovasc Dis. 2006;21 Suppl 2:71-9.

84. Rebel A, Koehler RC, Martin LJ. In situ immunoradiographic method for quantification of specific proteins in normal and ischemic brain regions. J Neurosci Methods. 2005;143:227-35.

85. Hata R, Maeda K, Hermann D, Mies G, Hossmann KA. Evolution of brain infarction after transient focal cerebral ischemia in mice. J Cereb Blood Flow Metab. 2000;20:937-46.

86. Picard FJ, Bergeron MG. Rapid molecular theranostics in infectious diseases. Drug Discov Today. 2002;7:1092-101.

87. Allen TM. The use of glycolipids and hydrophilic polymers in avoiding rapid uptake of liposomes by the mononuclear phagocyte system. Adv Drug Deliv Rev. 1994;13:285-309.

88. Drummond DC, Meyer O, Hong K, Kirpotin DB, Papahadjopoulos D. Optimizing liposomes for delivery of chemotherapeutic agents to solid tumors. Pharmacol Rev. 1999;51:691-743.

89. Kabanov AV. Polymer genomics: an insight into pharmacology and toxicology of nanomedicines. Adv Drug Deliv Rev. 2006;58:1597-621.

90. Kataoka K, Harada A, Nagasaki Y. Block copolymer micelles for drug delivery: design, characterization and biological significance. Adv Drug Deliv Rev. 2001;47:113-31.

91. Lee CC, MacKay JA, Frechet JM, Szoka FC. Designing dendrimers for biological applications. Nat Biotechnol. 2005;23:1517-26.

92. Lu Y, Low PS. Folate-mediated delivery of macromolecular anticancer therapeutic agents. Adv Drug Deliv Rev. 2002;54:675-93.

93. Nori A, Kopecek J. Intracellular targeting of polymer-bound drugs for cancer chemotherapy. Adv Drug Deliv Rev. 2005;57:609-36.

94. Widera A, Norouziyan F, Shen WC. Mechanisms of TfR-mediated transcytosis and sorting in epithelial cells and applications toward drug delivery. Adv Drug Deliv Rev. 2003;55:1439-66.

95. Jaffer FA, Weissleder R. Molecular imaging in the clinical arena. JAMA. 2005;293:855-62.

96. Massoud TF, Gambhir SS. Molecular imaging in living subjects: seeing fundamental biological processes in a new light. Genes Dev. 2003;17:545-80.

97. Krohn KA, Link JM, Mason RP. Molecular imaging of hypoxia. J Nucl Med. 2008;49 Suppl 2:129S-48S.

98. Nighswander-Rempel SP, Kupriyanov VV, Shaw RA. Regional cardiac tissue oxygenation as a function of blood flow and pO2: A near-infrared spectroscopic imaging study. J Biomed Opt. 2006;11:054004.

99. Hartmann P, Mirtolouei R, Untersberger S, Ziegler W, Hermann Z, Richtig E, Hofmann-Wellenhof R, Grinschgl S, Kerl H, Smolle J. Non-invasive imaging of tissue PO2 in malignant melanoma of the skin. Melanoma Res. 2006;16:479-86.

100. Thiagarajah JR, Papadopoulos MC, Verkman AS. Noninvasive early detection of brain edema in mice by near-infrared light scattering. J Neurosci Res. 2005;80:293-9.

101. Alavi A, Kung JW, Zhuang H. Implications of PET based molecular imaging on the current and future practice of medicine. Semin Nucl Med. 2004;34:56-69.

102. Heiss WD. Ischemic penumbra: evidence from functional imaging in man. J Cereb Blood Flow Metab. 2000;20:1276-93.

103. Herholz K, Heiss WD. Positron emission tomography in clinical neurology. Mol Imaging Biol. 2004;6:239-69.

104. Golman K, Petersson JS. Metabolic imaging and other applications of hyperpolarized 13C1. Acad Radiol. 2006;13:932-42.

105. Mansson S, Johansson E, Magnusson P, Chai CM, Hansson G, Petersson JS, Stahlberg F, Golman K. 13C imaging-a new diagnostic platform. Eur Radiol. 2006;16:57-67.

106. Pichler BJ, Wehrl HF, Judenhofer MS. Latest advances in molecular imaging instrumentation. J Nucl Med. 2008;49 Suppl 2:5S-23S.

107. van Laar PJ, van der Grond J, Hendrikse J. Brain perfusion territory imaging: methods and clinical applications of selective arterial spin-labeling MR imaging. Radiology. 2008;246:354-64.

108. Lu H, Law M, Johnson G, Ge Y, van Zijl PC, Helpern JA. Novel approach to the measurement of absolute cerebral blood volume using vascular-space-occupancy magnetic resonance imaging. Magn Reson Med. 2005;54:1403-11.

109. Wu CW, Chuang KH, Wai YY, Wan YL, Chen JH, Liu HL. Vascular space occupancy-dependent functional MRI by tissue suppression. J Magn Reson Imaging. 2008;28:219-26.

110. Moseley ME. Molecular imaging and stroke. Stroke. 2009;40:S30-3.

111. Sheth VR, Li Y, Chen LQ, Howison CM, Flask CA, Pagel MD. Measuring in vivo tumor pHe with CEST-FISP MRI. Magn Reson Med. 2011.

112. Sun PZ, Murata Y, Lu J, Wang X, Lo EH, Sorensen AG. Relaxation-compensated fast multislice amide proton transfer (APT) imaging of acute ischemic stroke. Magn Reson Med. 2008;59:1175-82.

113. Zhou J, Payen JF, Wilson DA, Traystman RJ, van Zijl PC. Using the amide proton signals of intracellular proteins and peptides to detect pH effects in MRI. Nat Med. 2003;9:1085-90.

114. Sun PZ, Zhou J, Sun W, Huang J, van Zijl PC. Detection of the ischemic penumbra using pH-weighted MRI. J Cereb Blood Flow Metab. 2007;27:1129-36.

115. Querol M, Bogdanov A, Jr. Amplification strategies in MR imaging: activation and accumulation of sensing contrast agents (SCAs). J Magn Reson Imaging. 2006;24:971-82.

116. Bellin MF. MR contrast agents, the old and the new. Eur J Radiol. 2006;60:314-23.

117. Frullano L, Meade TJ. Multimodal MRI contrast agents. J Biol Inorg Chem. 2007;12:939-49.

118. Jun YW, Jang JT, Cheon J. Magnetic nanoparticle assisted molecular MR imaging. Adv Exp Med Biol. 2007;620:85-106.

119. Rhyner MN, Smith AM, Gao X, Mao H, Yang L, Nie S. Quantum dots and multifunctional nanoparticles: new contrast agents for tumor imaging. Nanomedicine (Lond). 2006;1:209-17.

120. Zabow G, Dodd S, Moreland J, Koretsky A. Micro-engineered local field control for high-sensitivity multispectral MRI. Nature. 2008;453:1058-63.

121. Strijkers GJ, Mulder WJ, van Tilborg GA, Nicolay K. MRI contrast agents: current status and future perspectives. Anticancer Agents Med Chem. 2007;7:291-305.

122. Yoo B, Pagel MD. An overview of responsive MRI contrast agents for molecular imaging. Front Biosci. 2008;13:1733-52.

123. Woods M, Woessner DE, Sherry AD. Paramagnetic lanthanide complexes as PARACEST agents for medical imaging. Chem Soc Rev. 2006;35:500-11.

124. Zhang S, Merritt M, Woessner DE, Lenkinski RE, Sherry AD. PARACEST agents: modulating MRI contrast via water proton exchange. Acc Chem Res. 2003;36:783-90.

125. Gallagher FA, Kettunen MI, Day SE, Hu DE, Ardenkjaer-Larsen JH, Zandt R, Jensen PR, Karlsson M, Golman K, Lerche MH, Brindle KM. Magnetic resonance imaging of pH in vivo using hyperpolarized 13C-labelled bicarbonate. Nature. 2008;453:940-3.

126. Schlageter KE, Molnar P, Lapin GD, Groothuis DR. Microvessel organization and structure in experimental brain tumors: microvessel populations with distinctive structural and functional properties. Microvasc Res. 1999;58:312-28.

127. Weiss N, Miller F, Cazaubon S, Couraud PO. The blood-brain barrier in brain homeostasis and neurological diseases. Biochim Biophys Acta. 2009;1788:842-57.

128. Stewart PA, Wiley MJ. Developing nervous tissue induces formation of blood-brain barrier characteristics in invading endothelial cells: a study using quail--chick transplantation chimeras. Dev Biol. 1981;84:183-92.

129. Kimelberg HK, Norenberg MD. Astrocytes. Sci Am. 1989;260:66-72, 4, 6.

130. Goldstein GW. Endothelial cell-astrocyte interactions. A cellular model of the blood-brain barrier. Ann N Y Acad Sci. 1988;529:31-9.

131. Begley DJ. The blood-brain barrier: principles for targeting peptides and drugs to the central nervous system. J Pharm Pharmacol. 1996;48:136-46.

132. Oldendorf WH. Blood brain barrier permeability to lactate. Eur Neurol. 1971;6:49-55.

133. Oldendorf WH. Carrier-mediated blood-brain barrier transport of short-chain monocarboxylic organic acids. Am J Physiol. 1973;224:1450-3.

134. Takanaga H, Tamai I, Inaba S, Sai Y, Higashida H, Yamamoto H, Tsuji A. cDNA cloning and functional characterization of rat intestinal monocarboxylate transporter. Biochem Biophys Res Commun. 1995;217:370-7.

135. Cornford EM, Braun LD, Oldendorf WH. Carrier mediated blood-brain barrier transport of choline and certain choline analogs. J Neurochem. 1978;30:299-308.

136. Kang YS, Terasaki T, Ohnishi T, Tsuji A. In vivo and in vitro evidence for a common carrier mediated transport of choline and basic drugs through the blood-brain barrier. J Pharmacobiodyn. 1990;13:353-60.

137. Kurihara A, Suzuki H, Sawada Y, Sugiyama Y, Iga T, Hanano M. Uptake of propranolol by microvessels isolated from bovine brain. J Pharm Sci. 1987;76:759-64.

138. Pardridge WM, Sakiyama R, Fierer G. Transport of propranolol and lidocaine through the rat blood-brain barrier. Primary role of globulin-bound drug. J Clin Invest. 1983;71:900-8.

139. Shimon M, Egozi Y, Kloog Y, Sokolovsky M, Cohen S. Kinetics of choline uptake into isolated rat forebrain microvessels: evidence of endocrine modulation. J Neurochem. 1988;50:1719-24.

140. Yamazaki M, Fukuoka H, Nagata O, Kato H, Ito Y, Terasaki T, Tsuji A. Transport mechanism of an H1-antagonist at the blood-brain barrier: transport mechanism of mepyramine using the carotid injection technique. Biol Pharm Bull. 1994;17:676-9.

141. Banks WA, Kastin AJ, Barrera CM. Delivering peptides to the central nervous system: dilemmas and strategies. Pharm Res. 1991;8:1345-50.

142. Ringe K, Walz CM, Sabel BA. Nanoparticle Drug Delivery to the Brain. In: Nalwa HS, editor. Encyclopedia of Nanoscience and Nanotechnology: American Scientific Publishers; 2004. p. 91-104.

143. Kumagai AK, Eisenberg JB, Pardridge WM. Absorptive-mediated endocytosis of cationized albumin and a beta-endorphin-cationized albumin chimeric peptide by isolated brain capillaries. Model system of blood-brain barrier transport. J Biol Chem. 1987;262:15214-9.

144. Pardridge WM. Drug delivery to the brain. J Cereb Blood Flow Metab. 1997;17:713-31.

145. Pardridge WM, Triguero D, Buciak J. Transport of histone through the blood-brain barrier. J Pharmacol Exp Ther. 1989;251:821-6.

146. Smith KR, Borchardt RT. Permeability and mechanism of albumin, cationized albumin, and glycosylated albumin transcellular transport across monolayers of cultured bovine brain capillary endothelial cells. Pharm Res. 1989;6:466-73.

147. Pardridge WM, Buciak JL, Friden PM. Selective transport of an anti-transferrin receptor antibody through the blood-brain barrier in vivo. J Pharmacol Exp Ther. 1991;259:66-70.

148. Pardridge WM, Kumagai AK, Eisenberg JB. Chimeric peptides as a vehicle for peptide pharmaceutical delivery through the blood-brain barrier. Biochem Biophys Res Commun. 1987;146:307-13.

149. Levin VA. Relationship of octanol/water partition coefficient and molecular weight to rat brain capillary permeability. J Med Chem. 1980;23:682-4.

150. Pardridge WM, Triguero D, Yang J, Cancilla PA. Comparison of in vitro and in vivo models of drug transcytosis through the blood-brain barrier. J Pharmacol Exp Ther. 1990;253:884-91.

151. Bradley G, Juranka PF, Ling V. Mechanism of multidrug resistance. Biochim Biophys Acta. 1988;948:87-128.

152. Juliano RL, Ling V. A surface glycoprotein modulating drug permeability in Chinese hamster ovary cell mutants. Biochim Biophys Acta. 1976;455:152-62.

153. Gros P, Ben Neriah YB, Croop JM, Housman DE. Isolation and expression of a complementary DNA that confers multidrug resistance. Nature. 1986;323:728-31.

154. Safa AR. Photoaffinity labeling of the multidrug-resistance-related P-glycoprotein with photoactive analogs of verapamil. Proc Natl Acad Sci U S A. 1988;85:7187-91.

155. Safa AR, Glover CJ, Meyers MB, Biedler JL, Felsted RL. Vinblastine photoaffinity labeling of a high molecular weight surface membrane glycoprotein specific for multidrug-resistant cells. J Biol Chem. 1986;261:6137-40.

156. Tamai I, Safa AR. Azidopine noncompetitively interacts with vinblastine and cyclosporin A binding to P-glycoprotein in multidrug resistant cells. J Biol Chem. 1991;266:16796-800.

157. Dehouck MP, Dehouck B, Schluep C, Lemaire M, Cecchelli R. Drug transport to the brain: comparison between in vitro and in vivo models of the blood-brain barrier. Eur J Pharm Sci. 1995;3:357-65.

158. Habgood MD, Begley DJ, Abbott NJ. Determinants of passive drug entry into the central nervous system. Cell Mol Neurobiol. 2000;20:231-53.

159. Crivori P, Cruciani G, Carrupt PA, Testa B. Predicting blood-brain barrier permeation from three-dimensional molecular structure. J Med Chem. 2000;43:2204-16.

160. Filmore D. Breeching the blood-drain barrier. Modern Drug Discov. 2002;5:22 -7.

161. Madrid Y, Langer LF, Brem H, Langer R. New directions in the delivery of drugs and other substances to the central nervous system. Adv Pharmacol. 1991;22:299-324.

162. Thorne RG, Frey WH, 2nd. Delivery of neurotrophic factors to the central nervous system: pharmacokinetic considerations. Clin Pharmacokinet. 2001;40:907-46.

163. Begley DJ, Squires LK, Zlokovic BV, Mitrovic DM, Hughes CC, Revest PA, Greenwood J. Permeability of the blood-brain barrier to the immunosuppressive cyclic peptide cyclosporin A. J Neurochem. 1990;55:1222-30.

164. Jaehde U, Langemeijer MW, de Boer AG, Breimer DD. Cerebrospinal fluid transport and disposition of the quinolones ciprofloxacin and pefloxacin in rats. J Pharmacol Exp Ther. 1992;263:1140-6.

165. de Lange EC, Danhof M, de Boer AG, Breimer DD. Methodological considerations of intracerebral microdialysis in pharmacokinetic studies on drug transport across the blood-brain barrier. Brain Res Rev. 1997;25:27-49.

166. Terasaki T, Deguchi Y, Kasama Y, Pardridge WM, Tsuji A. Determination of in vivo steady-state unbound drug concentration in the brain interstitial fluid by microdialysis. Int J Pharm. 1992;81:143-52.

167. Menacherry S, Hubert W, Justice JB, Jr. In vivo calibration of microdialysis probes for exogenous compounds. Anal Chem. 1992;64:577-83.

168. Tewes B, Franke H, Hellwig S, Hoheisel D, Decker S, Griesche D, Tilling T, Wegener J, Galla HJ. Preparation of endothelial cells in primary cultures obtained from the brains of 6-month old pigs. In: de Boer AG, Sutanto W, editors. Transport across the blood-brain barrier: In-vitro and in-vivo techniques. Leiden University, Netherlands: CRC Press; 1997.

169. Erben M, Decker S, Franke H, Galla HJ. Electrical resistance measurements on cerebral capillary endothelial cells--a new technique to study small surface areas. J Biochem Biophys Methods. 1995;30:227-38.

170. Gath U, Hakvoort A, Wegener J, Decker S, Galla HJ. Porcine choroid plexus cells in culture: expression of polarized phenotype, maintenance of barrier properties and apical secretion of CSF-components. Eur J Cell Biol. 1997;74:68-78.

171. Hurst RD, Fritz IB. Properties of an immortalised vascular endothelial/glioma cell co-culture model of the blood-brain barrier. J Cell Physiol. 1996;167:81-8.

172. Wegener J, Sieber M, Galla HJ. Impedance analysis of epithelial and endothelial cell monolayers cultured on gold surfaces. J Biochem Biophys Methods. 1996;32:151-70.

173. Iyer M, Mishru R, Han Y, Hopfinger AJ. Predicting blood-brain barrier partitioning of organic molecules using membrane-interaction QSAR analysis. Pharm Res. 2002;19:1611-21.

174. Siegal T, Zylber-Katz E. Strategies for increasing drug delivery to the brain: focus on brain lymphoma. Clin Pharmacokinet. 2002;41:171-86.

175. Aragnol D, Leserman LD. Immune clearance of liposomes inhibited by an anti-Fc receptor antibody in vivo. Proc Natl Acad Sci U S A. 1986;83:2699-703.

176. Derksen JT, Morselt HW, Scherphof GL. Uptake and processing of immunoglobulin-coated liposomes by subpopulations of rat liver macrophages. Biochim Biophys Acta. 1988;971:127-36.

177. Gabizon A, Papahadjopoulos D. The role of surface charge and hydrophilic groups on liposome clearance in vivo. Biochim Biophys Acta. 1992;1103:94-100.

178. Papahadjopoulos D, Allen TM, Gabizon A, Mayhew E, Matthay K, Huang SK, Lee KD, Woodle MC, Lasic DD, Redemann C, et al. Sterically stabilized liposomes: improvements in pharmacokinetics and antitumor therapeutic efficacy. Proc Natl Acad Sci U S A. 1991;88:11460-4.

179. Allen TM. Long-circulating (sterically stabilized) liposomes for targeted drug delivery. Trends Pharmacol Sci. 1994;15:215-20.

180. Moghimi SM, Patel HM. Opsonophagocytosis of liposomes by peritoneal macrophages and bone marrow reticuloendothelial cells. Biochim Biophys Acta. 1992;1135:269-74.

181. Klibanov AL, Maruyama K, Beckerleg AM, Torchilin VP, Huang L. Activity of amphipathic poly(ethylene glycol) 5000 to prolong the circulation time of liposomes depends on the liposome size and is unfavorable for immunoliposome binding to target. Biochim Biophys Acta. 1991;1062:142-8.

182. Torchilin VP. Immunoliposomes and PEGylated immunoliposomes: possible use for targeted delivery of imaging agents. Immunomethods. 1994;4:244-58.

183. Lee YJ, Corry PM. Metabolic oxidative stress-induced HSP70 gene expression is mediated through SAPK pathway. Role of Bcl-2 and c-Jun NH2-terminal kinase. J Biol Chem. 1998;273:29857-63.

184. Allen TM, Brandeis E, Hansen CB, Kao GY, Zalipsky S. A new strategy for attachment of antibodies to sterically stabilized liposomes resulting in efficient targeting to cancer cells. Biochim Biophys Acta. 1995;1237:99-108.

185. Hansen CB, Kao GY, Moase EH, Zalipsky S, Allen TM. Attachment of antibodies to sterically stabilized liposomes: evaluation, comparison and optimization of coupling procedures. Biochim Biophys Acta. 1995;1239:133-44.

186. Maruyama K, Takizawa T, Yuda T, Kennel SJ, Huang L, Iwatsuru M. Targetability of novel immunoliposomes modified with amphipathic poly(ethylene glycol)s conjugated at their distal terminals to monoclonal antibodies. Biochim Biophys Acta. 1995;1234:74-80.

187. Shahinian S, Silvius JR. A novel strategy affords high-yield coupling of antibody Fab' fragments to liposomes. Biochim Biophys Acta. 1995;1239:157-67.

188. Sadeque AJ, Wandel C, He H, Shah S, Wood AJ. Increased drug delivery to the brain by P-glycoprotein inhibition. Clin Pharmacol Ther. 2000;68:231-7.

189. Savolainen J, Edwards JE, Morgan ME, McNamara PJ, Anderson BD. Effects of a P-glycoprotein inhibitor on brain and plasma concentrations of anti-human immunodeficiency virus drugs administered in combination in rats. Drug Metab Dispos. 2002;30:479-82.

190. Fellner S, Bauer B, Miller DS, Schaffrik M, Fankhanel M, Spruss T, Bernhardt G, Graeff C, Farber L, Gschaidmeier H, Buschauer A, Fricker G. Transport of paclitaxel (Taxol) across the blood-brain barrier in vitro and in vivo. J Clin Invest. 2002;110:1309-18.

191. Gupta SP. QSAR studies on drugs acting at the central nervous system. Chem Rev. 1989;89:1765-800.

192. van De Waterbeemd H, Smith DA, Beaumont K, Walker DK. Property-based design: optimization of drug absorption and pharmacokinetics. J Med Chem. 2001;44:1313-33.

193. Lewis DF, Dickins M. Substrate SARs in human P450s. Drug Discov Today. 2002;7:918-25.

194. Lin JH, Lu AY. Role of pharmacokinetics and metabolism in drug discovery and development. Pharmacol Rev. 1997;49:403-49.

195. Cornford EM, Oldendorf WH. Epilepsy and the blood-brain barrier. Adv Neurol. 1986;44:787-812.

196. Oldendorf WH. Measurement of brain uptake of radiolabeled substances using a tritiated water internal standard. Brain research. 1970;24:372-6.

197. Abraham MH, Chadha HS, Mitchell RC. Hydrogen bonding. 33. Factors that influence the distribution of solutes between blood and brain. J Pharm Sci. 1994;83:1257-68.

198. de Boer AG, Gaillard PJ. In vitro models of blood-brain barrie : when to use which. Curr Med Chem. 2002;2:203-9.

199. Mertsch K, Maas J. Blood-brain barrier penetration and drug development from an industrial point of view. Curr Med Chem. 2002;2:189-209.

200. Bodor N, Buchwald P. Drug targeting via retrometabolic approaches. Pharmacol Ther. 1997;76:1-27.

201. Han HK, Amidon GL. Targeted prodrug design to optimize drug delivery. AAPS PharmSci. 2000;2:E6.

202. Orive G, Anitua E, Pedraz JL, Emerich DF. Biomaterials for promoting brain protection, repair and regeneration. Nat Rev Neurosci. 2009;10:682-92.

203. Bodor N, Prokai L, Wu WM, Farag H, Jonalagadda S, Kawamura M, Simpkins J. A strategy for delivering peptides into the central nervous system by sequential metabolism. Science. 1992;257:1698-700.

204. Palomino E, Kessel D, Horwitz JP. A dihydropyridine carrier system for sustained delivery of 2',3'-dideoxynucleosides to the brain. J Med Chem. 1989;32:622-5.

205. Pardridge WM. The blood-brain barrier: bottleneck in brain drug development. NeuroRx. 2005;2:3-14.

206. Neuwelt E, Abbott NJ, Abrey L, Banks WA, Blakley B, Davis T, Engelhardt B, Grammas P, Nedergaard M, Nutt J, Pardridge W, Rosenberg GA, Smith Q, Drewes LR. Strategies to advance translational research into brain barriers. Lancet Neurol. 2008;7:84-96.

207. Beduneau A, Saulnier P, Benoit JP. Active targeting of brain tumors using nanocarriers. Biomaterials. 2007;28:4947-67.

208. Weinstein JN, Blumenthal R, Sharrow SO, Henkart PA. Antibody-mediated targeting of liposomes. Binding to lymphocytes does not ensure incorporation of vesicle contents into the cells. Biochim Biophys Acta. 1978;509:272-88.

209. Siwak DR, Tari AM, Lopez-Berestein G. The potential of drug-carrying immunoliposomes as anticancer agents. Commentary re: J. W. Park et al., Anti-HER2 immunoliposomes: enhanced efficacy due to targeted delivery. Clin. Cancer Res., 8: 1172-1181, 2002. Clin Cancer Res. 2002;8:955-6.

210. Begley DJ. Delivery of therapeutic agents to the central nervous system: the problems and the possibilities. Pharmacol Ther. 2004;104:29-45.

211. Denora N, Trapani A, Laquintana V, Lopedota A, Trapani G. Recent advances in medicinal chemistry and pharmaceutical technology--strategies for drug delivery to the brain. Curr Top Med Chem. 2009;9:182-96.

212. Sahoo SK, Labhasetwar V. Nanotech approaches to drug delivery and imaging. Drug Discov Today. 2003;8:1112-20.

213. Schnyder A, Huwyler J. Drug transport to brain with targeted liposomes. NeuroRx. 2005;2:99-107.

214. Lian T, Ho RJ. Trends and developments in liposome drug delivery systems. J Pharm Sci. 2001;90:667-80.

215. Misra A, Ganesh S, Shahiwala A, Shah SP. Drug delivery to the central nervous system: a review. J Pharm Pharm Sci. 2003;6:252-73.

216. Pardridge WM, Boado RJ, Black KL, Cancilla PA. Blood-brain barrier and new approaches to brain drug delivery. West J Med. 1992;156:281-6.

217. Zhang Y, Calon F, Zhu C, Boado RJ, Pardridge WM. Intravenous nonviral gene therapy causes normalization of striatal tyrosine hydroxylase and reversal of motor impairment in experimental parkinsonism. Hum Gene Ther. 2003;14:1-12.

218. Lockman PR, Mumper RJ, Khan MA, Allen DD. Nanoparticle technology for drug delivery across the blood-brain barrier. Drug Dev Ind Pharm. 2002;28:1-13.

219. Zhong Y, Bellamkonda RV. Biomaterials for the central nervous system. J R Soc Interface. 2008;5:957-75.

220. Kreuter J, Ramge P, Petrov V, Hamm S, Gelperina SE, Engelhardt B, Alyautdin R, von Briesen H, Begley DJ. Direct evidence that polysorbate-80-coated poly(butylcyanoacrylate) nanoparticles deliver drugs to the CNS via specific mechanisms requiring prior binding of drug to the nanoparticles. Pharm Res. 2003;20:409-16.

221. Menei P, Pean JM, Nerriere-Daguin V, Jollivet C, Brachet P, Benoit JP. Intracerebral implantation of NGF-releasing biodegradable microspheres protects striatum against excitotoxic damage. Exp Neurol. 2000;161:259-72.

222. McRae A, Dahlstrom A. Transmitter-loaded polymeric microspheres induce regrowth of dopaminergic nerve terminals in striata of rats with 6-OH-DA induced parkinsonism. Neurochem Int. 1994;25:27-33.

223. Schubert D, Dargusch R, Raitano J, Chan SW. Cerium and yttrium oxide nanoparticles are neuroprotective. Biochem Biophys Res Commun. 2006;342:86-91.

224. Blasi P, Giovagnoli S, Schoubben A, Ricci M, Rossi C. Solid lipid nanoparticles for targeted brain drug delivery. Adv Drug Deliv Rev. 2007;59:454-77.

225. Kaur IP, Bhandari R, Bhandari S, Kakkar V. Potential of solid lipid nanoparticles in brain targeting. J Control Release. 2008;127:97-109.

226. Brioschi A, Zenga F, Zara GP, Gasco MR, Ducati A, Mauro A. Solid lipid nanoparticles: could they help to improve the efficacy of pharmacologic treatments for brain tumors? Neurol Res. 2007;29:324-30.

227. Chattopadhyay N, Zastre J, Wong HL, Wu XY, Bendayan R. Solid lipid nanoparticles enhance the delivery of the HIV protease inhibitor, atazanavir, by a human brain endothelial cell line. Pharm Res. 2008;25:2262-71.

228. Liu L, Guo K, Lu J, Venkatraman SS, Luo D, Ng KC, Ling EA, Moochhala S, Yang YY. Biologically active core/shell nanoparticles self-assembled from cholesterol-terminated PEG-TAT for drug delivery across the blood-brain barrier. Biomaterials. 2008;29:1509-17.

229. Shigeno T, Teasdale GM, McCulloch J, Graham DI. Recirculation model following MCA occlusion in rats. Cerebral blood flow, cerebrovascular permeability, and brain edema. J Neurosurg. 1985;63:272-7.

230. Longa EZ, Weinstein PR, Carlson S, Cummins R. Reversible middle cerebral artery occlusion without craniectomy in rats. Stroke. 1989;20:84-91.

231. Shevchenko A, Wilm M, Vorm O, Mann M. Mass spectrometric sequencing of proteins silver-stained polyacrylamide gels. Anal Chem. 1996;68:850-8.

232. Rouser G, Fkeischer S, Yamamoto A. Two dimensional then layer chromatographic separation of polar lipids and determination of phospholipids by phosphorus analysis of spots. Lipids. 1970;5:494-6.

233. Lowry OH, Rosebrough NJ, Farr AL, Randall RJ. Protein measurement with the Folin phenol reagent. J Biol Chem. 1951;193:265-75.

234. McCarthy KD, de Vellis J. Preparation of separate astroglial and oligodendroglial cell cultures from rat cerebral tissue. J Cell Biol. 1980;85:890-902.

235. Rodriguez-Gonzalez R, Agulla J, Perez-Mato M, Sobrino T, Castillo J. Neuroprotective effect of neuroserpin in rat primary cortical cultures after oxygen and glucose deprivation and tPA. Neurochem Int. 2011;58:337-43.

236. Fedoroff S, Richardson A. Protocols for neural cell culture. New Jersey: Humana Press; 2001.

237. Gill RR, Gbur CJ, Jr., Fisher BJ, Hess ML, Fowler AA, 3rd, Kukreja RC, Sholley MM. Heat shock provides delayed protection against oxidative injury in cultured human umbilical vein endothelial cells. J Mol Cell Cardiol. 1998;30:2739-49.

238. Gilany K, Van Elzen R, Mous K, Coen E, Van Dongen W, Vandamme S, Gevaert K, Timmerman E, Vandekerckhove J, Dewilde S, Van Ostade X, Moens L. The proteome of the human neuroblastoma cell line SH-SY5Y: an enlarged proteome. Biochim Biophys Acta. 2008;1784:983-5.

239. Kokubo Y, Matson GB, Liu J, Mancuso A, Kayama T, Sharp FR, Weinstein PR. Correlation between changes in apparent diffusion coefficient and induction of heat shock protein, cell-specific injury marker expression, and protein synthesis reduction on diffusion-weighted magnetic resonance images after temporary focal cerebral ischemia in rats. J Neurosurg. 2002;96:1084-93.

240. Sanz O, Estrada A, Ferrer I, Planas AM. Differential cellular distribution and dynamics of HSP70, cyclooxygenase-2, and c-Fos in the rat brain after transient focal ischemia or kainic acid. Neuroscience. 1997;80:221-32.

241. Datta A, Park JE, Li X, Zhang H, Ho ZS, Heese K, Lim SK, Tam JP, Sze SK. Phenotyping of an in vitro model of ischemic penumbra by iTRAQ-based shotgun quantitative proteomics. J Proteome Res. 2010;9:472-84.

242. Multhoff G. Heat shock protein 70 (Hsp70): membrane location, export and immunological relevance. Methods. 2007;43:229-37.

243. Stangl S, Gehrmann M, Riegger J, Kuhs K, Riederer I, Sievert W, Hube K, Mocikat R, Dressel R, Kremmer E, Pockley AG, Friedrich L, Vigh L, Skerra A, Multhoff G. Targeting membrane heat-shock protein 70 (Hsp70) on tumors by cmHsp70.1 antibody. Proc Natl Acad Sci U S A. 2011;108:733-8.

244. Allen TM, Hansen C, Martin F, Redemann C, Yau-Young A. Liposomes containing synthetic lipid derivatives of poly(ethylene glycol) show prolonged circulation half-lives in vivo. Biochim Biophys Acta. 1991;1066:29-36.

245. Olivier JC. Drug transport to brain with targeted nanoparticles. NeuroRx. 2005;2:108-19.

246. Lanza GM, Yu X, Winter PM, Abendschein DR, Karukstis KK, Scott MJ, Chinen LK, Fuhrhop RW, Scherrer DE, Wickline SA. Targeted antiproliferative drug delivery to vascular smooth muscle cells with a magnetic resonance imaging nanoparticle contrast agent: implications for rational therapy of restenosis. Circulation. 2002;106:2842-7.

247. Sipkins DA, Cheresh DA, Kazemi MR, Nevin LM, Bednarski MD, Li KC. Detection of tumor angiogenesis in vivo by alphaVbeta3-targeted magnetic resonance imaging. Nat Med. 1998;4:623-6.

248. Sipkins DA, Gijbels K, Tropper FD, Bednarski M, Li KC, Steinman L. ICAM-1 expression in autoimmune encephalitis visualized using magnetic resonance imaging. J Neuroimmunol. 2000;104:1-9.

249. Glogard C, Stensrud G, Hovland R, Fossheim SL, Klaveness J. Liposomes as carriers of amphiphilic gadolinium chelates: the effect of membrane composition on incorporation efficacy and in vitro relaxivity. Int J Pharm. 2002;233:131-40.

250. Leclercq F, Cohen-Ohana M, Mignet N, Sbarbati A, Herscovici J, Scherman D, Byk G. Design, synthesis, and evaluation of gadolinium cationic lipids as tools for biodistribution studies of gene delivery complexes. Bioconjug Chem. 2003;14:112-9.

251. Storrs RW, Tropper FD, Li HY, Song CK, Sipkins DA, Kuniyoshi JK, Bednarski MD, Strauss HW, Li KC. Paramagnetic polymerized liposomes as new recirculating MR contrast agents. J Magn Reson Imaging. 1995;5:719-24.

252. Gao K, Jiang X. Influence of particle size on transport of methotrexate across blood brain barrier by polysorbate 80-coated polybutylcyanoacrylate nanoparticles. Int J Pharm. 2006;310:213-9.

253. Redhead HM, Davis SS, Illum L. Drug delivery in poly(lactide-co-glycolide) nanoparticles surface modified with poloxamer 407 and poloxamine 908: in vitro characterisation and in vivo evaluation. J Control Release. 2001;70:353-63.

254. Ramos-Cabrer P, Agulla J, Argibay B, Pérez-Mato M, Castillo J. Serial MRI study of the enhanced therapeutic effects of liposome-encapsulated citicoline in cerebral ischemia. Int J Pharm. 2011;405:228-33.

255. Fresta M, Puglisi G. Survival rate improvement in a rat ischemia model by long circulating liposomes containing cytidine-5i-diphosphate choline. Life Sciences. 1997;61:1227-35.

256. Adibhatla RM, Hatcher JF, Tureyen K. CDP-choline liposomes provide significant reduction in infarction over free CDP-choline in stroke. Brain research. 2005;1058:193-7.

257. Wegener S, Weber R, Ramos-Cabrer P, Uhlenkueken U, Wiedermann D, Kandal K, Villringer A, Hoehn M. Subcortical lesions after transient thread occlusion in the rat: T2-weighted magnetic resonance imaging findings without corresponding sensorimotor deficits. J Magn Reson Imaging. 2005;21:340-6.

APENDIX: SUMMARY

Theranostics was initially defined in the context of cancer treatment and personalized medicine, however, the tremendous potential of this strategy has captured the attention of many biomedical researchers who are trying to export this concept to other fields, including the study and treatment of cerebrovascular diseases.

Cerebrovascular diseases are the second cause of death and the first cause of disability in developed countries. However, despite their social and economical importance, therapies for these diseases are quite limited. The most common etiology of stroke, ischemic stroke, consists of the reduction of blood flow in a brain area by occlusion of a major cerebral artery. This process triggers a series of events at molecular and cellular levels (the so-called ischemic cascade), that leads to energy depletion in the affected area, yielding on a quick process of cell death by necrosis. This area is called the infarct core. The surrounding zone, usually called the ischemic penumbra but probably better defined as the peri-infarct area, it is constituted by hypo-perfused tissue in which blood flow is too low to maintain electric activity, but sufficient to preserve ion channels. This area is subjected to a wave of deleterious metabolic processes that propagate from the ischemic core to the neighboring tissue, including excitotoxicity, spreading depression, oxidative stress, and inflammatory response, all of them leading to the expansion of the ischemic core into the peri-infarct region, and subsequent worsening of clinical outcome.

There is a hot debate on the stroke community about strategies to be followed to treat this disease. While neuroreparative therapies are under development, and seem to be far from being translated into the clinics, most neuroprotective strategies with impressive results in preclinical research have failed in the clinical setting, for different reasons. In this regard, some authors claim that research should not be focused just on the

development of new treatments for stroke, but must also consider how to deliver those agents efficiently to the stroke-stricken brain. A good example of this disjunctive is citicoline (Cytidine-5'-diphosphocholine) an essential intermediate in the synthesis of Phosphatidylcholine (a major brain phospholipid). Citicoline is believed to interfere in cell membrane damage, providing a benefit in for disorders of the central nervous system, including stroke. After the demonstration of efficiency in the preclinical field, citicoline has also been tested in several clinical trials with unclear outcome, and its usefulness for the treatment of stroke is under discussion. One of the main reasons for the controversy on the efficiency of citicoline in the clinics is the different ways of administration used for the drug (oral versus intravenous), especially considering that only 0.2-2.0% of the administered citicoline ends up in the brain parenchyma, depending on the administration route. This fact is highly influenced by the polar nature of citicoline, which hampers the crossing of the drug through the blood-brain barrier. Therefore, the use of alternative ways of administration for citicoline, or any other drug for that matter, to increase its bioavailability in the brain parenchyma, would potentially enhance the therapeutic effects of this drug for the treatment of stroke.

The aim of this study was to develop a nanoparticle system that would act as a theranostic agent for ischemic stroke. For this purpose a liposome-based nanoparticle system was synthesized. The lipophilic nature of the liposomes makes them ideal carriers to enhance blood brain barrier crossing, due to the lipidic composition of several components of the blood-brain barrier. It has been described, though, that the size of the liposome correlates with its ability to effectively cross the blood-brain barrier. Therefore our liposomes were designed to have around 100 nm in diameter, which would facilitate their blood-brain barrier crossing. We also used PEG-coupled lipids that enhance the circulation time of said liposomes, which increased the clearance time for said nanoparticle. In order to be able to use them as a diagnostic tool we loaded the liposomes with both Gd and rhodamine, which allowed us to identify them *in vivo*

and *in vitro* (by MRI) and *ex vivo* and *in vitro* (by fluorescence microscopy).

To determine the capacity of this liposome to penetrate the cellular membrane, astrocyte cell cultures were incubated with the liposomes an later on underwent fluorescence microscopy procedures to determine their capacity to transfect these cells. Not only did the liposomes transfect the astrocytes, but the efficacy was concentration-dependant, reaching a plateau at 4.8 μM. To determine the viability of this system to be identified *in vivo* in an ischemic rat brain, we injected a particular amount of substance that theoretically would allow us to differentiate it from both normal and ischemic tissue. We were able to corroborate that the paramagnetic liposomes synthesized could be visualized as long as they reached a 70 μM concentration of gadolinium. Since fluorescence microscopy is a more sensible technique, even lower concentrations of the nanocarrier can be identified by this technique.

The exact definition of the location and extension of the peri-infarct region (diagnosis), as well as targeted therapeutic approaches to treat it, based either on stopping the deleterious processes triggered by the ischemia (neuroprotective strategies) or on the enhancement of brain plasticity and neuroreparative processes, are key factors for the development of effective therapies heading for the improvement of patients' outcome. Therefore, it becomes necessary to define suited biomarkers that allow for the identification of this region. Although there are some scattered reports in the literature that identify up-regulated proteins in the peri-infarct area, only the expression of individual and selected proteins have been studied, so far. We believe that a global study of protein expression of the peri-infarct area is needed, to find adequate biomarkers, to compare their potential as theranostic targets in the context of cerebral ischemia. Since theranostics is based on molecular recognition processes between the theranostic agent and cells within the target tissue, it is preferable to define protein biomarkers that are located in the cellular plasma membrane, rather than

intracellular in order to facilitate the molecular interaction between the cell and the theranostic agents. Therefore, we have performed a proteomic analysis of peri-infarct tissue and compared it to healthy brain tissue in an animal model of stroke, using two different proteomic techniques (two-dimensional electrophoresis; 2-DE, and combined fractional diagonal chromatography; COFRADIC). Results have been validated by immunohistochemical techniques and Western blotting. All differences on protein expression found by proteomic approaches were quantitative, and no qualitative differences were found. This fact does not discard the existence of specific proteins for the peri-infarct tissue, whose concentration remain under the detection limits of the aforementioned techniques. It is noteworthy the particular case of the HSP70 family of proteins, cited as specific for the peri-infarct tissue by some authors and the only one coincidental result for both proteomic approaches. Therefore, we decided to deep into the analysis of the expression of the HSP70 protein family by western-blot and immunohistochemical analysis. 2D WB studies indicated the existence of a minor fraction of HSP70 proteins, specific for the peri-infarct tissue, which was revealed to be the inducible form of the heat shock protein family HSP70 also called HSP72 by immunohistochemistry. Constitutively expressed HSP70 was found across all the brain, whereas HSP72 was only identified specifically in the peri-infarct region. A double immunofluorescence approach was taken to determine what type of cell overexpressed HSP72. Since the presence of the protein was mainly restricted to the cortical area of the brain we tested both astrocytes and neurons for HSP72 expression. We found that mainly neurons are responsible for the expression of this protein, at least at 48 hours. The spatio-temporal dynamics of HSP72 expression indicate that HSP72 can be found as early as 6 hours after an ischemic event, although at this time point the expression is limited to the infarct core, and only a minimal positive staining can be seen at the peri-infarct region. Global expression of HSP72 peaks around 12 hours post ischemia and diminishes over time from that point, turning practically

anecdotic by day 14. The expression of HSP72 is not restricted to the peri-infarct area but also includes the infarct core at early time points (6-24 hours). It is only from ca. 24 hours on that HSP72 becomes practically exclusive for the peri-infarct region. 48 hours post ischemia is the most suitable time for the use of HSP72 as biomarker of the per-infarct tissue, since at this time point the expression of HSP72 at the peri-infarct region outweighs the one present at the ischemic core. The amount of cells that express HSP72 seems to be high enough to consider it an effective target for theranostics.

Once defined a proper target, an antibody against HSP72 was coupled to a set of paramagnetic (Gd^{3+} loaded) fluorescent liposomes, vectorized towards cells expressing HSP72. The HSP72-targeted liposomes were tested *in vitro* on astrocyte and endothelial cell cultures that underwent a heat shock process by which they overexpressed HSP72. The cell cultures were then incubated with both HSP72-targeted and non-targeted liposomes for 30 min or 1 hour to test the efficacy of both systems to label the stress induced cells. Transfection efficiency was not significantly affected by the incubation time. Cells overexpressing HSP72 showed a strong fluorescence signal after incubation with targeted liposomes while a low (residual) fluorescence signal was detected when cells were incubated with untargeted liposomes instead. A residual fluorescence signal was also detected when control cells where incubated with both targeted and untargeted liposomes. Using MRI, only the combination of HSP72 positive cells with HSP72 targeted liposomes led to a noticeable reduction of T1 relaxation time. Neither the combination of HSP72 positive and negative cells with untargeted liposomes, nor the combination of HSP72 negative cells with HSP72 targeted liposomes induced a significant reduction of T1 relaxation times with respect to cell culture media, used as control. All this experiments confirm the capacity of anti-HSP72 liposomes to target cells that overexpress this protein (such is the case of neurons of the peri-infarct region) and interact with them by molecular recognition processes,

confirming the validity of the biomarker selected as target for out theranostic agents.

We performed a serial MRI study on an animal model of cerebral ischemia, comparing both the therapeutic and diagnostic effects of HSP72-targeted liposomes encapsulating citicoline versus the untargeted-liposome as well as the free form of the drug, administered by two different routes (i.p. versus i.v.). Our intention was to investigate whether this well-known pharmacological approach to facilitate the trespassing of hydrophilic compounds through the BBB could be enhanced even more, aimed at the specific region of the brain were the of citicoline are needed, bringing some light to the existing doubts of its possibilities for the treatment of stroke. First we determined the capacity of the targeted-liposomes to accumulate in the peri-infarct region. Due to the low concentration of liposomes that crossed the BBB there was not enough contrast to be able to identify them on T1WI, but after acquiring T1 maps and processing them, establishing a threshold of 2.25 s, in the control group, only a group of pixels are presented at the most caudal slice of the brain, and no presence of liposomes (pixels with T1 < 2.25 s) is detected in the brain of this animals. For animals treated with regular (untargeted) liposomes, liposomes (pixels with T1 < 2.25) are distributed along most of the brain, without preference for any region in particular. Finally, anti-HSP72 vectorized liposomes tend to accumulate in the periphery of the ischemic lesion, as correspond to the distribution of the HSP72 protein for this period of time.

The therapeutic effect of the citicoline-loaded liposomes was evaluated by MRI over a 7 day period. The groups studied included citicoline administered free by systemic injection (either ip or iv), as well as non-targeted liposomes either unloaded or loaded with citicoline, finally HSP72-targeted liposomes loaded with citicoline were also studied. No statistically significant differences were found on basal infarct volumes for all groups. Lesions had a tendency to grow at days 1 and 3, dropping later by day 7 (typical behavior on this animal model). In those groups

were citicoline was used infarct volumes experiment a decrease from basal volumes at day 7, this phenomenon (not observed for both control groups) is more noticeable when citicoline is encapsulated in untargeted, and specially, in HSP72 targeted liposomes. Infarct volumes were significantly lower in the citicoline-loaded liposome groups with respect to free citicoline, administered either intravenously or intraperitoneally. In the case of HSP72-targeted liposomes, an improved effect compared with untargeted liposomes was only appreciated at day 7. It should be appreciated that the number of animals per group was reduced (only 4 animals per group) and further studies should be carried in the future to add robustness to our study.

Further optimization of the diagnostic and therapeutic activity of our theranostic agent is possible by modifying the nature or structure of the base liposomes (for example, with double targeting to facilitate the crossing of the BBB after IV administration), by using an enhanced T1 contrast agent, by optimization of the encapsulating process and by using different therapeutic agents, etc.

In conclusion, this study has demonstrated:

- That the peri-infarct region of the brain of ischemic animals presents a characteristic protein expression, with over-expression of particular molecular markers that allows its identification by molecular biology techniques.
- It also shows that 15 molecular markers of the peri-infarct region have been identified. Among them, the HSP72 or inducible HSP70 member of the Heat Shock Proteins family is the only truly specific one.
- The spatiotemporal dynamics of expression of the HSP72 protein has been characterized by immuno-histochemistry techniques, showing a maximal expression at the peri-infarct region 12-24 h after the induction of ischemia, and continues up to 14 days post ischemia.
- HSP72 protein is mostly expressed by neurons of the peri-infarct region, as demonstrated by immunofluorecence techniques.

- It is feasible the synthesis of theranostic agents, with a phospholipid liposome based structure, that contain imaging probes for their detection by conventional imaging techniques, and able to carry drugs on their structure for their transport and controlled release at target tissues.
- MRI techniques allow the detection of the gadolinium doped theranostic agents *in vivo*, either after their intraparenchymal or systemic injection in the rat.
- Fluorescence microscopy techniques allow the detection of the Rhodamine doped theranostic agents *in vitro* and *ex vivo*, of cell cultures and brain tissue samples.
- It is feasible to attach anti-HSP72 antibodies to the surface of the aforementioned theranostic agents, so they participate in molecular recognition processes at the peri-infarct region.
- It is feasible to load the aforementioned theranostic agents with citicoline (a known therapeutic agent for stroke).
- Constructed anti-HSP72 magnetoliposomes do effectively participate in molecular recognition processes with cells that overexpress HSP72 protein *in vitro*, allowing the identification (by MRI and fluorescence microscopy) of such cells.
- Constructed anti-HSP72 magnetoliposomes have been detected *ex vivo* (by fluorescence microscopy) in tissue samples of the peri-infarct region of ischemic animals.
- Constructed anti-HSP72 magnetoliposomes have been detected *in vivo* (by MRI) showing a preferential accumulation of the agent at the peri-infarct area of ischemic animals, as compared to animals treated with non-vectorized magneto-liposomes (controls).
- Citicoline doped anti-HSP72 magnetoliposomes show an enhanced therapeutic action in ischemic animals (defined as reduced lesion volumes on MRI), as compared with animals treated with citicoline doped non-targeted liposomes and animals treated with non-encapsulated (free) citicoline.

In summary, we have provided prove of principle that theranostics of the peri-infarct tissue is possible, and truly

enhances the diagnosis and therapeutic action of drugs for the treatment of stroke.

APÉNDICE: RESUMEN

El término teranóstica fue acuñado por primera vez en el contexto de la medicina personalizada para el tratamiento del cáncer, sin embargo, el tremendo potencial que esta estrategia posee, ha llamado la atención de numerosos investigadores en el campo de la biomedicina, los cuales están tratando de exportar este concepto a otros campos, incluido el estudio y tratamiento de la enfermedad vascular cerebral.

La enfermedad vascular cerebral es la segunda causa de muerte y la primera causa de discapacidad en los países desarrollados. Sin embargo, a pesar de su importancia tanto a nivel social como económico, las terapias para el tratamiento de esta enfermedad son todavía bastante limitadas. La etiología más común del ictus, el ictus isquémico, consiste en la reducción del flujo sanguíneo en un área del cerebro debido a la oclusión de una de las arterias cerebrales principales. Este proceso desencadena una serie de eventos tanto a nivel celular como molecular (la también denominada cascada isquémica), que conducen a la depleción de energía en el área afectada, produciendo rápidamente la muerte celular por necrosis. Este área se conoce como núcleo del infarto. La zona que lo rodea, denominada normalmente penumbra isquémica, aunque probablemente estaría mejor definida como zona peri-infarto, está compuesta por tejido hipo-perfundido, en el cual el flujo sanguíneo está demasiado reducido, de forma que las células no son capaces de mantener su actividad eléctrica, pero es suficiente como para mantener la actividad de los canales iónicos, preservando la viabilidad celular. Esta área se encuentra sometida a una ola de procesos metabólicos deletéreos que se propagan desde el núcleo isquémico hacia el tejido periférico e incluyen fenómenos de excitotoxicidad, depresión propagada, estrés oxidativo y respuestas inflamatorias. Todos estos procesos conducen a la propagación del núcleo isquémico en detrimento de la región peri-infarto, y al consiguiente empeoramiento del pronóstico clínico.

En la comunidad científica dedicada a la investigación del ictus existe un debate animado acerca de las posibles estrategias a seguir para el tratamiento de esta enfermedad. Mientras que las terapias de tipo regenerativo se encuentran todavía en fases iniciales de su desarrollo, y todavía están lejos de ser trasladadas a la práctica clínica, la mayoría de las terapias neuroprotectoras, pese a obtener resultados esperanzadores en investigación preclínica, han fallado al ser testadas en el ámbito clínico por diferentes razones. A este respecto, algunos autores piden que la investigación no debería estar sólo centrada en el desarrollo de nuevos tratamientos para el ictus, sino que deberían tener en consideración los métodos para conseguir una administración eficiente de esos agentes terapéuticos al cerebro isquémico. Un buen ejemplo de esta disyuntiva es la citicolina (o CDP-colina, citidina-5'-difosfocolina), un intermediario esencial en la síntesis de fosfatidilcolina (uno de los principales fosfolípidos en el cerebro). Se cree que la citicolina es capaz de interferir en el daño a las membranas celulares, pudiendo ser un agente beneficioso para el tratamiento de distintas enfermedades del sistema nervioso central, incluyendo el ictus. Tras haber demostrado su eficacia en el ámbito preclínico, la citicolina ha sido testada en distintos ensayos clínicos que han generado resultados poco concisos. Su utilidad para el tratamiento del ictus, por lo tanto, está todavía discutida. Una de las razones principales de la controversia acerca de la eficacia de la citicolina en el ámbito clínico parte de las diferentes vías de administración que pueden utilizarse para administrar este medicamento (oral frente a intravenosa), especialmente importante, si tenemos en cuenta que solo entre un 0.2 y un 2 % de la citicolina administrada termina en el parénquima cerebral, dependiendo de la vía de administración utilizada. Este hecho se encuentra influenciado en gran medida por la naturaleza polar de la citicolina, la cual obstaculiza su paso a través de la barrera hematoencefálica. Por lo tanto, el desarrollo de nuevas vías de administración para la citicolina, así como para cualquier otra droga dirigida hacia el cerebro,

incrementaría su biodisponibilidad en el parénquima cerebral, pudiendo llegar a incrementar los efectos terapéuticos de este fármaco para el tratamiento del ictus.

El propósito de este trabajo consiste en el desarrollo de un sistema basado en nanopartículas que tenga propiedades teranósticas para su utilización en el ictus isquémico. Para ello hemos elegido liposomas como nanopartícula a utilizar, en parte debido a que su naturaleza lipofílica facilita su paso a través de la barrera hematoencefálica, pues gran parte de sus componentes son también de naturaleza lipídica. El tamaño de los liposomas es una de las principales características que se tuvieron en cuenta durante su síntesis, pues está descrito que diámetros de partícula superiores a 100 μm, la cantidad de nanopartículas que llegan al cerebro disminuye enormemente. En condiciones normales, los liposomas administrados por vía sistémica son rápidamente opsonizados y retirados de la circulación. El incluir lípidos con polietilen- glicol en su estructura aumenta enormemente su tiempo de aclaramiento. El objetivo es utilizar este sistema como agente teranóstico, por ello es necesario el marcaje de los liposomas de forma que nos permita observarlos tanto *in vivo* e *in vitro* (al marcarlos con gadolinio para seguirlos por resonancia magnética), como *ex vivo* e *in vitro* (al incluir un lípido marcado con un fluoróforo, rodamina, en su estructura).

Para determinar la capacidad de estos liposomas de atravesar la membrana celular, se realizaron los siguientes experimentos *in vitro*: cultivos celulares de astrocitos fueron incubados con distintas concentraciones de liposomas y observados a continuación por microscopía de fluorescencia. Se pudo comprobar así, la capacidad de estos liposomas ser incorporados por los astrocitos, además, su acumulación fue concentración dependiente, alcanzándose un umbral máximo al incubar estas células con una solución de liposomas 4.8 μM. Para determinar la viabilidad de este sistema de ser observado mediante técnicas de resonancia magnética, se inyectaron liposomas en cerebros de animales isquémicos, tanto en

regiones del infarto, como en áreas de cerebro sano. Fue posible la identificación de liposomas, y su diferenciación en ambos tipos de tejido, siempre que la concentración de gadolinio alcanzada fuese superior a 70 μM. Debido a que las técnicas de microscopía de fluorescencia son mucho más sensibles, fue posible identificar los liposomas en concentraciones inferiores a partir de muestras de tejido cerebral (*ex vivo*).

La definición de la localización y extensión de la región peri-infarto (con fines diagnósticos), así como las aproximaciones terapéuticas dirigidas hacia esta zona en concreto para su tratamiento, bien sean basadas en el bloqueo de procesos deletéreos desencadenados por la isquemia (neuroprotección), como en el potenciamiento de la plasticidad cerebral y los procesos neurorreparativos, son factores clave para el desarrollo de terapias efectivas destinadas a mejorar el pronóstico funcional del paciente. Por lo tanto, es fundamental el definir cuál o cuáles son los biomarcadores que nos definan de forma más eficaz esta región del cerebro. Aunque existen algunos trabajos en la literatura que identifican proteínas sobre-expresadas en el área peri-infarto, hasta la fecha sólo han sido estudiadas una pequeña parte de ellas. Es necesario pues un estudio global de la expresión proteica de la región peri-infarto que nos permita identificar biomarcadores adecuados, y comparar su potencial como agentes teranósticos en el ámbito de la isquemia cerebral. Ya que la teranóstica se basa en procesos de reconocimiento molecular entre el agente teranóstico y las células dentro del tejido diana, es preferible definir biomarcadores que estén localizados en la membrana celular, en lugar de marcadores intracelulares, lo que facilita la interacción molecular entre la célula y el agente teranóstico. Para identificar estos posible biomarcadores realizamos un análisis proteómico del tejido peri-infarto frente a tejido cerebral sano en un modelo animal de isquemia cerebral. Utilizamos dos técnicas proteómicas diferentes, electroforesis bidimensional y cormatografía fraccional diagonal combinada (COFRADIC). Los resultados positivos fueron validados mediante técnicas de

western-blot (WB) e inmunohistoquímicas. Todas las diferencias en la expresión proteica que se encontraron mediante aproximaciones proteómicas fueron cuantitativas, no se encontró ninguna diferencia cualitativa entre ninguna de las fracciones estudiadas. Este hecho no descarta la existencia de proteínas exclusivas de la zona peri-infarto, simplemente la técnica no es suficientemente resolutiva como para detectar proteínas a concentración inferior a su límite de detección. Entre las proteínas identificadas destaca el caso de la HSP70 un miembro de la familia de proteínas de choque térmico, que ya había sido citada previamente por algunos autores como específica de la región peri-infarto. Esta proteína fue el único resultado común a ambas técnicas. Por lo tanto decidimos analizar en más detalle la expresión de las distintas formas de HSP70 tanto por WB como por inmunohistoquímicas. Los WB bidimensionales indican la presencia de una pequeña fracción de proteínas HSP70 que se expresa de forma específica en la región peri-infarto. Esta pequeña fracción se identificó como la forma inducible de la HSP70 también denominada HSP72 mediante técnicas de inmunohistoquímicas. La HSP70 expresada de forma constitutiva aparecía por todo el cerebro, mientras que la HSP72 se encontraba expresada de forma específica en la región peri-infarto. Mediante técnicas de doble inmunofluorescencia se trató de identificar qué tipo o tipos celulares expresaban esta proteína de forma diferencial. Debido a que la presencia de HSP72 se encontraba restringida a la región cortical del cerebro se decidió comprobar si astrocitos o neuronas eran las responsables de esta expresión. La expresión de HSP72 en la región peri-infarto de animales sometidos a isquemia cerebral está principalmente producida por las neuronas, al menos 48 horas tras la inducción de la isquemia. La dinámica espacio-temporal de expresión de la HSP72 revela que esta proteína se encuentra ya expresada 6 horas tras la inducción de la isquemia, aunque en este punto temporal la expresión se encuentra limitada al núcleo isquémico, y sólo una pequeña región del células en el peri-infarto aparece marcada. La expresión global de la HSP72

alcanza su máximo entorno a las 12 horas tras la isquemia y va disminuyendo con el tiempo a partir de ese punto, siendo prácticamente anecdótica a los 14 días tras la inducción de la isquemia. En tiempos de evolución cortos (entre 6 y 24 horas tras la isquemia) la expresión de HSP72 no se encuentra restringida a la zona peri-infarto, sino que incluye también el núcleo de la lesión. Es sólo a partir de las 24 horas cuando la HSP72 se encuentra expresada prácticamente de forma exclusiva en el peri-infarto. Por lo tanto, 48 horas tras la inducción de la isquemia, la HSP72 se confirma como la proteína más adecuada para su uso como biomarcador de tejido peri-infarto. La cantidad de células que expresan HSP72 parece ser lo suficientemente elevada como para considerarla como una diana efectiva con fines teranósticos.

Una vez se ha definido una diana adecuada, durante la síntesis de liposomas paramagnéticos y fluorescentes, se unión un anticuerpo contra la HSP72, con lo cual estos quedaban vectorizados frente a células que sobrexpresen HSP72. Estos liposomas fueron testados *in vitro* frente a cultivos celulares de astrocitos y células endoteliales en los que se indujo la sobreexpresión de HSP72. Estos cultivos fueron incubados entonces tanto con liposomas vectorizados como sin vectorizar durante 30 minutos o 1 hora, lo que permitió comparar la eficacia de transfección de ambos sistemas. La eficacia de transfección fue independiente del tiempo de incubación utilizado. Las células que sobreexpresaban HSP72 mostraron una fuerte señal en fluorescencia tras su incubación con liposomas vectorizados, mientras que sólo aparecía una señal residual cuando eran incubados con liposomas sin vectorizar. Una señal residual se encontraba también en el caso de que células que no expresasen HSP72 fueran incubadas tanto con liposomas vectorizados como no vectorizados. Estas células fueron recogidas y los pellets analizados por resonancia magnética. Sólo la combinación de células que sobreexpresasen HSP72 con liposomas vectorizados frente a esta proteína produjeron una reducción significativa de los tiempos de relajación T1 con respecto a células control, a las que no se añadió ningún

liposoma. Ni la combinación de células que sobreexpresasen HSP72 con liposomas no vectorizados ni células que no sobreexpresasen HSP72 con liposomas vectorizados produjo una reducción significativa de los tiempos de relajación T1 con respecto al control. Todos estos experimentos confirman la capacidad de liposomas vectorizados frente a HSP72 de unirse específicamente a células que sobreexpresen esta proteína (como sería el caso de las neuronas de la zona peri-infarto) e interaccionar con ellas mediante mecanismos de reconocimiento molecular, confirmando la validez de este biomarcador como diana para ser utilizado en agentes teranósticos.

Se han realizado una serie de estudios por resonancia magnética en un modelo animal de isquemia cerebral, comparando tanto el efecto terapéutico como diagnóstico de liposomas vectorizados frente a HSP72 en los cuales se encapsuló citicolina, frente a liposomas no vectorizados, así como a la administración sistémica del fármaco libre (bien por vía intraparenquimal, como por vía intravenosa). Nuestra intención fue investigar si esta aproximación farmacológica ampliamente estudiada para facilitar el paso de la barrera hematoencefálica podía ser mejorada, dirigiendo el fármaco hacia la región del cerebro donde se requiere su acción terapéutica. En primer lugar determinamos la capacidad de los liposomas vectorizados frente a HSP72 para acumularse de forma específica en la región peri-infarto. Debido a la baja concentración en cerebro que alcanzaron los liposomas, las imágenes con peso T1 adquiridas no mostraron el contraste suficiente para ser capaz de identificar los liposomas a simple vista. Sin embargo, tras generar mapas T1 a partir de las imágenes y establecer un umbral de corte de 2.25 s, en el grupo control, sólo un pequeño grupo de pixeles a nivel caudal presentaban pixeles positivos, que reflejarían la presencia de liposomas. No se observó señal positiva en la mayor parte del cerebro. En animales tratados con liposomas no vectorizados, éstos mostraban una distribución uniforme por todo el cerebro. Finalmente, en el caso de animales tratados con liposomas

vectorizados frente a HSP72, se observaba un acumulo de éstos en la periferia de la lesión, lo que coincide con la distribución de HSP72 observada previamente por estudios de inmunohistoquímica.

El efecto terapéutico de la citicolina encapsulada en liposomas se evaluó como una reducción del infarto por resonancia magnética durante un período de observación de 7 días. Los grupos estudiados incluyeron tanto un control, como animales tratados con citicolina libre por vía sistémica (ip o iv), animales tratados con liposomas no vectorizados vacíos y con citicolina, así como liposomas vectorizados con citicolina. No se encontraron diferencias significativas en los infartos basales para ninguno de los grupos estudiados. Las lesiones mostraban una tendencia a aumentar a días 1 y 3, reduciéndose a día 7. En aquellos grupos tratados con citicolina, los volúmenes de infarto sufrieron una reducción respecto al basal a día 7, este fenómeno no se observó en los grupos control y fue más pronunciado cuando la citicolina se administraba encapsulada en liposomas. Los volúmenes de infarto fueron significativamente inferiores en los grupos tratados con citicolina encapsulada en liposomas frente a los que se les administró citicolina libre de forma sistémica. En el caso de animales tratados con liposomas vectorizados, sólo se observó una reducción significativa del infarto frente a animales tratados con liposomas no vectorizados (que incluían citicolina) a día 7.

La optimización de las actividades diagnóstica y terapéutica del agente teranóstico mostrado es posible mediante modificaciones bien en su estructura base, como el agente de contraste utilizado, así como en la capacidad de encapsulación o el uso de diferentes sustancias terapéuticas, etc.

En conclusión, el presente estudio demuestra que:

- La región peri-infarto del cerebro de animales isquémicos muestra una expresión proteica característica, en la que se encuentra la sobre-expresión de determinados marcadores

moleculares, lo que permite su identificación mediante técnicas de biología molecular.

- Hemos identificado 15 marcadores moleculares de la región peri-infarto. Entre ellos, la forma inducible de la proteína de choque térmico HSP70 o HSP72 ha sido la única que ha mostrado ser específica de esta región.
- La dinámica espaciotemporal de expresión de la proteína HSP72 ha sido caracterizada por técnicas inmunohistoquímicas, mostrando una expresión máxima en la región peri-infarto entre las 12 y 24 horas tras la inducción de la isquemia. La HSP72 ha conseguido identificarse hasta 14 días tras la inducción de la isquemia.
- Mediante técnicas de inmunofluorescencia, se ha revelado que la proteína HSP72 se expresa fundamentalmente en las neuronas de la región peri-infarto.
- Ha sido posible la síntesis de liposomas como agentes teranósticos, a partir de una estructura fosfolipídica basal, que contienen tanto sondas de imagen que permiten su detección mediante técnicas de imagen convencional, así como son capaces de transportar drogas en su estructura para su posterior liberación controlada en los tejidos diana.
- Las técnicas de MRI han permitido la detección de los agentes teranósticos marcados con gadolinio, bien tras su inyección intraparenquimal, o sistémica en ratas.
- Técnicas de microscopía de fluorescencia han sido utilizadas para la detección de agentes teranósticos marcados con rodamina tanto *in vitro* (en cultivos celulares), como *ex vivo* (en muestras de tejido cerebral).
- Ha sido posible la unión de anticuerpos frente a la proteína HSP72 en la superficie de los agentes teranósticos ya mencionados, de tal modo que estos participan en procesos de reconocimiento molecular en la región peri-infarto.
- Ha sido posible la inclusión de citicolina (un agente cuya actividad neuroprotectora ha sido ampliamente demostrada) en los agentes teranósticos sintetizados.
- Los magnetoliposomas anti-HSP72 construidos participan en procesos de reconocimiento molecular de forma efectiva en

cultivos celulares con células que sobreexpresan la proteína HSP72, lo que permite su identificación mediante MRI y microscopía de fluorescencia.

- Los magnetoliposomas anti-HSP72 construidos se han detectado *ex vivo* (mediante microscopía de fluorescencia) en muestras de tejido cerebral de la región peri-infarto de animales isquémicos.
- Los magnetoliposomas anti-HSP72 construidos han sido detectados *in vivo* (mediante técnicas de MRI) y han mostrado una acumulación diferencial en el área peri-infarto de animales isquémicos, en comparación con animales tratados con magnetoliposomas no vectorizados (controles).
- Los magnetoliposomas anti-HSP72 cargados de citicolina han mostrado un incremento en la acción terapéutica sobre animales con isquemia cerebral (entendiéndose ésta como una reducción en el volumen de lesión en MRI), comparado con animales tratados con liposomas no vectorizados, también cargados de citicolina, así como con animales tratados con citicolina no encapsulada.

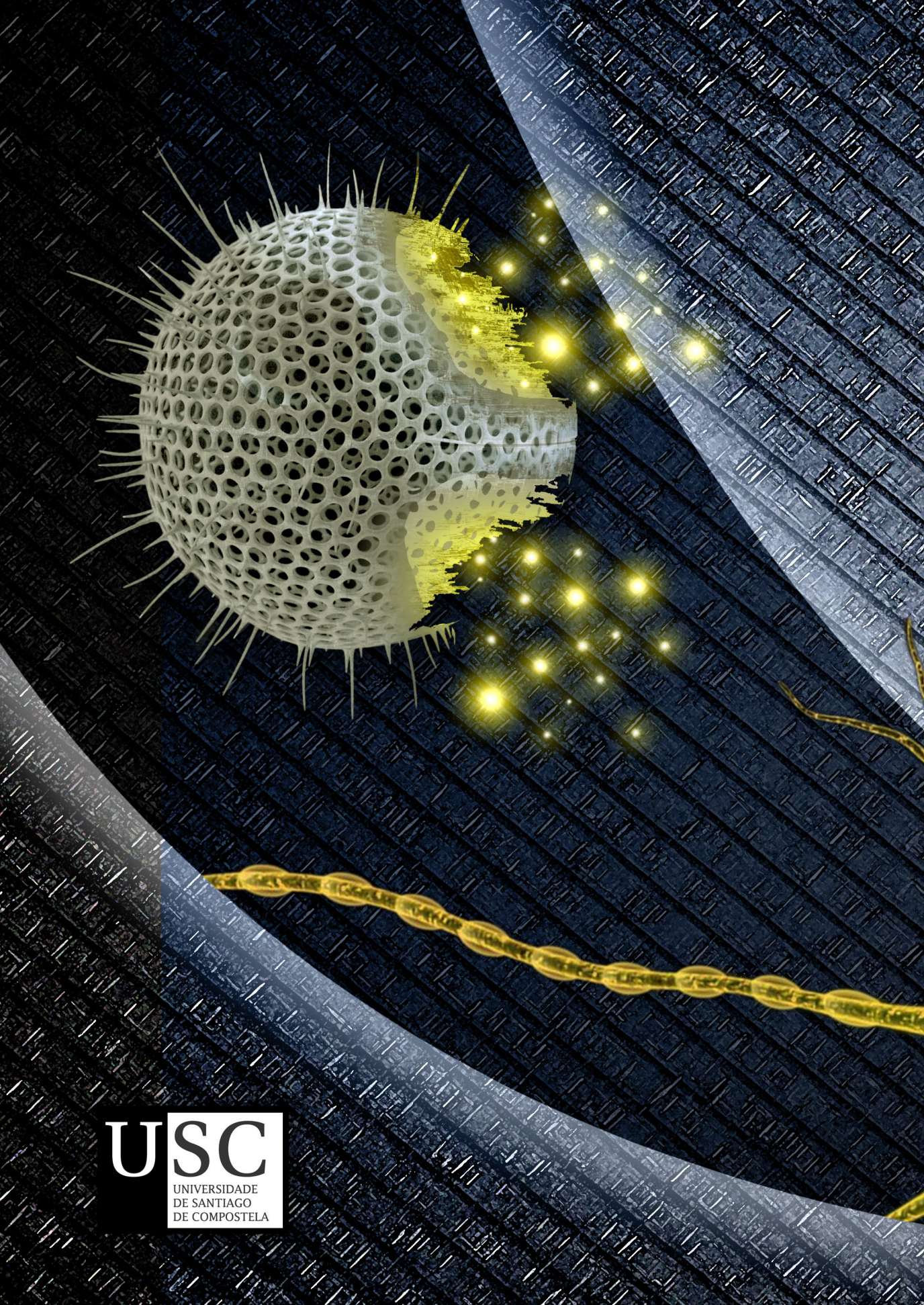

USC
UNIVERSIDADE
DE SANTIAGO
DE COMPOSTELA